Analysis of different levels of constraint in a total knee arthroplasty: a finite element study

Master thesis carried out with the aim of obtaining a master degree in Biomedical Engineering by

Laurence Rapallo

Supervisors:
Prof. Davide Ruffoni (ULG)
Prof. Bernardo Innocenti (ULB)

Collaborators:
Orthopaedic surgeon: G. Castellarin
Marketing and technology manager: C. Dottino (Adler Ortho)
R&D engineer: Silvia Pianigiani (Adler Ortho)

Academic year 2020-2021
University of Liège - School of Engineering and Computer Science

Abstract

The total knee arthroplasty is one of the most common orthopaedic surgical procedure. This one aims to relieve the pain and improve the mobility of the patients suffering from conditions leading to the deterioration of the knee joint. This surgery is only considered when the medical treatments such as the anti-inflammatory medications and physiotherapy are no longer sufficient to improve the patient's condition. According to the American Academy of Orthopedic Surgeons (AAOS), 90% of the patients undergoing a knee arthroplasty experience a significant reduction in pain. Besides, over 90 % of the prosthetic knees are still functioning after 15 years. For most of the patients, this procedure enable them to return to simple activities such as walking or climbing stairs, and leads to an improved quality of life with less pain and more mobility.

This thesis focuses on the clinical case of a patient who was suffering from osteoarthritis and had to undergo a total knee arthroplasty. The choice of the surgeon *Gianluca Castellarin* was to preserve as much as possible the soft tissues of the patients including the posterior cruciate ligament. He made the choice of using a cruciate retaining prosthesis. The goal of this thesis is to model the knee of the patient with four different types of prostheses with different levels of constraint using finite element analysis to confirm/invalidate the choice made by the surgeon.

Acknowledgment

The future belongs to those who believe in the beauty of their dreams (Eleanor Roosevelt). The development of a master thesis represents the final stretch in the completion of an academic course. During my studies at the Faculty of Applied Sciences of the University of Liège, I was surprised to discover the beautiful spirit of mutual supportiveness not only among fellow students but also with the teachers of the faculty. Without a doubt, I will enter the professional world with this same state of mind that has accompanied me throughout my studies.

A little particular wink in the native language (italian) of my external promoter, his team of PhD students from the BEAMS unit of the ULB, the company Adler Ortho and the surgeon Gianluca Castellarin (Italy) who gave me their help in the realization of this thesis.

Al termine della mia formazione, vorrei ringraziare in particolare il mio promotore esterno, Bernardo Innocenti, professore di Biomeccanica presso il dipartimento BEAMS dell'Università Libre de Bruxelles, il quale a gentilmente diretto questo lavoro, realizzando diverse revisioni con particolare attenzione . La sua disponibilità e il suo supporto mi hanno reso molto nella realizzazione di questo lavoro. Desidero esprimere i miei ringraziamenti alla supervisione della mia facoltà e in particolare al mio relatore di tesi Professor Davide Ruffoni, Responsabile del Laboratorio di Meccanica dei Materiali Biologici e Bioispirati, Dipartimento di Ingegneria Aerospaziale e Meccanica che durante lo sviluppo della mia tesi mi ha dato i suoi preziosi consigli e incoraggiamento. I miei ringraziamenti vanno anche a Silvia Pianingiani e Carlo Dottino dell'azienda italiana Adler Ortho, che mi hanno gentilmente fornito i dati di modellazione con cui ho potuto iniziare e sviluppare la mia tesi. I consigli della Silvia su come usarli sono stati preziosi. Ringrazio inoltre il dottor Gianluca Castellarin, chirurgo specialista in ortopedia e traumatologia, responsabile della seconda unità funzionale di ortopedia dell'ospedale di Suzzara di Mantova (Italia), operante anche presso l'ospedale privato "Villa Laura" di Bologna (Italia), che ha condiviso con me la sua conoscenza in termini di analisi riguardante la scelta di una protesi che possa soddisfare al meglio le aspettative dei pazienti. Vorrei anche ringraziare la team di dottorandi che mi hanno accolto e mi ha fatto sentire parte della loro squadra. Sono trascorsi sei mesi alla velocità della luce dove ho potuto apprezzare particolarmente la loro professionalità e il buonumore con cui hanno condiviso le loro conoscenze specifiche per rispondere alle mie domande! Rivolgo quindi questi ringraziamenti a Edoardo e Nicola.

My thanks also go to my precious friends who have given me their support, help and encouragement: Donna and Laura Pereira Barbon, Michaël Stappers, Gaelle Idczak, and especially Martin Purnode. Finally, I would like to thank my parents for their patience, and their incredible support and encouragement during all these years, but especially in the last 6 months. They made themselves available to drive me to the BEAMS department on the mornings and to pick me up in the evenings to ensure that I could realize this thesis in the best possible conditions.

Contents

List of Figures

List of Tables

Nomenclature

Latin Symbol

E	Young Modulus, $[MPa]$
F	Force, $[N]$
G	Shear Modulus, $[MPa]$
VM	Von Mises (stress), $[MPa]$

Greek symbol

α	Expansion coefficient, [-]
ε	Pre-strain of the ligament, [-]
ν	Poisson Ratio, [-]

Subscript

h	Horizontal
v	Vertical

Abreviation

A	Anterior
$AAOS$	American Academy of Orthopedic Surgeons
ACL	Anterior Cruciate Ligament
$aMCL$	Anterior Medial Collateral Ligament
BC	Boundary Conditions
$BEAMS$	Bio Electro And Mechanical Systems
CCK	Constrained Condylar Knee
$CoCr$	Cobalt-Chromium
CR	Crutiate Retaining
$dMCL$	Deep Medial Collateral Ligament

FB	Fixed Bearing
FM	Femoral Mechanical Axis
HKA	Hip-Knee Ankle angle
L	Lateral
LCL	Lateral Collateral Ligament
LBA	Load Bearing Axis
M	Medial
MCL	Medial Collateral Ligament
MB	Mobile Bearing
P	Posterior
PCL	Posterior Cruciate Ligament
$pMCL$	Posterior Medial Collateral Ligament
PS	Posterior Stabilized
RP	Reference point
$sMCL$	Superficial Medial Collateral Ligament
TKA	Total Knee Arthroplasty
TKR	Total Knee Replacement
TM	Tibial Mechanical Axis
$UHMWPE$	Ultra-High-Molecular-Weight Polyethylene
ULB	Université Libre de Bruxelles VM
Von Mises	

Chapter 1

Human knee joint

The knee joint is considered as the largest and most complex articulation of the human body, regarding its geometry but also its biomechanical functions. It is a synovial joint connecting four bones: the femur (thigh bone), the tibia (shin bone), the patella (kneecap) and fibula (calf bone). The knee joint is composed of two joints:

- the tibio-femoral joint corresponding to the articulation between the femoral condyles and the tibial condyles;
- the patello-femoral joint corresponding to the articulation between the femoral trochlear groove and the patella.

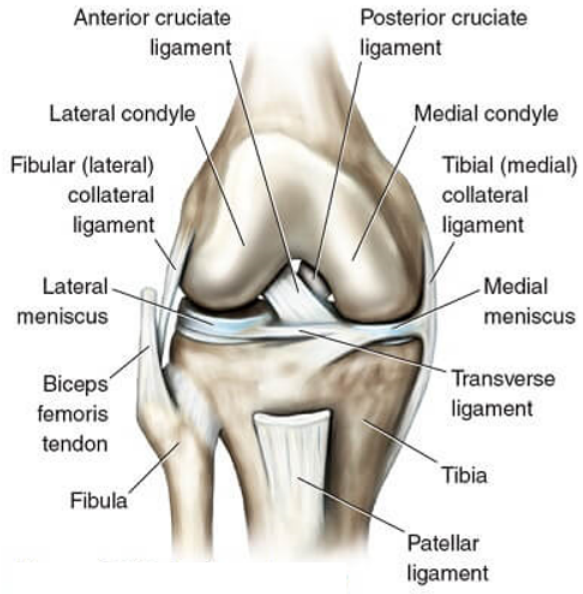

Figure 1.1: Anatomy of the knee joint [1]

1.1 Anatomy of the knee joint

1.1.1 Bones and cartilage

1.1.1.1 Femur

The femur, also known as thigh bone, is the longest, strongest and heaviest bone in the human body, extending from the hip to the knee. This bone articulates proximally with the pelvic bone and distally with the patella and the proximal aspect of the tibia.

The distal extremity of the femur is constituted of two convex areas: the medial and lateral condyles which articulate with the tibia and the patella. Those condyles are separated posteriorly by the intercondylar fossa and connected anteriorly by the femoral trochlear groove. The trochlear groove is a smooth shallow articular depression limited anteriorly by the patellar surface and posteriorly by the intercondylar line. The intercondylar fossa is delimitated by two walls: the medial and lateral ones. The first one corresponds to the lateral surface of the medial condyle while the second one corresponds to the medial surface of the lateral condyle. Each condyle presents a convex eminence, named medial and lateral epicondyles, to which the collateral ligaments are attached [2]. The condyles differ from their shape and location, with the medial one being elliptic with a large posterior offset and the lateral one being spherical with a smaller posterior offset.

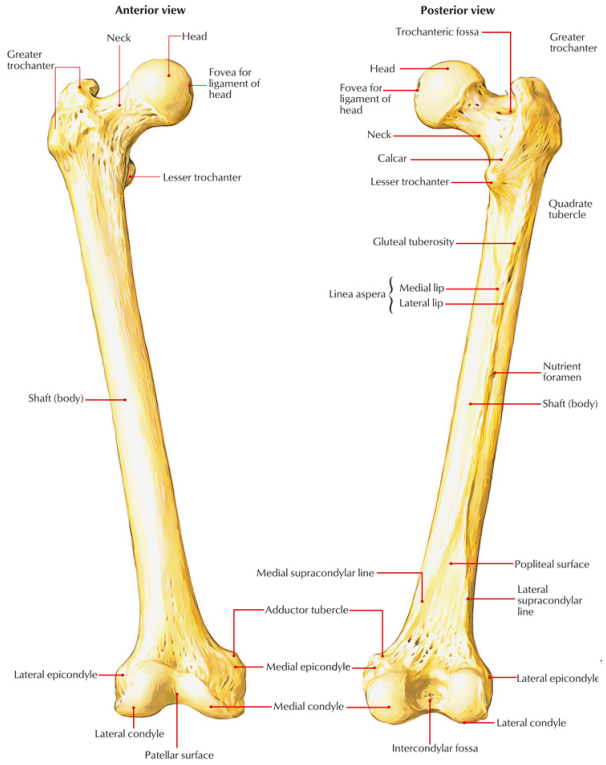

(a) Anterior and posterior view of the femur [3]

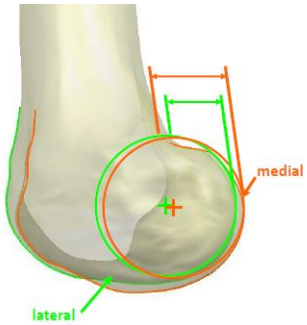

(b) Shape of the femoral condyles [4]

Figure 1.2: Anatomy of the femur

1.1.1.2 Tibia and fibula

There are two long bones located in the lower leg: the tibia and the fibula. The tibia, also called shin bone, is the second largest and strongest bone of the human body. The tibia is found on the medial side of the leg and extends from the knee joint to the ankle. The proximal extremity of the tibia is composed of two plateaus, the medial and lateral tibial condyles, constituting the distal articular surface of the knee joint.

Those condyles are separated by the intercondylar eminence consisting in a roughened area and two bony spines (medial and lateral) which serves as the attachment point for the cruciate ligaments and the menisci. During knee extension, the intercondylar eminence of the tibia slides in the intercondylar fossa of the femur, helping to prevent rotation. In the medio-lateral direction, both tibial plateaus are concave whereas in the antero-posterior direction, only the medial one is concave, the lateral one being convex. This asymmetry increases the mobility of the knee joint in the lateral side. Moreover, the medial plateau presents a larger and thicker articular surface compared to the lateral one. On the lateral side of the tibia is located the fibula, connected to the tibia in the proximal and distal extremity [5].

The fibula is smaller and much thinner than the tibia making the tibia the main weight-bearing bone of the two. The fibula represents an important attachment site for muscles. Those two bones work together to stabilize the ankle and provide support to the muscles of the lower leg.

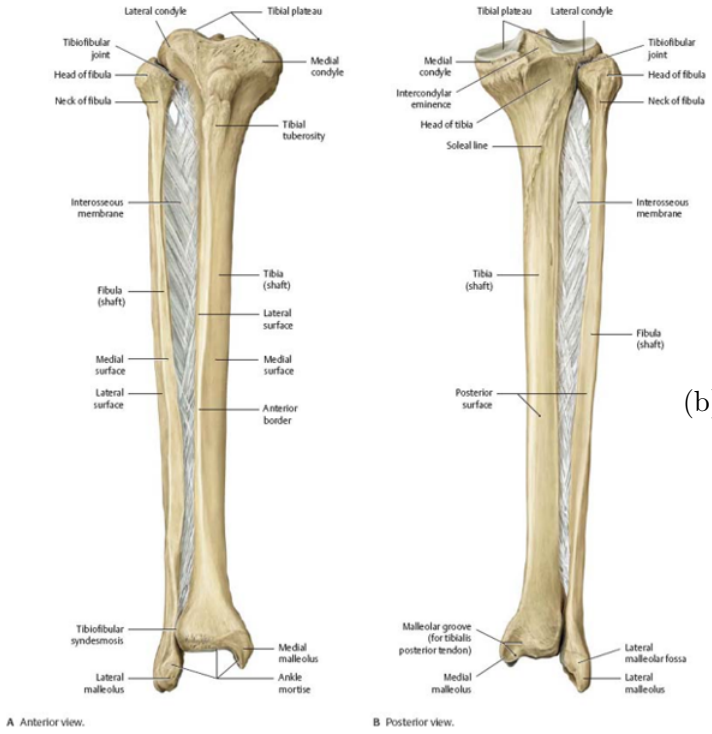

(a) Anterior and posterior view of the tibia [6]

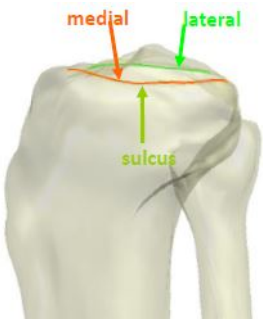

(b) Medial and lateral tibial plateaus - medial view [4]

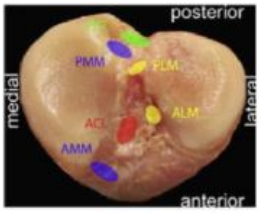

(c) Medial and lateral tibial plateaus - superior view [4]

Figure 1.3: Anatomy of the tibia

1.1.1.3 Patella

The patella, most commonly referred to as the kneecap, is a triangular-shaped bone articulating with the patellar surface of the distal femur and located in the intercondylar notch [2]. The apex of the patella points downward towards the tibia while the base of the bone sits upward towards

the femur. The patella is embedded in the tendon of the quadriceps femoris at its base and in the patellar tendon at its apex. The patellar tendon originates from the apex of the patella and connects to the front of the tibia whereas the quadriceps tendon originates from the base and connects to the quadriceps muscles. The posterior surface of the patella is divided into its medial and lateral facets articulating respectively with the medial and lateral femoral condyles [7]. The patella is allowed to slide up and down in the patellar groove during the knee flexion and extension.

The main functions of the patella are the followings [8]:

- increasing the leverage that the quadriceps tendon can exert on the femur and therefore increase the efficiency of the muscle during the knee extension;
- offering protection to the anterior aspect of the knee joint against trauma or to the quadriceps tendon from tear or wear caused by daily activities such as walking.

The articular surfaces of the femur, tibia and fibula are covered with articular cartilage which enables smooth and almost frictionless movements and provides shock absorption.

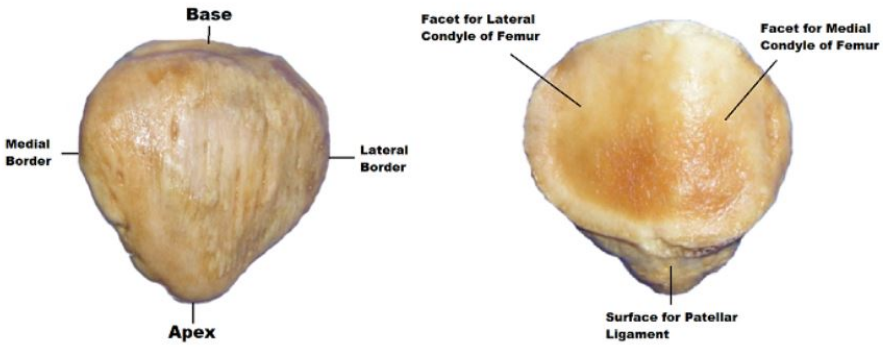

Figure 1.4: Anatomy of the patella [9]

1.1.2 Soft tissues

1.1.2.1 Menisci

The knee joint contains two menisci (medial and lateral), both made of fibrocartilage material. Those menisci consist in a pair of wedge-shaped semi-lunar cartilage and are situated between the corresponding femoral condyle and tibial plateau. The lateral meniscus is smaller and thinner but is more mobile than its medial counterpart. However, the lateral meniscus covers a larger portion of the tibial plateau compared to the medial one.

The presence of the menisci is crucial to ensure the functioning of a normal healthy knee joint. The functions ensured by the menisci include load bearing, load transmission, shock absorption, lubrication, nutrition of the articular cartilage, as well as joint stability.

The menisci reduce the incongruency between the spherical-shaped femoral condyles and the flat tibial plateaus, presenting a concave upper surface in contact with the femoral condyles and a flat lower surface in contact with the tibial plateaus. The increase of the congruency allows to extend the contact area at the tibio-femoral joint and reduce the stresses acting on the tibial cartilage. Thanks to this configuration, the menisci act as shock absorbers as the weight is spread out across a larger surface and protect the articular cartilage from excessive forces. The menisci also serve as joint lubricant reducing the friction between the two articular surfaces. Moreover, the menisci distribute the load more evenly from the femur to the tibia and stabilize the knee joint by preventing the sliding of the femur with respect to the tibia [10], [11].

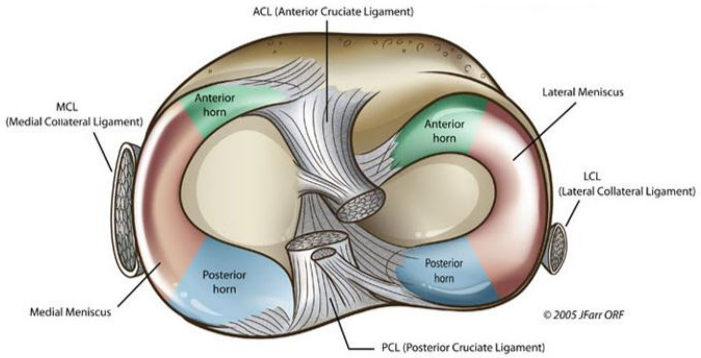

Figure 1.5: Menisci - superior view [12]

1.1.2.2 Ligaments and tendons

The ligaments involved in the tibio-femoral joint are the cruciate ligaments (anterior and posterior) and the collateral ligaments (medial and lateral) while the ones involved in the patello-femoral joint are the medial patella-femoral ligament and the lateral retinaculum. The collateral ligaments are found on both medial and lateral sides of the knee joint and provide medio-lateral stability prohibiting the knee from moving side to side. There are two collateral ligaments: the medial collateral ligament (MCL) located on the medial side of the knee and the lateral collateral ligament (LCL) located on the lateral side of the knee [13], [14].

The lateral collateral ligament originates from the lateral epicondyle of the femur and attaches on the head of the fibula. The LCL is shorter than the MCL making it less prone to injuries. The main function of the LCL is to stabilize the lateral side of the knee by resisting to varus forces (coming from the medial to the lateral side) and avoid excessive postero-lateral rotation of the tibia relative to the femur. When the cruciate ligaments are torn, the LCL acts a secondary restraint to the anterior and posterior tibial translation [15].

The medial collateral ligament contains two portions: the superficial (sMCL) and the deep one (dMCL). The MCL originates from the medial epicondyle of the femur and inserts into the posterior medial surface of the proximal tibia. The MCL stabilizes the medial side of the knee by resisting to valgus forces (coming from the lateral to medial side) through all degrees of knee flexion and extension. The MCL also acts as a secondary restraint to the anterior tibial translation of the tibia on the femur when the first restraint, the anterior cruciate ligament (ACL), is injured [16].

There are two cruciate ligaments: the anterior cruciate ligament (ACL) and the posterior cruciate ligament (PCL) located inside the knee joint, in the intercondylar region. Those ligaments ensure the anterior-posterior stability of the knee joint. The anterior cruciate ligament is attached to the posterior aspect of the medial surface of the lateral femoral condyle. From its femoral attachment, it runs inferiorly, medially and anteriorly and attaches the tibia in a fossa in front of and lateral to the anterior spine. The ACL provides 85% of the restraining force to anterior translation during the knee flexion preventing excessive anterior sliding of the tibia relative to the femur. The ACL also resists to varus and valgus stresses and prevents internal rotation of the tibia [17]. The PCL attaches to the posterior part of the lateral surface of the medial condyle of the femur and inserts distally on the posterior surface of the tibia. The main functions of the PCL are to prevent the posterior displacement of the tibia relative to the femur (sliding backwards) and the tibial external rotation. Both cruciate ligaments work together to lock the knee when it is fully extended [18].

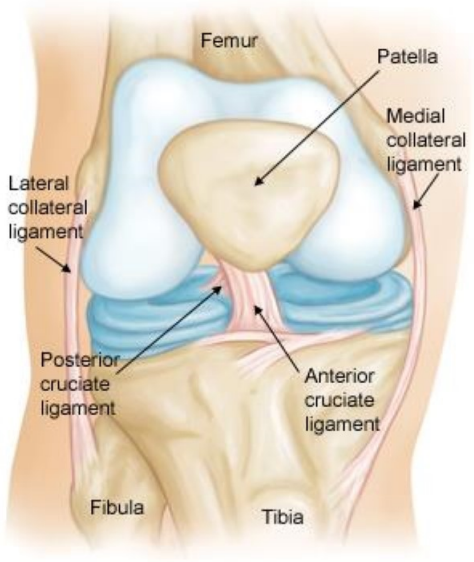

Figure 1.6: Knee joint ligaments [19]

1.1.2.3 Muscles

The two groups of muscles acting on the knee joint are the knee extensors (quadriceps femoris) and flexors (hamstrings).

The quadriceps femoris is the strongest muscle in the human body and extends along the anterior compartment of the femur. This muscle is composed of four individual muscles: vastus medialis (on the medial side of the femur), vastus lateralis (on the lateral side of the femur), vastus intermedius (in between the vastus lateralis and medialis), and rectus femoris (in the middle of the femur). Those muscles differ from their origin, with the rectus arising from the anterior inferior iliac spine and the upper part of the acetabulum at the ilium while the others arise from the surface of the femur. Out of all four muscles, the rectus femoris is the only bi-articular muscle crossing both hip and knee joints. Those four muscles join each other above the patella forming the quadriceps femoris tendon, connecting the quadriceps muscle to the patella. The patella is attached to the tibia through the patellar tendon which begins where the quadriceps tendon ends [20], [21]. The contraction of this group of muscles allows the extension of the leg at the knee joint. As the rectus femoris attaches the ilium, it also allows the flexion of the leg at the hip joint. Those muscles have therefore a crucial role in activities such as walking, running and jumping.

The hamstrings constitute a group of three muscles extending along the posterior surface of the femur. It comprises the semitendinosus and semimembranosus (both located at the medial part of the thigh with the semimembranosus being the most medial one) and the biceps femoris. The biceps femoris occupies the lateral region at the back of the thigh and includes a long and short head. All three muscles proximally attach at the ischial tuberosity but differ in their distal attachment. The semitendinosus inserts at the pes anserine (an area of the tibia near the tibial tuberosity), the semimembranosus attaches to the posterior part of the medial condyle of the tibia while the biceps femoris attaches to the fibula head. The main function of those muscles is to flex the knee and extend the hip. When the knee is in flexion, the semitendinosus and semimembranosus also control the internal rotation of the knee while the biceps femoris controls the external one [22], [23].

(a) Quadriceps muscles [24]

(b) Hamstring muscles [25]

Figure 1.7: Knee muscles

1.2 Kinematics of an healthy knee

The complex knee kinematics can be described through six degrees of freedom, with 3 translations and 3 rotations. The three translations and rotations are:

- medial/lateral translation and flexion/extension occurring respectively along and about the epicondylar femoral axis;
- proximal/distal translation (or superior/inferior translation) and internal/external rotation (or axial rotation) occurring respectively along and about the long tibial axis;
- anterior/posterior translation and varus/valgus rotation occurring respectively along and about a floating axis perpendicular to the tibia mechanical axis.

The primary motion of the tibio-femoral joint is the flexion/extension. Full-extension of the knee (0° of flexion) corresponds to the configuration in which the femoral and tibial axes are aligned in the sagittal plane. The knee can flex up to 130° in the case of an active flexion and up to 160° in the case of a passive flexion. Negative flexion, known as hyper-extension can occur up to -5° of flexion for some individuals. During the last 30° of knee extension, the tibia externally rotates up to 20° while during the first 30° of flexion, the tibia internally rotates up to 20°. This slight rotation is due to the anatomical difference between the articular surfaces of the femoral condyles, with the medial femoral condyle being longer than the lateral one, and must occur to achieve the full-extension of the knee. Moreover, it is responsible for the tightening of the ligamentous structures that lock the knee, assuring maximal stability. This kinematic phenomenon is known as the "screw-home" mechanism [26], [27], [28].

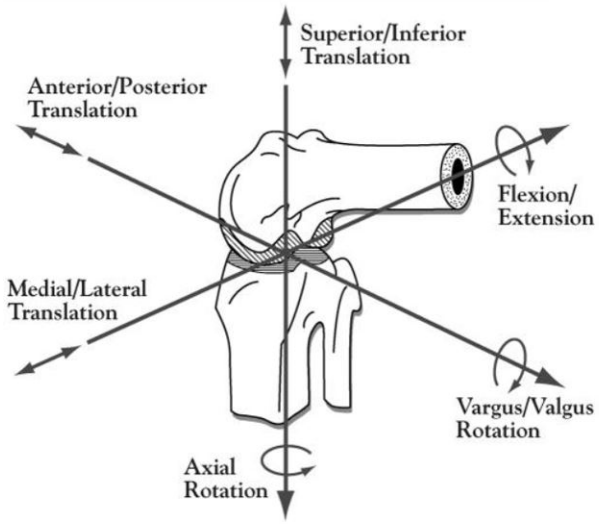

Figure 1.8: The six degrees of freedom of the knee - translations and rotations [29]

1.3 Alignment of the lower limb

The accurate alignment of the lower limbs is determined by the orientation of an anatomical or mechanical axis of the tibia and the femur. The mechanical axis of the leg (or load-bearing axis) corresponds to the line extending from the center of the femoral head to the center of the ankle joint. The anatomical axis of the femur and the tibia coincides with the mid-diaphyseal line of each bone. An angle of 6° is formed between the mechanical and anatomical axis of the femur whereas the mechanical and anatomical axis of the tibia coincide. A healthy knee is in a neutrally aligned configuration in which the mechanical axis of the femur and the tibia form an angle of 180° [30], [31], [32].

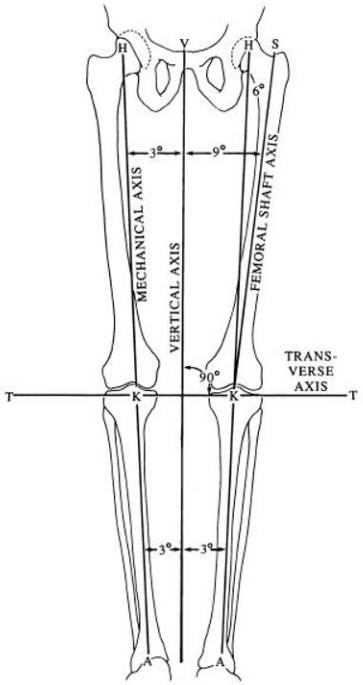

Figure 1.9: Alignment of the lower limb - anatomical and mechanical axes [33]

1.4 Malalignment of knee joint

If the center of the knee joint is shifted laterally or medially with respect to the load-bearing axis of the knee, this indicates either a varus or valgus malalignment. The valgus deformity is therefore a condition in which the distal part of the tibia is turned outward in relation to the femur resulting in a knock-kneed appearance. In opposition, the varus deformity exhibits a bowlegged with the tibia turned inward with respect to the femur. Both deformities increase the risk of developing osteoarthritis. The anatomical restoration of the femoral and tibial alignment is therefore important to achieve an optimal functioning of the knee [34], [35], [36].

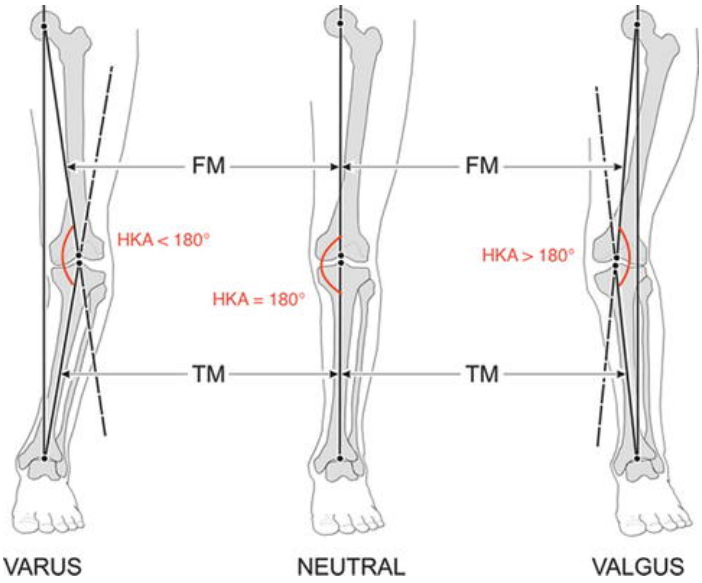

Figure 1.10: Varus, Neutral and Valgus alignment of the lower limbs with LBA=Load Bearing Axis, TM=Tibial Mechanical Axis, FM=Femoral Mechanical Axis, HKA= Hip-Knee-Ankle angle [37].

Chapter 2

Total knee arthroplasty

Total knee arthroplasty (TKA), also known as total knee replacement (TKR) is a surgical procedure replacing the articular surfaces of the knee joint with prosthetic components. TKA helps to return to a normal knee biomechanics, reducing the pain and improving the knee mobility [38], [39], [40]. This procedure is indicated for patients suffering from conditions leading to the deterioration of the knee joint. One of the most common pathological cause of TKA is arthritis comprising mainly osteoarthritis, rheumatoid arthritis and post-traumatic arthritis. TKA is also practiced to correct severe knee deformities (such as varus and valgus) and repair knee injuries [38]. Osteoarthritis is a condition in which the joint cartilage degrades progressively with time, faster than the body's ability to repair it [41]. Rheumatoid arthritis is an autoimmune disorder in which the immune system doesn't recognize the body tissues and attacks them by mistake. The lining of the joints becomes inflamed, causing the synovial membrane surrounding the joints to swell and resulting in joint deformity, bone erosion and loss of function [42]. Post-traumatic arthritis is a form of cartilage degeneration resulting from sudden injury fractures, meniscal or knee ligaments' tear. Those conditions all lead to the degradation of the articular surfaces causing the underlying bones to rub against each other. This bone-to bone contact is painful and limits significatively the mobility of the patient. When non-surgical treatments such as anti-inflammatory medications and knee injections are no longer sufficient to improve the patient's condition, total knee replacement should be considered[43].

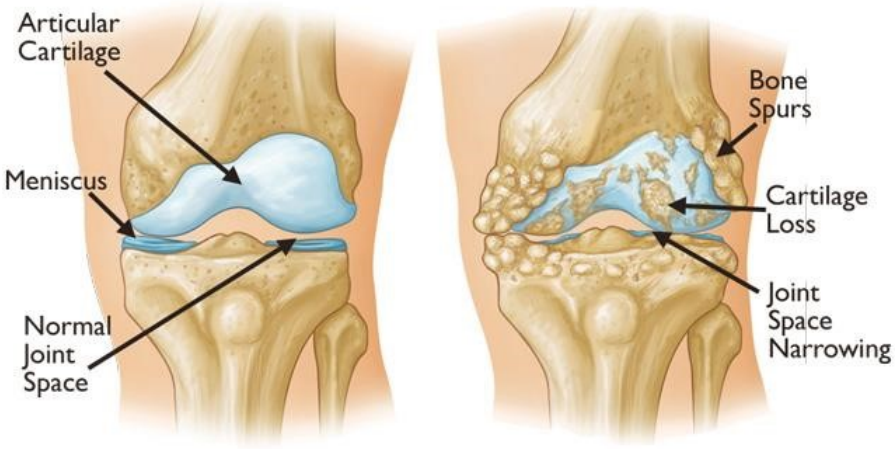

Figure 2.1: Healthy knee and arthritic knee [44]

2.0.1 TKA components

The knee prosthesis is made up of four components [43], [45], [46]:

- the femoral component usually made of metal, most commonly cobalt-chrome;
- the patellar component usually made of polyethylene;
- the tibial insert typically made of high-density polyethylene;
- the tibial component made of metal, either cobalt-chrome or titanium alloy.

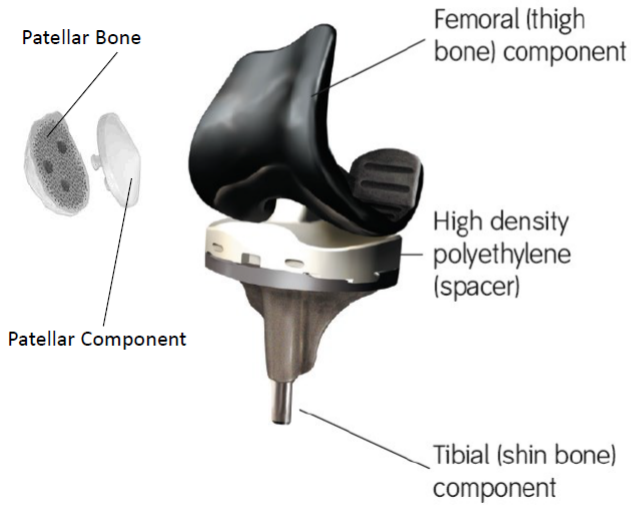

Figure 2.2: TKA components [47]

2.0.2 Mechanical and kinematic alignment

The alignment refers to the axis following which the cut is realized for the TKA. A mechanical alignment is achieved when the tibia is cut perpendicularly to the mechanical axis of the bones. A kinematic alignment is achieved when the tibial cut is realized following the joint line (with an angle of 3°). In the first case, the cut bone thickness varies along the cutting axis whereas in the second case, the cut bone thickness is constant.

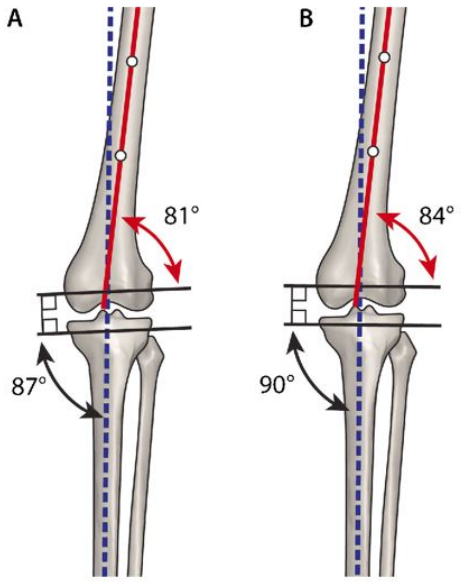

Figure 2.3: A: Kinematic alignment - B: Mechanical alignment during TKA [48]

2.0.3 TKA designs

2.0.3.1 Cruciate retaining knee

If the posterior cruciate ligament is healthy enough to continue stabilizing the knee, the surgeon will retain it when implanting the prosthesis and only remove the anterior cruciate ligament. A groove is present in the posterior aspect of the tibial components for the native PCL. Those prostheses are categorized as non-constrained implants as the femoral and tibial components are not linked together and rely on the patient's ligaments to ensure the stability of the knee [46], [45], [49], [50].

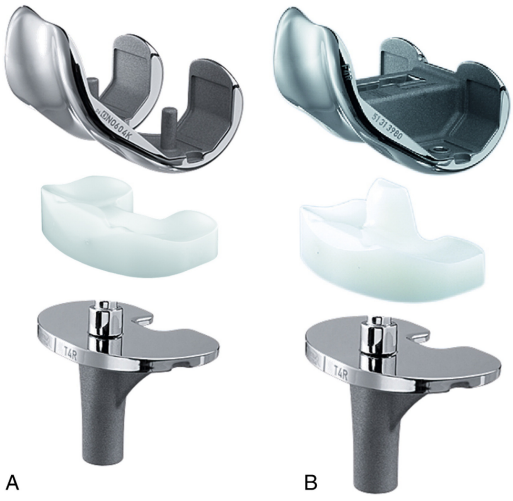

Figure 2.4: A: Cruciate retaining knee - B: Posterior stabilized knee [51]

There are several advantages in using the CR knee over the PS [52]:

- The CR knee preserves femoral bone as it doesn't require to cut a groove on the distal femur to accommodate to the tibial post. The depth of resected distal femoral bone typically matches the thickness of the femoral implant.
- The motion obtained while preserving the posterior cruciate ligament is closer to the normal knee kinematics.
- The CR design increases proprioception of the motion by the patient.

There are also disadvantages associated with the use of the CR knee [52]:

- Appropriate soft tissue balancing is more challenging in the case of a CR knee as the PCL tension should be considered when balancing the flexion and extension gaps. It is even more difficult with larger knee deformities (with varus lower than 10° or valgus higher than 15°) because the varus or valgus ligamentous imbalance should first be corrected.
- The CR knee stability relies on the integrity of the PCL. The rupture of the PCL or its attenuation (being over laxed or excessively thigh) leads to the knee instability.

2.0.3.2 Posterior stabilized knee

When the surgeon considers that the cruciate ligaments are too weak to ensure the knee stability, those ligaments are removed and substituted by a post-cam system incorporated in the implant. The tibial component has a raised surface with an internal post that articulates with a rectangular box-like opening (cam) between the condyles of the femoral component. This mechanism supports the posterior movement of the femur, known as the femoral rollback, which is essential to achieve deep knee flexion and prevents the anterior translation of the femur on the tibia during knee flexion. Those prostheses are classified as semi-constrained as they rely on the post-cam system to ensure the stability of the knee [46], [45], [49].

Figure 2.5: Posterior stabilized knee [53]

The use of the PS design has some advantages [54]:

- The PS knee is often easier to balance as it doesn't rely on abnormal PCL morphology and function.
- It allows the reliable restoration of the knee kinematics.

- It provides small improvements in the range of motion compared to CR knees with a difference in the maximal flexion angle up to 8 °.
- It reduces the polyethylene wear as the surface of the polyethylene component better matches the radius of curvature of the femoral component, increasing the area of contact and decreasing the stress to which the polyethylene is subjected.
- It avoids the possible post-operative rupture of the PCL as it can occur with the use of CR knees.

However, the use of the PS knee presents some disadvantages[54]:

- A tibio-femoral dislocation might occur when there is a significant flexion-extension gap mismatch. Indeed, the post "jumps" over the cam when the flexion gap is larger than the extension one due to PCL resection. The dislocation occurrence is very rare as the surgeon performs a larger distal femoral cut to balance the extension gap.
- The friction between the prosthesis' components could cause polyethylene wear and a breakage at the post-cam interface can occur.
- The use of this implant leads to excessive bone resection. Indeed, the PS design requires an additional bone removal from the distal femur, the "box cut", to accommodate to the tibial post.

2.0.3.3 Constrained implants

The constrained condylar knee (CCK) is a constrained prosthesis based on a post-cam sytem comparable to the one found in the posterior stabilized designs but presenting a larger post. In this type of prosthesis, the femoral and tibial components are not linked together, allowing a smaller range of motion compared to the posterior stabilized knee.

The most constrained type of prostheses are the hinged prostheses. In those implants, the femoral and tibial components are linked together with a hinged mechanism. The hinge is either fixed or allowing some degrees of internal/external rotation. Those prostheses are reserved for seriously damaged knees and are rarely the first-choice option. They are most commonly used for revision surgery to improve the stability of the knee joint providing a more constrained articulation. However, they can also be used in primary knee arthroplasty if the knee presents a significant instability.

They are used in the case of:

- severe deformities associated with knee arthritis;
- collateral ligament deficiency which would be unable to support any other type of prosthesis;
- inadequate bone support;
- and TKA trauma.

They are usually coupled with stems (cemented or cementless) to transfer the load to the intramedullary canal and augments or wedge to cover the bone defect. However, in the case of revision surgery, the stems are difficult to remove, especially when cemented. In addition, the surgical time is significantly higher as the stems have to be positioned correctly otherwise a diaphyseal fracture can occur. Due to their high level of constraint, the hinged prostheses are mostly destined to elderly patients being less physically active than younger ones. Besides, as they subjected to higher mechanical stress they are not expected to last as long as other less-constrained designs [55], [56].

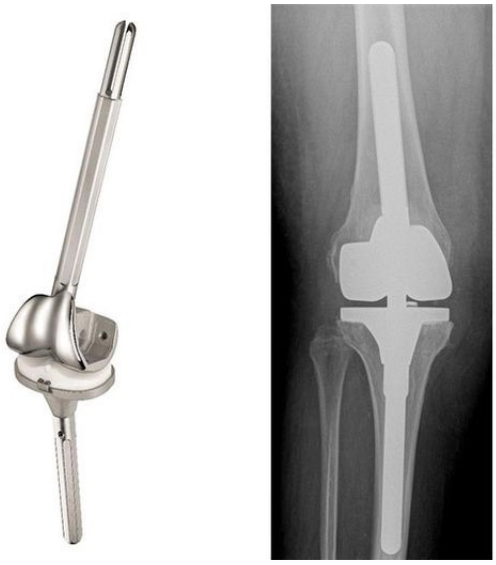

Figure 2.6: Hinged prosthesis model and radiography of the implanted hinged prosthesis [57]

2.0.3.4 Tibial ultracongruent insert

Some mobile bearing devices contain an ultracongruent insert enabling to stabilize the knee joint even with PCL deficiency. Those inserts are characterized by a high anterior wall and a deep-dished plate. The articulation provided by those inserts is more conforming, ensuring the stability of the knee.

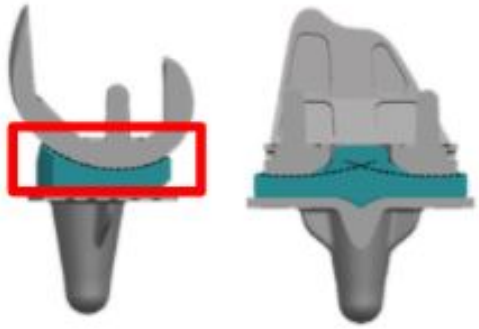

Figure 2.7: Ultracongruent insert - *Smith & Nephew - Adler Ortho - Link Orthopaedic*

2.0.3.5 Fixed bearing implant

In a fixed bearing implant, the tibial insert is fixed firmly to the metal tibial tray. The femoral component then rolls over it. Extreme physical activities and weight gain should be avoided as it could cause the fixed implant to wear down more quickly. The fixed bearing implants are less expensive than the mobile bearing models [46], [58].

2.0.3.6 Mobile bearing implant

In a mobile bearing implant, the tibial insert can rotate upon the tibial component. This type of prosthesis replicates the small rotation occurring in a healthy knee to achieve full-extension or to go from full-extension to flexion, providing a more physiological motion of the implant. Mobile bearing inserts were developed to minimize the wear occurring with the post-cam system. However, this type of implant is not suitable for every patient since it requires more support from the surrounding soft tissues especially the ligaments to avoid the knee dislocation. Moreover, the surgical costs associated with those implants are higher than those of the fixed bearing implants. Those prostheses are recommended for young and more active patients as they have a longer lifetime [46], [58].

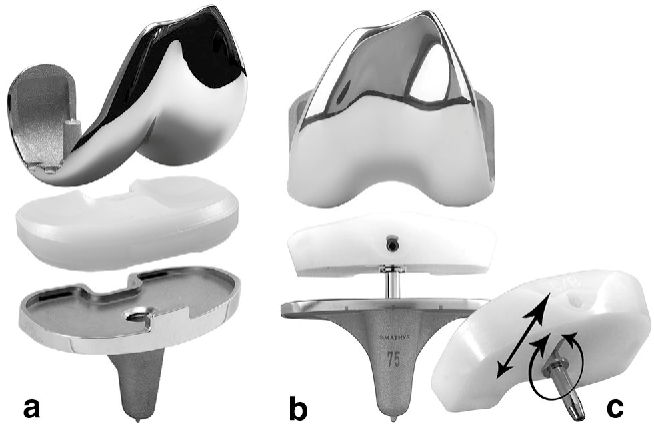

Figure 2.8: Example of - a: fixed-bearing implant - b: mobile-bearing implant [59]

2.0.3.7 Cemented and cementless total knee replacement

Three different types of fixations are used to connect knee implants to the bone [46]:

- cemented fixation in which the insert and the tibial tray are fixed together with a fast-curing bone cement (polymethylmethacrylate);
- cementless fixation where the implants are press-fitted onto bone. Most are designed with a porous surface, textured or coated with hydroxyapatite to promote the growth of the new bone into the surface of the implant;
- hybrid fixation in which the femoral component is inserted without cement while the tibial and patellar components are fixed with a bone cement.

The majority of the knee prostheses are cemented. The main advantage of that technique is that the bone cement dries very quickly providing an immediate fixation between the prosthesis's components and the bone surface. Moreover, cemented implants are highly recommended for old, obese and osteoporosis patients as it provides a better fixation for poor bone quality. This type of fixation also presents some drawbacks. The layer of cement formed between the bone and the implant component may become loose over time. Furthermore, third body wear can be caused by the presence of cement. Due to the friction of the different parts, small particles of cement are released in the body which causes an inflammation reaction as the body tries to remove the debris. This condition is called osteolysis as the inflammatory cells may also dissolve the bone surrounding the prosthesis, leading to the loosening of the implant. In this particular case, a revision surgery is needed. Additionally, the hardening of the cement releases a lot of thermal energy causing thermal necrosis to the surface of the surrounding bone.

The surgery procedure remains the same for both fixations, excepting that in the case of a cementless fixation, the components are press-fitted onto the bones, reducing significantly the surgery time compared to the cemented fixations. Cementless implants also require accurate bone cuts to avoid possible gaps between the prosthetic implant and the bone surface. The ideal candidates for cementless fixation prostheses are young patients as they usually present an excellent bone quality which is essential to have a good cementless fixation. Revision surgery is easier for cementless implants due to the availability of good bone stock but the implants are more difficult to remove [60].

2.0.4 Revision total knee arthroplasty

Total knee arthroplasty is one of the most successful surgical procedure. However, some patients achieve poor results after surgery or the implant may fail over time for many reasons and a revision surgery is required. The revisions in total knee arthroplasty are classified in two categories: early (within two years after the primary TKA) and late revisions. The main causes of TKA are: infection, fracture, implant failure, loosening, osteolysis, wear, instability, restricted range of motion, extensor mechanism insufficiency, allergy and pain [61]. The revision surgery is a longer and more complex surgical procedure than primary TKA as it requires an accurate preoperative planing (new radiographs of the patient's knee), specific prosthetic components, extraction devices and bone graft materials. There are different types of revision surgery depending on the number of prosthetic components that need to be replaced. In the most severe revision cases, all components must be removed and replaced. In order to cover the bone defect, augments/wedge or bone graft (to rebuilt the bone around the knee) could be used if bone cement is not sufficient [62] [63].

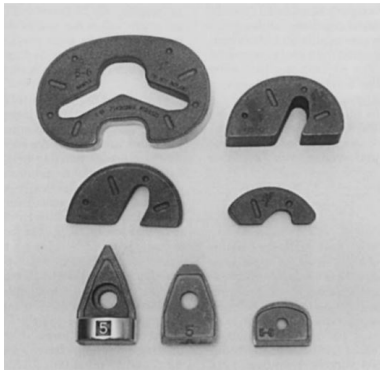

(a) Modular augments [64]

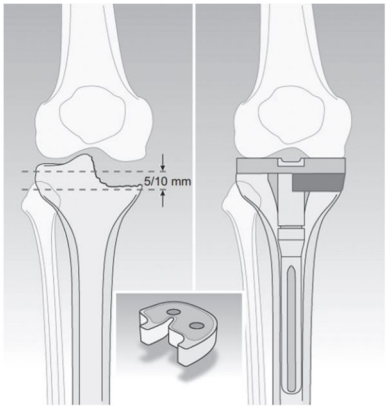

(b) Revision TKA with a wedge [65]

(c) Special implants for revision TKA [65]

Figure 2.9: Revision TKA

Chapter 3

Motivation - aim of the thesis - research question

This study is realized in collaboration with the company *Adler Ortho* and the surgeon *Gianluca Castellarin* who performed a total knee arthroplasty on the studied patient.

The patient suffered from femoral valgus: a condition in which the tibia is turned outward in relation to the femur. The orthopedic surgeon *Gianluca Castellarin* performed a femoral valgus osteotomy to correct the deformity of the femur by putting a blade plate. This one aimed to prevent the progression of the deformity and avoid the possible development of a fracture.

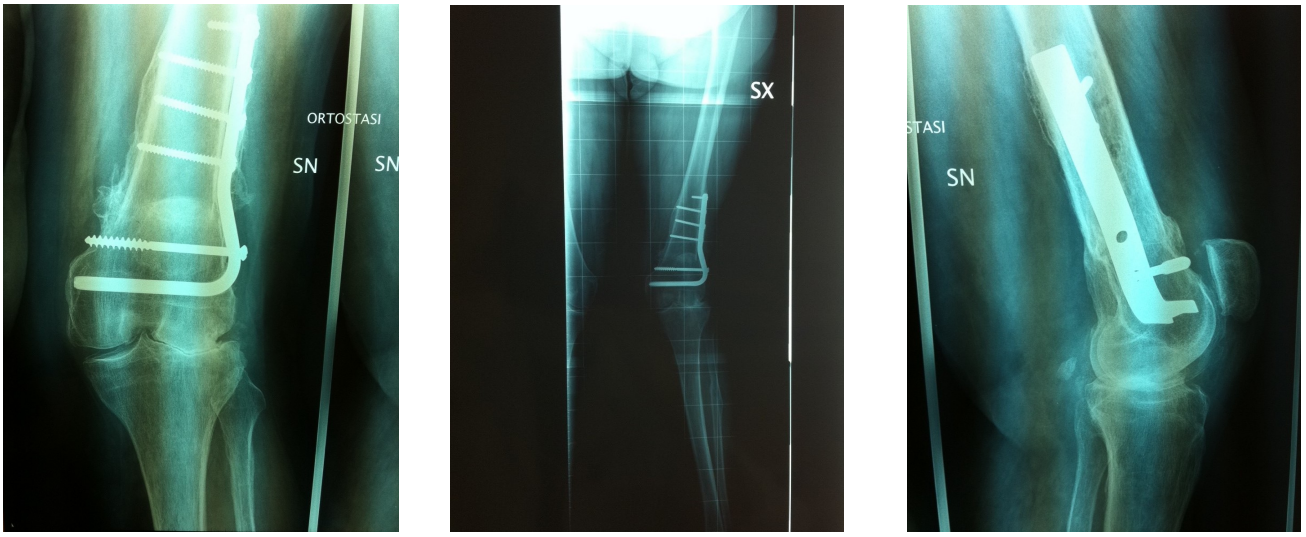

(a) Pre-operative X-rays (A/P view)

(b) Pre-operative X-rays (full leg)

(c) Pre-operative X-rays (lateral view)

Figure 3.1: Patient's pre-operative X-rays. These pictures were obtained in the courtesy of *Gianluca Castellarin*

The patient later suffered from osteoarthritis causing the knee cartilage to degenerate progressively. As it can be seen in the pre-operative X-ray in Figure 3.2, there was no more cartilage in between the femur and the tibia, causing the bones to grind painfully against each other. It was therefore necessary to perform a total knee arthroplasty on the patient. Since the patient was also suffering osteoporosis, removing the blade plate could have caused a bone fracture so the implant had to remain in place.

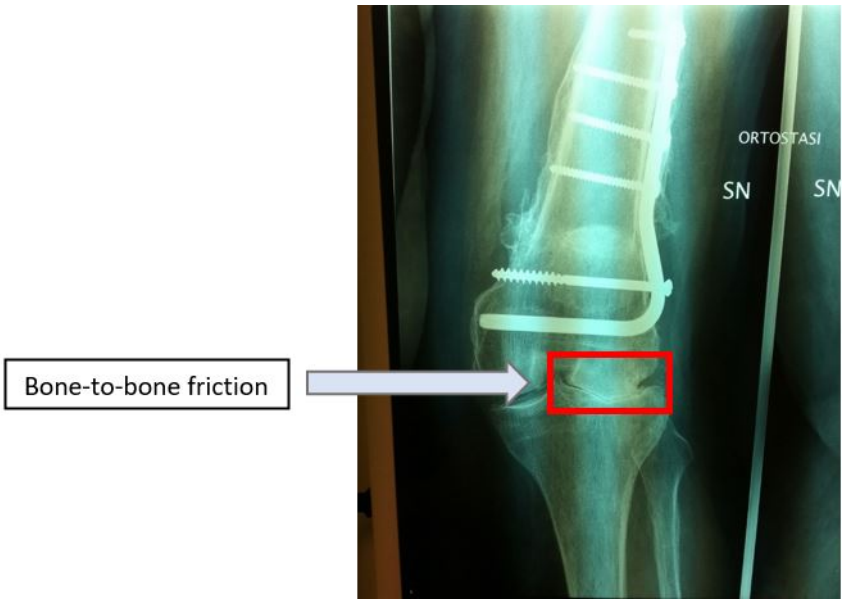

Figure 3.2: Patient's osteoarthritis and cartilage degeneration. This picture was obtained in the courtesy of *Gianluca Castellarin*

The goal of doctor *Gianluca Castellarin* was to preserve as much native soft tissue of the patient as possible, in opposition to the more conservative surgeons afraid of the new techniques. Due to the blade plate put in place, the best option was to implant a mobile bearing cruciate retaining prosthesis. The patient shows excellent results at 9 years post-up follow-up.

The purpose of this thesis is to study the impact of the different levels of constraint in the knee biomechanics of the patient at various loading conditions. This study will allow to approve or invalidate the decision made by the surgeon Gianluca Castellarin in the preservation of the PCL of the patient.

Chapter 4

Assembly

4.1 Geometry

The CAD files of all the prosthesis components (femoral component, tibial insert and tibial tray) were provided by the company Adler Ortho (Cormano, Milano, Italy). The geometry of those components is optimized, using the software `Abaqus`, by removing some design features such as the fillets, the chamfers and the holes in order to ease the meshing of the different parts. The initial geometries of the parts as well as the final geometries obtained for those ones can be found in the Annex (in Figure 10.1, 10.2, 10.3, 10.4, 10.5, 10.6, 10.7, 10.8, 10.9, 10.10).

4.2 Configurations

Four different models of prostheses were studied:

- Mobile bearing cruciate retaining knee with normal insert (MB CR knee);
- Mobile bearing cruciate retaining knee with ultracongruent insert (MB CR ultracongruent knee);
- Fixed bearing constrained condylar knee (FB CCK);
- Fixed bearing posterior stabilized knee (FB PS).

All the components of the prostheses are press-fitted. For the four models, three different configurations were analyzed: full-extension (0° of flexion), 30° of flexion (gait), and 90° of flexion (chair-rise). Those configurations represent the solicitations taken by the knee joint during the most frequent activities of daily life such as walking and sitting. The full-extension configuration represents the standing position. The configuration at 30° of flexion replicates the the maximal knee flexion angle occurring during the stance phase. This is in this configuration that the maximal force is observed in the gait cycle. The chair-rise investigates the sit-to-stand transfer from a chair [66].

4.3 Materials and properties

Linear elastic models were chosen for all the materials involved in this study, in agreement with the previous literature studies [67], [68], [69], [70], [71], [72]. This assumption provides a good approximation of all the mechanical properties to achieve an acceptable quantitative comparison among different configurations.

4.3.1 Prostheses components

The femoral components as well as the tibial components are made of cobalt-chromium alloy (CoCr). The tibial inserts are made of ultra-high-molecular-weight polyethylene (UHMWPE). They are all assumed to be homogeneous and isotropic [70], [67], [69], [73], [74]. The material properties are reported in Table 4.1.

Table 4.1: Material properties of the prostheses' components

Material	**Material model**	**Young's modulus [MPa]**	**Poisson's ratio**
CoCr	Elastic isotropic	240	0.3
UHMWPE	Elastic isotropic	0.7	0.40

4.3.2 Ligaments

For the FB CCK and PS prosthesis, the ligaments incorporated in the models are the lateral collateral ligament (LCL) and the medial collateral ligament (MCL). The medial collateral ligament is modeled in two distinct parts: anterior medial collateral ligaments (aMCL) and posterior medial collateral ligaments (pMCL) according to previous studies [67]. These ligaments were considered isotropic and modeled as beams with a specific cross-section and validated pre-strain [67], [68], [75], [69], [70]. The pre-strain of the ligaments is given by the following formula:

$$\varepsilon = \alpha \Delta t,$$

with ε, α and Δt representing respectively the pre-strain of the ligaments, the expansion coefficient and the variation of temperature. Δt is taken equal to 1.

The material properties of the collateral ligaments are gathered in Table 4.2.

Table 4.2: Material properties of the collateral ligaments

Material	**Material model**	**Density** $[kg/m^3]$	**Young's modulus** [MPa]	**Poisson's ratio** [-]	ε [-]
LCL	Elastic isotropic	310	345	0.45	0.08
MCL	Elastic isotropic	310	332	0.45	0.04

The MB CR prosthesis models (with the normal and the ultracongruent inserts) preserve the posterior cruciate ligament (PCL). This one is modeled as a spring with a stiffness of 350 [N/mm].

4.3.3 Bones

Both the femur and the tibia were modeled considering the cortical as well as the cancellous bone. The cortical bone was considered linear transversely isotropic (with the principal axis corresponding to the mechanical axis of the bone) whereas the cancellous bone was considered linear elastic isotropic [67], [76], [68], [75], [69], [70]. The material properties of the bones are gathered in the Table 4.3.
For the cortical bone, the direction E_3 represents the tibial mechanical axis.

Table 4.3: Material properties of the bones

Material	**Material model**	**Young's modulus** [MPa]	**Poisson's ratio** [-]	**Shear modulus** [MPa]
Cortical bone	Transversely isotropic	$E_1 = 11,500$ $E_2 = 11,500$ $E_3 = 17,000$	$\nu_{23} = 0.31$ $\nu_{13} = 0.31$ $\nu_{12} = 0.58$	$G_{23} = 4,400$ $G_{13} = 4,400$ $G_{12} = 3,800$
Cancellous bone	Elastic isotropic	2,130	0.31	/

4.4 Total models

The total models contain the prosthesis components, the bones (femur and tibia) and the ligaments.

4.4.1 Prosthesis components positioning

The next step consists in assembling the femoral component, the tibial insert as well as the tibial component and specify their relative positions. The positioning is realized following a mechanical alignment of the knee. This one aims to position both femoral and tibial components perpendicular to the mechanical axis of each bone. The software `Abaqus` contains a tool enabling to define position constraints in order to correctly position each component with respect to the others.

The position constraints that are applied on the prostheses' components in the three configurations are listed below.

- For all the models,the femoral distal bone cut surface is constrained to be parallel to the lower surface of the tibial insert. This constraint is only applied to the models in the full-extension configuration.
- For all the models in all the configurations, the lower surface of the tibial insert and the upper surface of the tibial tray are constrained to be "face-to-face".
- For the mobile bearing models, the peg of the mobile bearing (normal and ultracongruent) insert is constrained to be coaxial with the stem of the tibial tray.
- For the fixed bearing CCK model, the cylindrical hole of the insert is constrained to be coaxial with the stem of the tibial tray.

The models of the four assembled prostheses are illustrated in the full-extension configuration in the Figure 4.1.

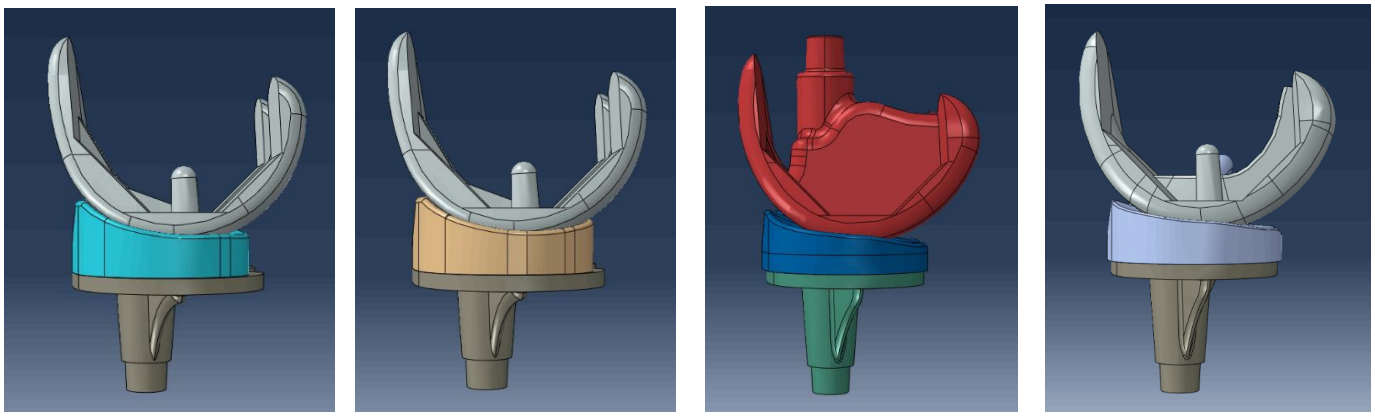

(a) MB CR knee

(b) MB CR ultracongruent knee

(c) FB CCK

(d) FB PS

Figure 4.1: Illustration of the four different models of prosthesis studied in the full-extension configuration

The upper, middle and lower components represent respectively the femoral component, the insert and the tibial tray of each type of knee prosthesis. At this stage, all the components of the TKA prostheses are fixed in place. The bones should therefore be incorporated in the model. Bones cutting and positioning

4.4.1.1 Femur

As the interaction between the femur and the femoral component is not studied, the femur used in the different models has been taken from a previous study [67]. The femoral cut has therefore been realized with respect to the femoral component of the previous study, perpendicularly to the mechanical axis of the femur, following a mechanical alignment technique. The femur model used can be found in the Annex in Figure 10.11. The same femur is used for all the models and consequently, the shape of the cut femur doesn't match any of the studied femoral component. However, since the interaction with the femur is not considered in the study, the femur model doesn't need to be rescaled. The femur has been positioned according to surgical techniques [70].

4.4.1.2 Tibia

In order to assemble the tibia with the tibial component, a tibial cut must be performed as it is realized during the total knee replacement surgical procedure. The tibial model was taken from the same study as the femur model [67], and can be found in the Annex in Figure 10.12. In this study, a resection of the proximal end of the intact tibia has been performed perpendicular (90°) to the mechanical axis of the tibia with a level of about 10 mm based on the less involved condyle. The tibial bone has already been cut into a shape that matches the corresponding surface of the tibial component from this previous study.

A solid extrusion is first applied to the stem of the tibial tray in order to fill the inside of the stem to realize a proper cut in the tibia. A solid extrusion is then applied to the tibial model in order to refill the hole resulting from the previous cut. The tibia is added to the model and correctly

positioned with respect to the tibial tray. In this purpose, three axes are constructed on the tibia, the first one corresponding to the mechanical axis of the tibia and the two other ones corresponding to the medio-lateral and antero-posterior axes, then those axes are aligned with the three axes of the tibial tray. The lower surface of the tibial tray and the upper surface of the tibia are put in contact and the extruded cut is then realized. The cut process is illustrated in the Figure 4.2 for the mobile bearing model and is similar for the other models.

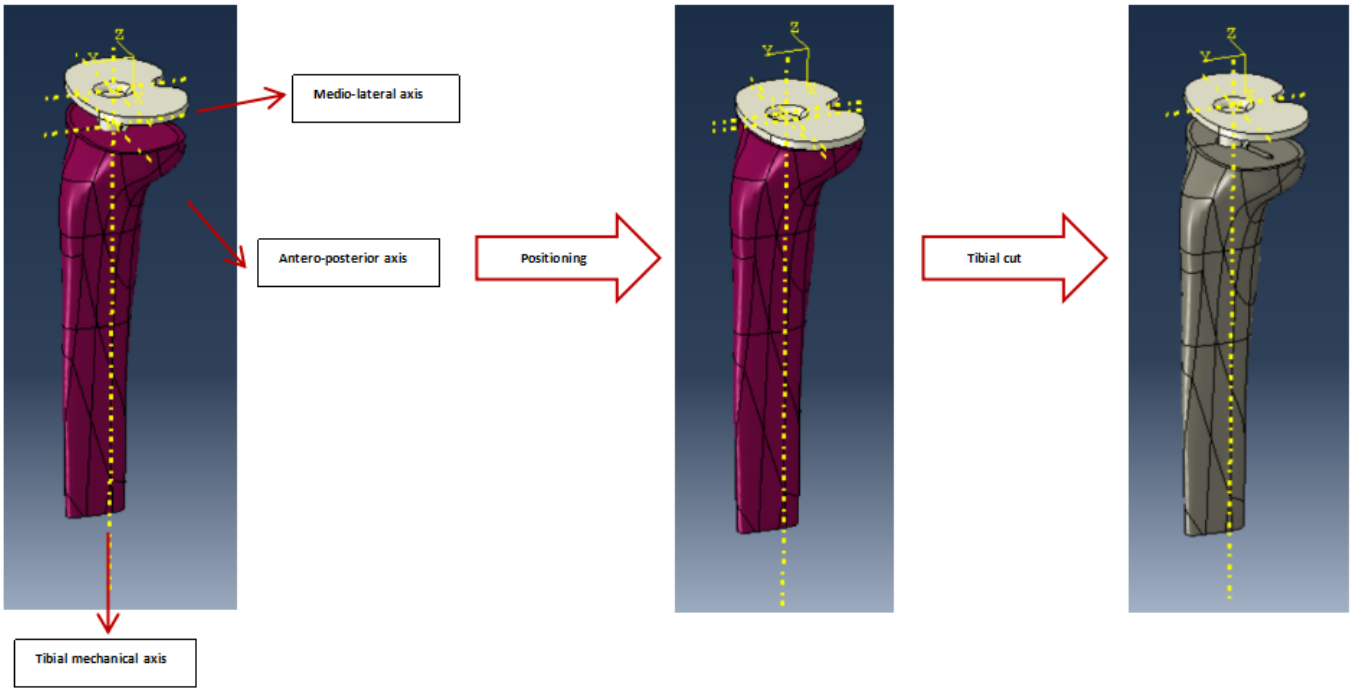

Figure 4.2: Illustration of the tibial cut process

After realizing the tibial cut, some position constraints are applied to the cut tibia in order to position it correctly with respect to the tibial tray.

- The upper surface of the cut tibia and the lower surface of the tibial tray are constrained to be ”face-to-face”.
- The stem of the tibial tray is constrained to be coaxial with the cylindrical axial hole of the cut tibia.

The next step consists in adding the ligaments in the models.

4.4.2 Ligaments positioning

4.4.2.1 Determination of the insertion points of each collateral ligament

The origin and the insertion points of each collateral ligament (lateral collateral ligament, anterior medial collateral ligament and posterior medial collateral ligament) were determined following the

Norm ISO 14243-1:2002 [77]. This norm aims to construct a plane passing through the faces of the femoral component containing the pegs and rotate it respectively at 30° and 60°. Both of the obtained planes are translated to become tangent with the condyles of the femoral component. Then two planes perpendicular respectively to each two previously obtained planes are constructed and those planes are translated up to the tangency point on the condyles. The axis resulting from the intersection of the two last obtained planes is then constructed. The medial and lateral most external point of the condyles are projected on this axis. The projected lateral point corresponds to the insertion point for the lateral collateral ligament. A reference point is created on this point. The obtained medial point is offset of 5mm in the anterior and posterior direction to obtain the insertion points for the anterior and posterior medial collateral ligament. Two reference points are also created on those points.

The base of each collateral ligament is positioned in order to coincide with its corresponding insertion point and then the ligaments are vertically aligned with the mechanical axis of the tibia.

The posterior cruciate ligament is modeled with its origin on the posterior part of lateral surface of the medial femoral condyle and its insertion on the posterior part of the proximal tibia.

4.4.3 Constraints

4.4.3.1 Femur

The surface interaction between the femur and the femoral component is considered rigidly bonded (tied constraint) as the interaction with the femur isn't studied. Indeed, the lower cut surface of the femur and the internal surface of the femoral component are tied together.

A reference point is created on the femur (RP-femur), located 15mm above the upper surface of the femur and aligned with the mechanical axis of the femur. As it can be seen in Figure 4.3, this reference point is constrained (coupling - continuum distributing) to the upper surface of the femur. This is on this reference point that the force as well as the boundary conditions (BC) are applied on the femur.

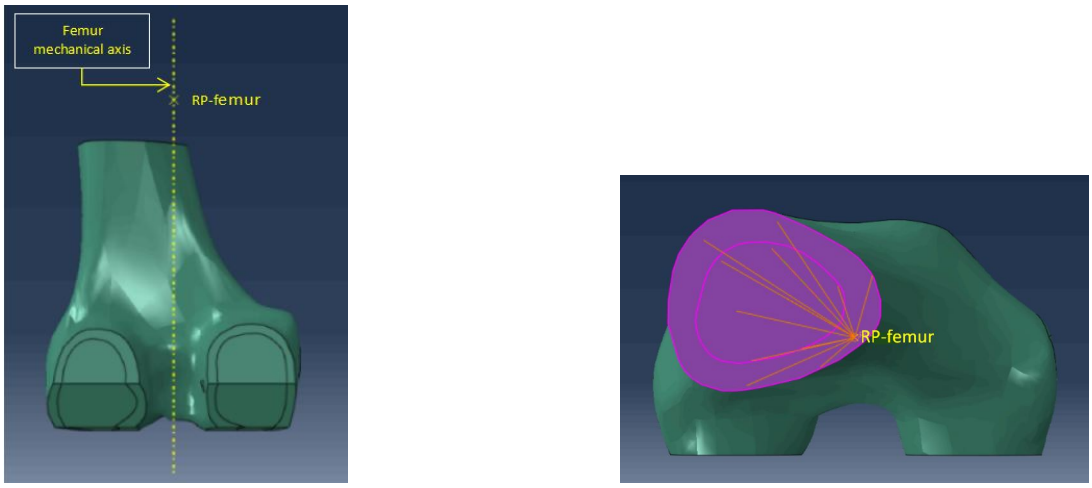

Figure 4.3: Illustration of the reference point and surfaces where the boundary conditions and the loads are applied on the femur

4.4.3.2 Ligaments

For the lateral collateral ligament, a coupling constraint is applied between the lateral epicondyle of the femur and the insertion point of the lateral collateral ligament (RP-lat_ligament). For the medial collateral ligaments, the medial epicondyle surface is divided in two parts: the anterior and posterior one. A coupling constraint is then applied bewteen the insertion point of the anterior medial collateral ligament (RP-ant_ligament) and the anterior surface of the medial epicondyle, and between the insertion point of the posterior medial collateral ligament (RP-post_ ligament) and the posterior surface of the medial epicondyle.

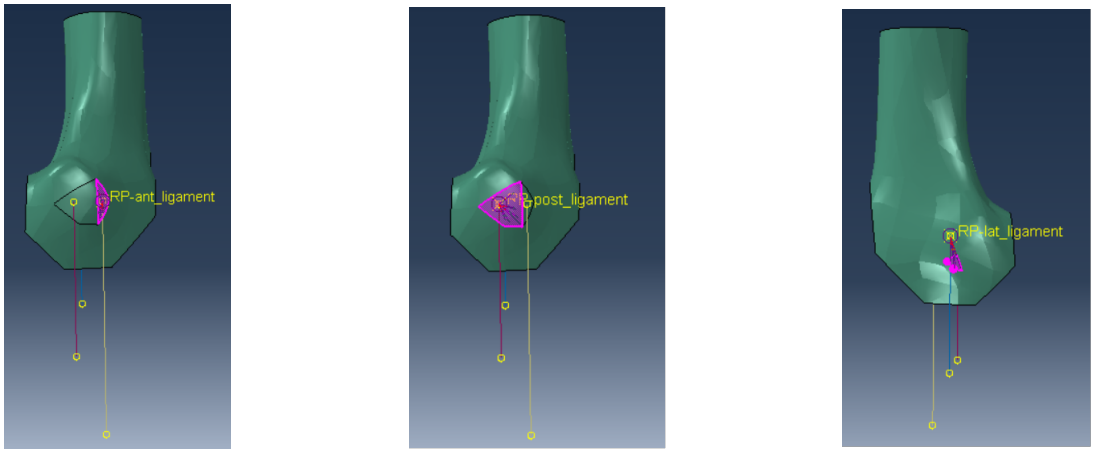

(a) Anterior medial collateral ligament

(b) Posterior medial collateral ligament

(c) Lateral collateral ligament

Figure 4.4: Illustration of the ligament insertion points and coupling epicondyle surfaces

4.4.4 Interactions

According to previous studies, the frictional behavior was modeled using general contact with the penalty function method. A coefficient of friction of 0.04 was considered for the interaction between the femoral component and the tibial insert, between the tibial insert and the tibial component as well as between the tibial component and the tibial bone [70].

4.4.5 Boundary conditions

4.4.5.1 Femur

For the femur, the boundary condition is applied to the reference point of the femur (RP-femur). Any form of rotation or displacement is allowed excepting for the anterior-posterior rotation in order to keep each model in the studied configuration with the appropriate flexion angle.

4.4.5.2 Inserts

For the FB PS and CCK models, the boundary conditions are applied to the lower surface of the insert. This one is allowed to rotate about the anterior-posterior axis and the medio-lateral axis in order to adjust its position with respect to the femoral component during the simulation. The insert can also translate along the longitudinal axis to allow the transmission of the forces and the constraints to the tibia. The surfaces on which the boundary conditions are applied to the FB PS and FB CCK inserts are illustrated respectively in Figure 4.5 and 4.6.

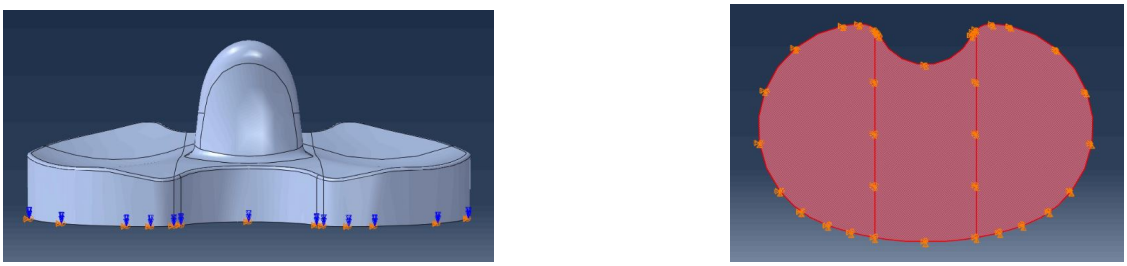

(a) Boundary conditions PS insert

(b) PS insert lower surface BC

Figure 4.5: Illustration of the surface where the boundary conditions are applied to the PS insert

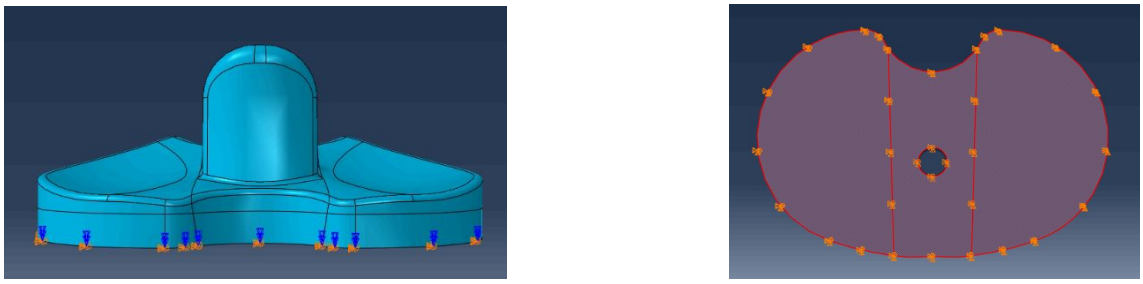

(a) Boundary conditions CCK insert

(b) CCK insert lower surface BC

Figure 4.6: Illustration of the surface where the boundary conditions are applied to the CCK insert

For the mobile bearing models, the boundary condition is applied to a reference point (RP) that coincides with the center of peg of the insert (Figure 4.7a and Figure 4.7b) which is constrained (Coupling - continuum distributing) to the lateral surfaces of the peg. This reference point is only allowed to move along and to rotate about a fixed vertical axis located in the middle of the tibial condyles.

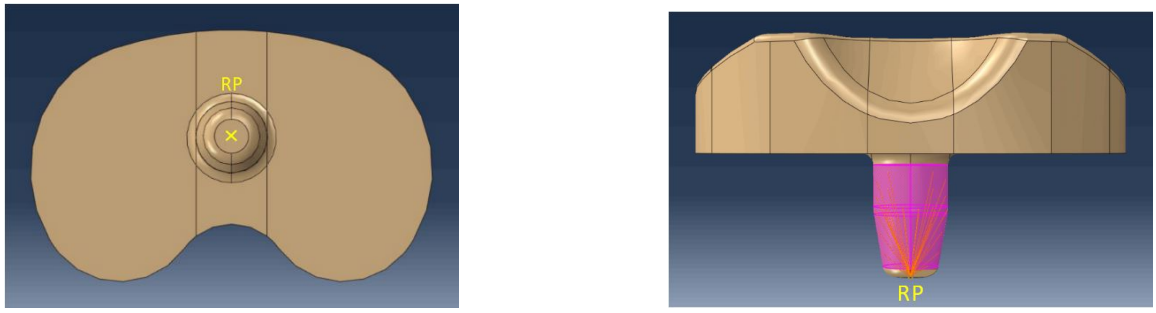

(a) MB CR insert reference point

(b) MB CR insert coupling surfaces

Figure 4.7: Illustration of the reference point and coupling surfaces where the boundary condition is applied for the MB CR normal and ultracongruent insert

In all the studied configurations, the tibia is distally fixed.
The anterior medial collateral ligament, posterior medial collateral ligament and the lateral collateral ligament are all distally fixed at their end.

4.4.6 Loadings

The loadings are defined according to a previous study [66]. The loading conditions in the three different configurations for the four studied models are the followings:

- Full-extension (0° of flexion): a vertical axial load of 2000N is applied on the reference point of the femur along the femoral mechanical axis.
- Gait (30° of flexion): a vertical axial load of 2200N is applied on the reference point of the femur with an inclination of 15° with respect to the longitudinal axis. The force is decomposed into its components to be applied to the model in the software `Abaqus`.

The two previous configurations replicated the maximal knee axial force during gait corresponding to about 3.1 times a 70 kg body weight as already implemented in previous studies [66].

- Chair-rise (90° of flexion): a vertical axial load of 1000N is applied on the reference point of the femur along the femoral mechanical axis. The force required in this configuration is not as high as in the two previous configurations since the sit-to-stand is performed with the help of the hands.

The different loading conditions are illustrated with the mobile bearing cruciate retaining knee model in Figure 4.8. The same loading conditions are applied to the three other models.

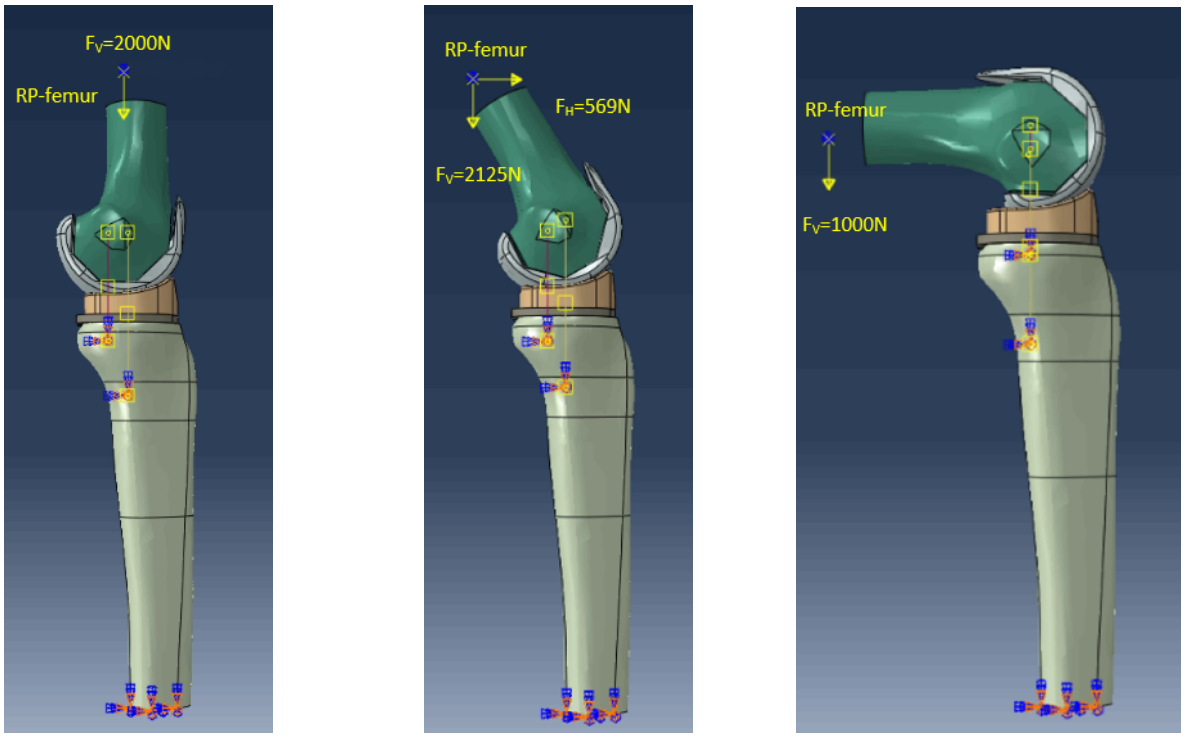

(a) Full-extension (0° of flexion) (b) Gait (30° of flexion) (c) Chair-rise (90° of flexion)

Figure 4.8: Forces applied to the MB CR model in the three analyzed configurations

4.4.7 Illustration of the total models

The total models containing the prostheses' components, the bones and the ligaments are illustrated for the mobile bearing and fixed bearing implants in the full-extension configuration in Figure 4.9.

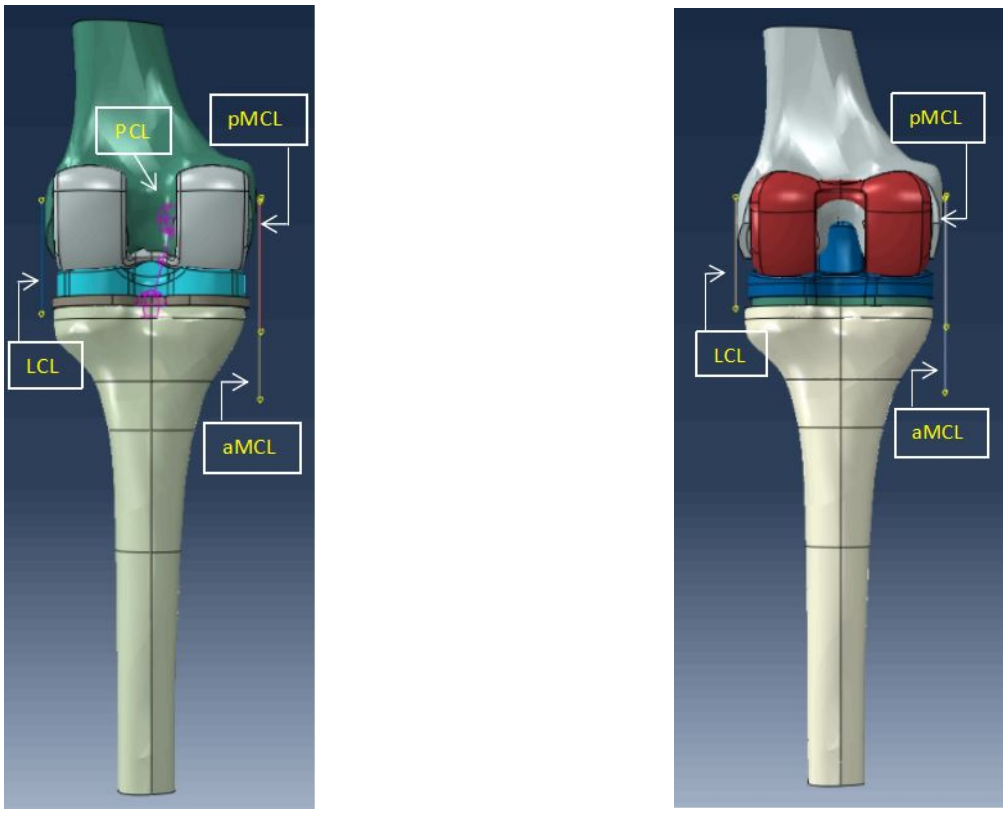

(a) Mobile bearing models

(b) Fixed bearing total models

Figure 4.9: Illustration of the total models for the mobile and fixed bearing models in the full-extension configuration

4.5 Models with the prosthesis components

4.5.1 Prosthesis components positioning

The prostheses' components are kept in the exact same position as in the total models (before adding the bones and the ligaments) and the position constraints applied to those components are exactly the same.

4.5.2 Constraints

A reference point (RP-fem_comp) was constructed on the femoral component to apply the load as well as the boundary condition acting on the femoral component. For the MB models and the FB CCK model, this reference point was taken at mid-distance from the top of the two pegs. For the FB PS model, the reference point was taken at the medio-lateral mid point of the cam slot.

This reference point is constrained (Coupling-continuum):

- to the femoral medial and lateral cut surfaces in the full-extension configuration;
- to the femoral medial, lateral, medial posterior and lateral posterior cut surfaces in the 30° of flexion configuration;
- to the femoral posterior cut surfaces in the 90° of flexion configuration.

The reference point and constrained surfaces are illustrated for the mobile bearing cruciate retaining knee model in the Figure 4.10. The same process is applied to the three other models.

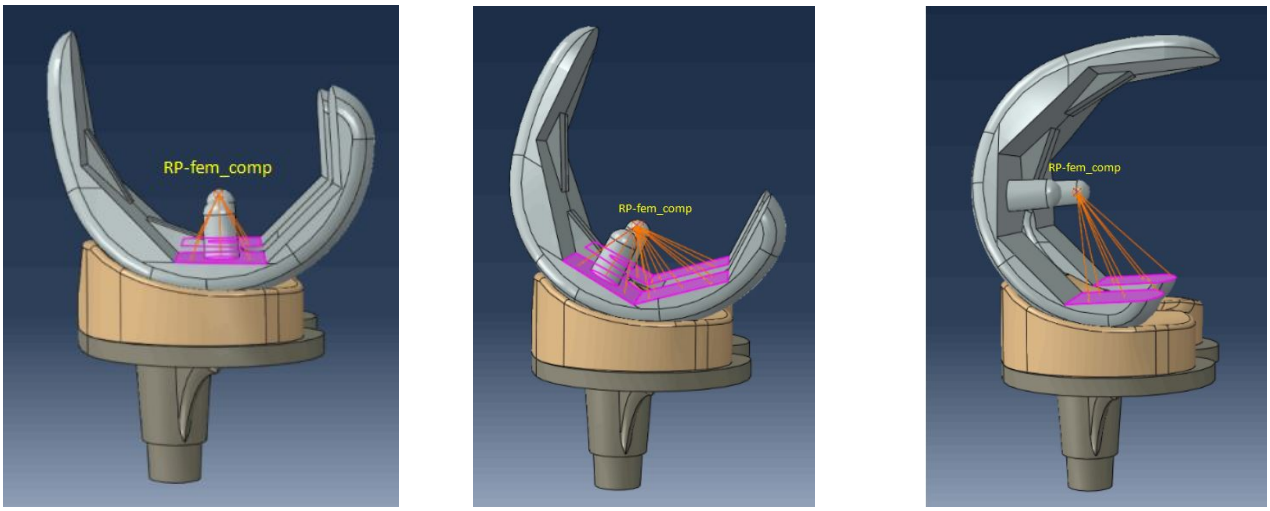

(a) Full-extension (0° of flexion) (b) Gait (30° of flexion) (c) Chair-rise (90° of flexion)

Figure 4.10: Illustration of the reference point and the coupling surfaces for the mobile bearing cruciate retaining knee

4.5.3 Interaction

The same method as in the total models was used to define the interaction between the femoral component and the insert as well as between the insert and the tibial tray.

4.5.4 Boundary conditions and loading

Instead of having the boundary condition applied on the reference point of the femur as it is the case in the total models, the boundary condition is applied to the reference point of the femoral component. The same boundary conditions as the ones applied on the inserts of the total models are applied on the inserts of the prostheses' models.
The lower surface of the tibial tray was encastered.
The loading conditions are the same as the ones applied to the total model. The load is applied to the reference point of the femoral component.

The different loading and boundary conditions are illustrated for the mobile bearing cruciate retaining model in Figure 4.11.

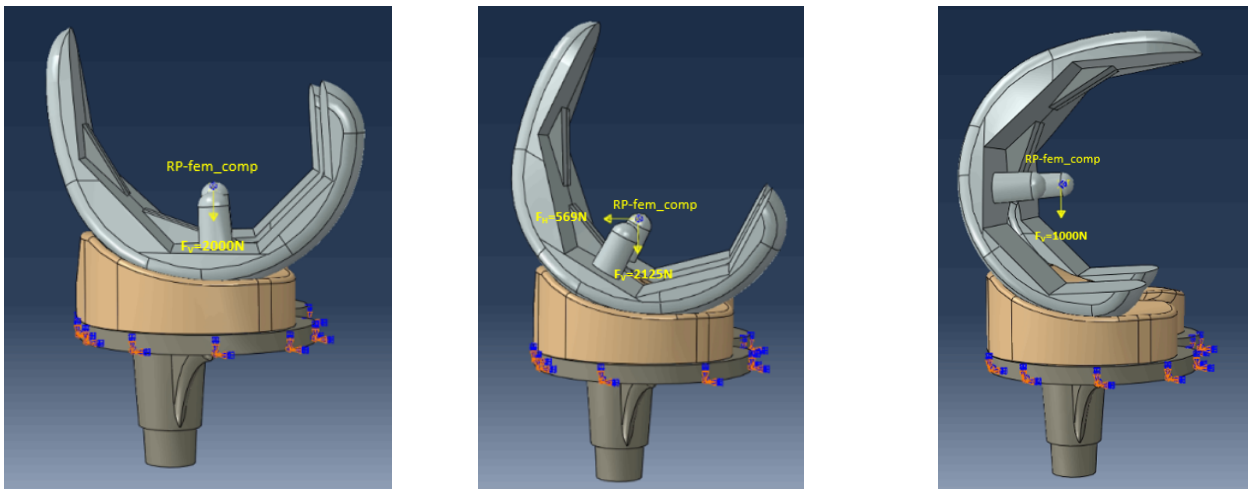

(a) Full-extension (0° of flexion) (b) Gait (30° of flexion) (c) Chair-rise (90° of flexion)

Figure 4.11: Illustration of the loading and boundary conditions for the mobile bearing cruciate retaining knee

Chapter 5

Finite element analysis

5.1 Finite element modeling

The finite element analysis is a numerical method used to find solutions for complex problems. This one aims to divide the complex geometry of a solid into smaller finite elements connected together through nodes, forming the finite element mesh. A solution is obtained for each finite element instead of obtaining an analytical solution for the studied problem, which provides an approximate result to the complex problem. By using mesh refinement, the approximate result approaches the true result.

5.2 Finite Element Mesh

The geometry of the different parts were simplified using the Virtual topology tool. All the parts were meshed using linear tetrahedral elements with the element sizes chosen accordingly to each part. `ABAQUS/ Standard version 2017 (Dassault Systèmes)` was used to perform all the finite element simulations.

5.2.1 Finite element modeling of the femoral component

The total number of nodes and elements used in the finite element modeling of the femoral component for each type of prosthesis in the three studied configurations can be found in Table 5.1.

Table 5.1: Number of nodes and elements used in the finite element model of the femoral component for the four models of prostheses considered in each studied configuration

Model	Number of nodes			Number of elements		
	0°	30°	90°	0°	30°	90°
MB CR	3650	3650	3650	14688	14688	14688
MB CR ultra	3650	3650	3650	14688	14688	14688
FB PS	6614	6614	6614	27925	27925	27925
FB CCK	7682	5353	8224	31052	20558	33629

5.2.2 Finite element modeling of the tibial tray

The total number of nodes and elements used in the finite element modeling of the tibial tray for each type of prosthesis in the three studied configurations can be found in Table 5.2.

Table 5.2: Number of nodes and elements used in the finite element model of the tibial tray for the four models of prostheses considered in each studied configuration

Model	Number of nodes			Number of elements		
	0°	30°	90°	0°	30°	90°
MB CR	3039	3039	3039	11406	11406	11406
MB CR ultra	3039	3039	3039	11406	11406	11406
FB PS	5676	5676	5676	24377	24377	24377
FB CCK	5676	5676	5676	24377	24377	24377

A medio-lateral partitioning was applied to the femoral components and the tibial trays of each model in order to study the parameters on the lateral and medial parts.

5.2.3 Finite element modeling of the insert

The inserts were divided in three parts: the medial, lateral and middle. The parameters of interest were studied on the medial and lateral parts corresponding respectively to the medial and lateral tibial plates. The partitioning planes were chosen according to the insert of each model.

For the FB CCK prosthesis, the partitioning planes were taken tangent to the peg of the insert. For the FB PS and mobile bearing prostheses, the partitioning planes were constructed based on already existing lines in the geometry of the insert. The partitioning applied to the insert of each model is illustrated in Figure 5.1.

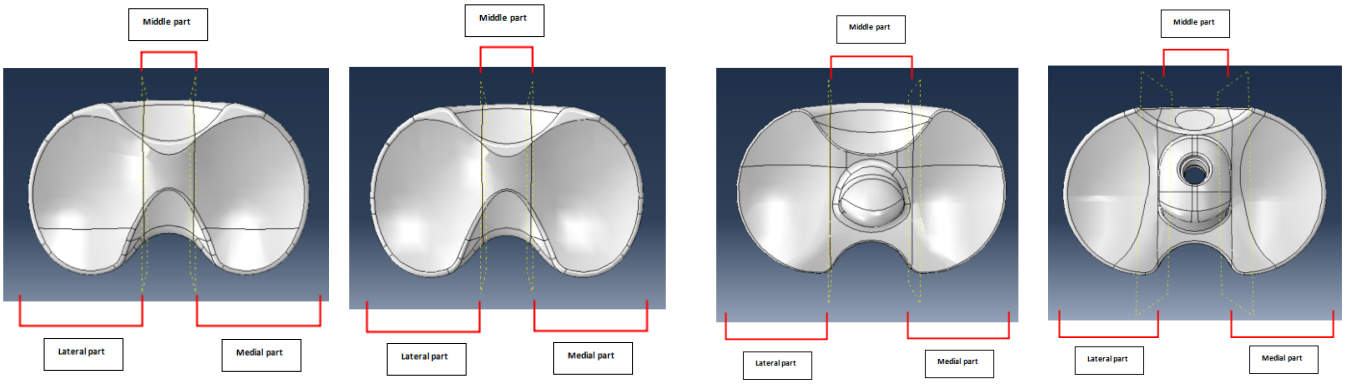

(a) MB CR insert (b) MB CR ultracongruent insert (c) FB PS insert (d) FB CCK insert

Figure 5.1: Illustration of the partitioning of the inserts

The total number of nodes and elements used in the finite element modeling of the tibial tray for each type of prosthesis in the three studied configurations can be found in Table 5.3.

Table 5.3: Number of nodes and elements used in the finite element model of the insert for the four models of prostheses considered in each studied configuration

Model	Number of nodes			Number of elements		
	0°	30°	90°	0°	30°	90°
MB CR	6770	6770	6770	32483	32483	32483
MB CR ultra	6251	6251	6251	29824	29824	29824
FB PS	6921	6856	6856	27925	32480	32480
FB CCK	7077	7077	7077	34222	34222	34222

5.2.4 Finite element modeling of the femur model

The geometry of the femur model is simplified using the Virtual topology tool by combining all the faces together on the cortical as well as the cancellous part, excepting for the ones representing the medial and lateral epicondyle. The final model of the femur presents about 23000 linear tetrahedral elements and 5000 nodes.

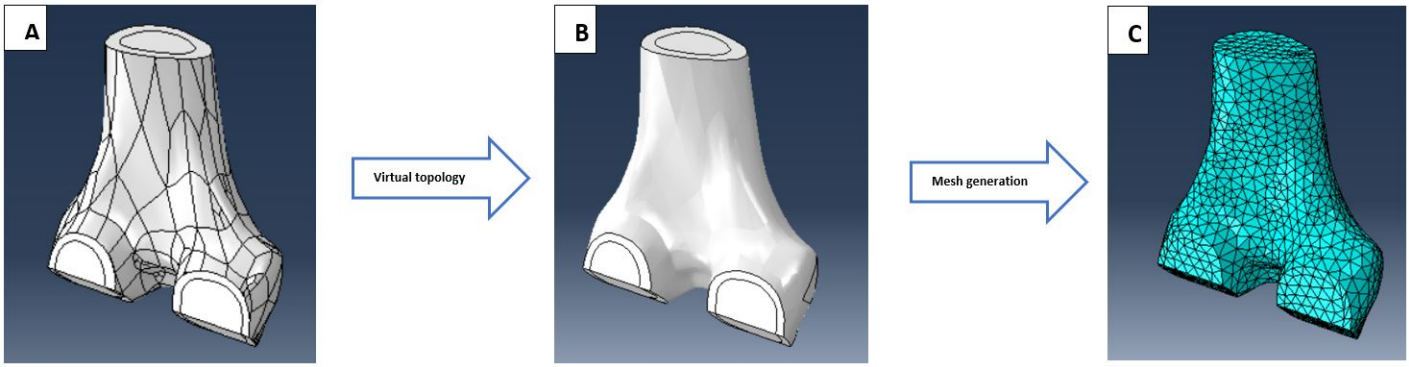

Figure 5.2: Process to obtain the final meshed femur model; A: Femur model initial geometry - B: Virtual topology - C: Generation of the mesh on the femur model

5.2.5 Finite element modeling of the tibial model

Due to the gross initial geometry of the tibial model, meshing the part as it is would produce a coarse mesh. The virtual topology tool was used to simplify the tibial geometry by combining faces or edges and ignoring some entities such as sharp angles in order to obtain a finer mesh.

The tibial model is first partitioned into its lateral and medial part with the use of the medio-lateral plane. Two other planes are constructed on the tibial model, one located at 5 mm from the top of the tibial model, and another one located at 30mm from the top of the tibial model. Those two planes are used to partition the tibia into its proximal (first 5 mm zone) and distal parts (20mm zone). The mesh is then generated individually on each partitioned part. The element size is chosen in order to obtain a finer mesh at the regions of interest (proximal and distal tibia) and a coarse mesh at the end of the tibial bone, as the results do not need to be precise in this zone.

For the mobile bearing models, the final model of the tibia presents about 60000 linear tetrahedral elements and about 12000 nodes. For the FB CCK and the FB PS models, the final model of the tibia presents about 100000 linear tetrahedral elements and 19000 nodes.

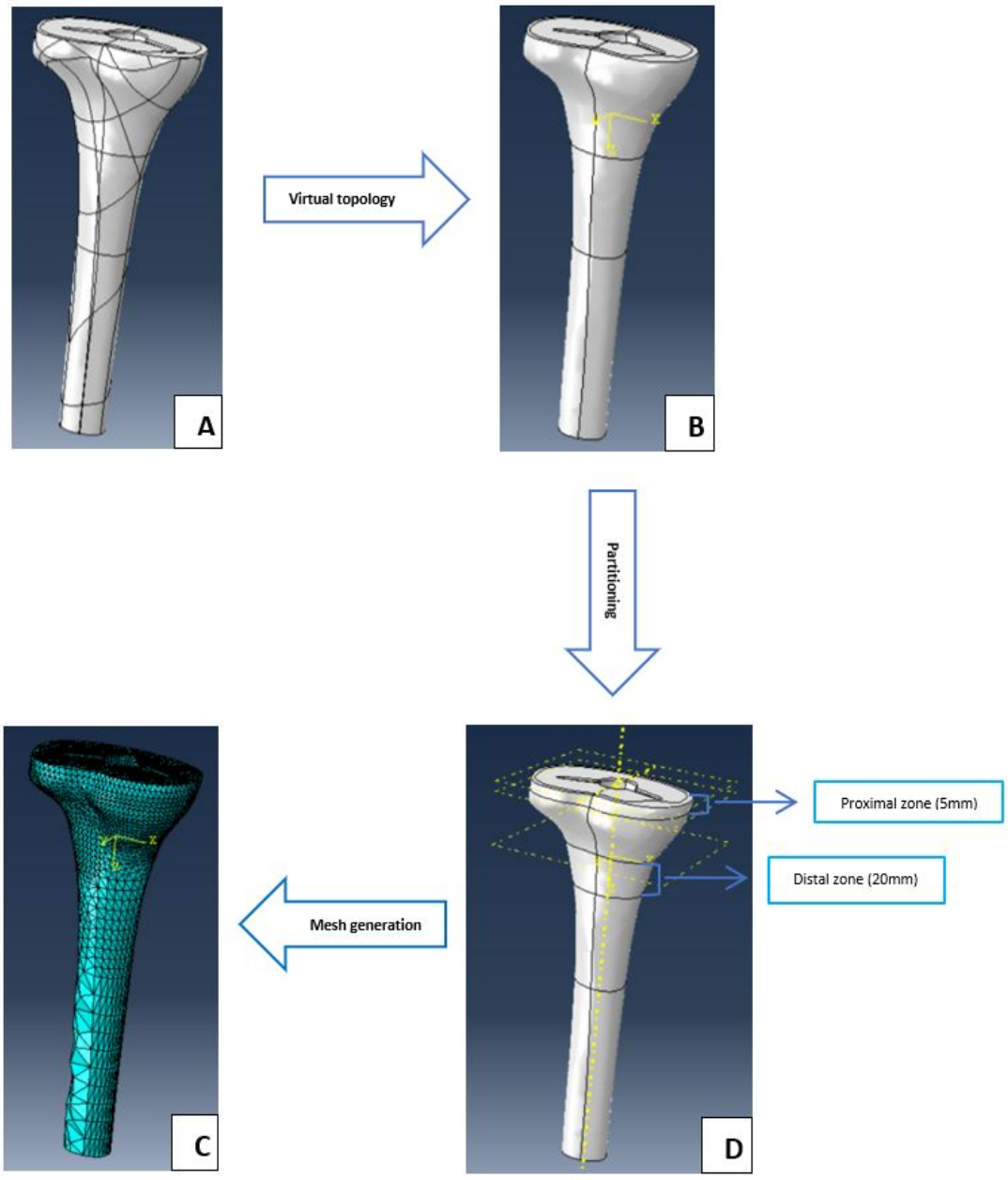

Figure 5.3: Process to obtain the final meshed tibial model; A: Tibial model initial geometry - B: Virtual topology - C: Definition of the partition planes and cell partition - D: Generation of the mesh on the tibial model

5.3 Regions of interest and output

Four regions of interest were defined on the tibia:

- two local regions close to the tibial tray: the medial and lateral proximal zone (investigated with a depth of 5mm);
- and two global regions located at 30mm from the top of the tibia: the medial and lateral distal zone (investigated with a depth of 20 mm).

Those two regions were selected to compare the stress distribution in the proximal and distal tibial bone (on both medial and lateral sides) for the four prosthesis models in the different configurations. The four regions of interest in the tibia are illustrated in Figure 5.4.

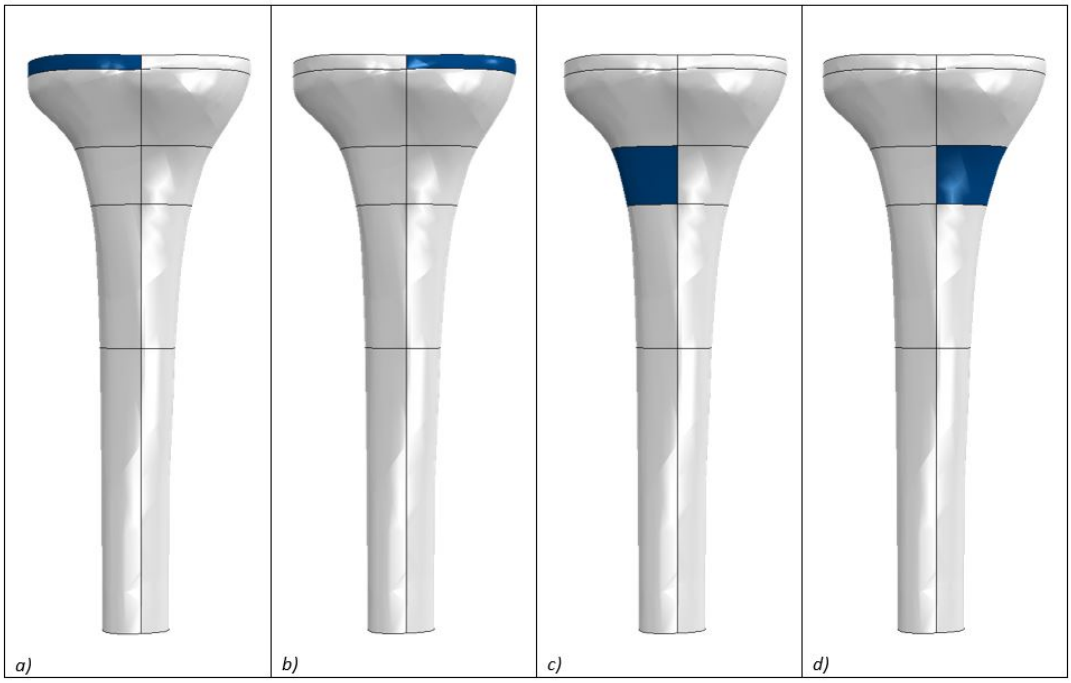

Figure 5.4: Regions of interest analyzed in the tibia: *a)* lateral proximal zone; *b)* medial proximal zone; *c)* lateral distal zone, and *d)* medial distal zone

As explained before, the insert of the different models was partitioned in three regions: the lateral, medial and middle regions. The regions of interest on which the parameters were studied were the medial and lateral tibial plates which are illustrated in the Figure 5.5 for each model.

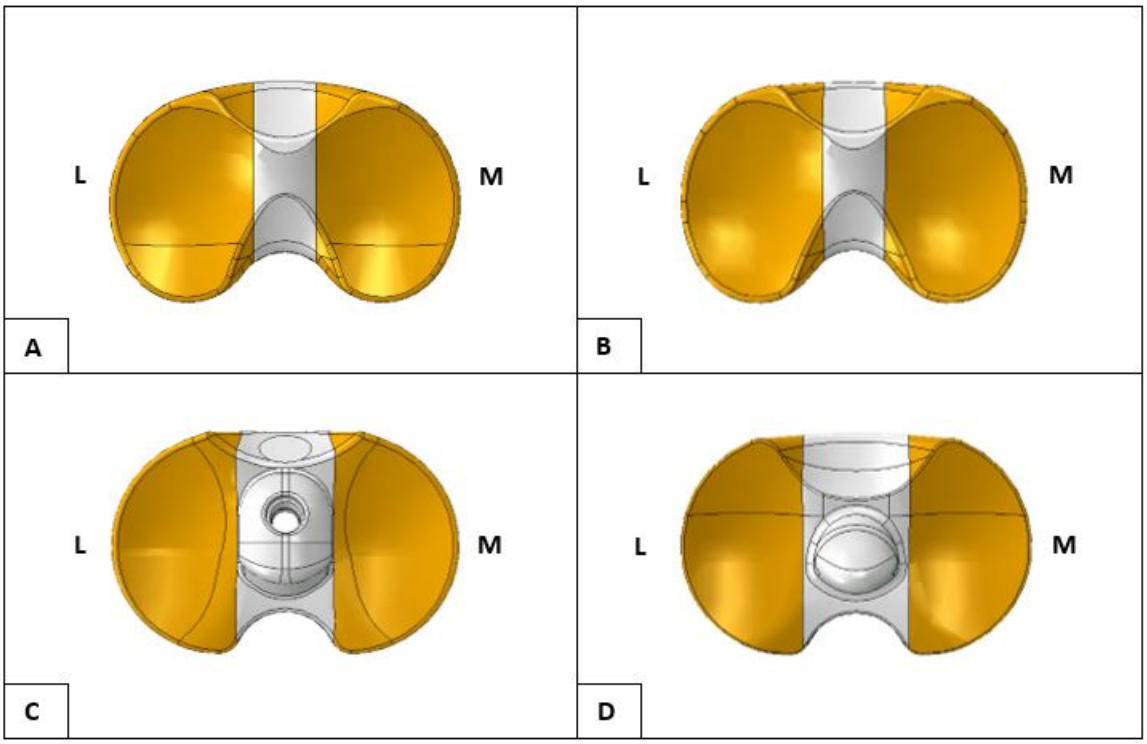

Figure 5.5: Regions of interest analyzed in the insert: M: medial tibial plate, L: lateral tibial plate for the **A**: MB CR insert; **B**: MB CR ultracongruent insert; **C**: FB CCK insert, and **D**: FB PS insert

For all the models in the studied configurations, the output that are requested are the followings:

- the medial and lateral contact areas between the femoral component and the tibial insert;
- the medial and lateral von Mises stresses taken by the tibial insert;
- the medial and lateral von Mises stresses taken by the tibial cortical bone in the proximal zone;
- the medial and lateral von Mises stresses taken by both cortical and cancellous tibial bone in the proximal zone;
- the medial and lateral von Mises stresses taken by the tibial cortical bone in the distal zone;
- and the medial and lateral von Mises stresses taken by both cortical and cancellous tibial bone in the distal zone.

Chapter 6

Simulations

6.1 Abaqus solvers

`Abaqus` contains two solvers to solve structural problems: Abaqus/standard and Abaqus/ explicit. The first one uses implicit methods to solve linear and nonlinear problems whereas the second one uses explicit methods.

6.2 Static analysis

A static analysis is implicit by definition. The static response only considers the behavior of the system once all the loads are completely applied to the structure and ignores the in-between behavior. The static general step does not take into account the inertial effects and is therefore not suitable to dynamic problems as they are highly dependent on inertia.

A static analysis was first performed on the models containing only the prosthesis components (without the bones and ligaments) at the three different flexion angles in order to see if the convergence was reached.

The problem was divided in two steps: the initial one in which all the initial conditions such as the boundary conditions are applied and the first step in which the load is applied. A linear amplitude was defined in order to apply the force progressively on the femoral component instead of applying all the load instantaneously. During the simulation, each step is divided in several time increments which are solved by the solver from the first to the last one. The time incrementation can be either fixed or controlled automatically by `Abaqus/Standard`. An automatic type of incrementation was chosen allowing `Abaqus/Standard` to determine the size of the time increments based on computational efficiency. For each increment, the convergence is checked. If the solver can reach the convergence easily, the increment size is increased and the solver jump to the next increment whereas if it is difficult for the solver to reach convergence or it is not reached at all, the solver reduces the increment size and reiterates the increment until convergence is reached. When the maximum increment size is reached, the simulation is completed and stops whereas if the minimum increment size value is reached, the simulation stops before completion.

The time period was set to 1. Since `Abaqus` has no default system unit, it is a user choice. The three base units: length/mass/time chosen were : [mm/ton/s]. All the material properties and loads were therefore defined using this system unit. The time period of 1 means that it requires 1 second for the load to be totally applied on the system. The initial increment size, minimal increment size, and maximum number of increments were respectively set to 10^{-2}, 10^{-6} and 10^{2}. The simulation stopped before completion, displaying an error message saying that the displacement increment for contact was too big. The values of the initial increment size, minimal increment

and maximum number of increments were therefore adjusted. The initial increment size as well as the minimal increment size were therefore reduced respectively up to 10^{-5} and 10^{-16} whereas the maximum number of increments was increased up to 10^{6}. However, even with those modifications, the simulation stopped after completing a few increments with a very high simulation time.

Convergence was never reached with the static analysis. Even increasing the maximal number of increments and decreasing the minimal increment size would not help reach the convergence. Indeed, in the static analysis, the femoral component needs to be perfectly positioned with respect to the tibial insert for the contact to occur during the simulation.

6.3 Static analysis with damping factor

One of the most common cause of non-convergence is the presence of instability. The static analysis was then performed adding a damping factor. The applied damping factor can be constant through the step or vary with time taking into account the changes occurring over the course of a step. This one was chosen to be constant over the duration of a step. This one allows to decrease the simulation time, with bigger time increment and therefore reducing the convergence issues. The damping factor used was the default parameter one: 0.0002. This value is appropriate for the study and does not need to be changed.

The time period was also set to 1. Several values of initial increment size, minimal increment size, and maximum number of increments were tested. The ultimate initial increment size, minimal increment size, and maximum number of increments were respectively set to 10^{-2}, 10^{-9} and 10^{6}. Even with the use of the damping factor, it was hard to reach convergence with the static analysis. The solution was to use `Abaqus/explicit` as no convergence issues will be encountered.

6.4 Dynamic explicit analysis

The dynamic explicit analysis was used so that during the simulation, the femoral component can adjust its position with respect to the tibial insert. At the end of the simulation, the femoral component reaches its equilibrium position and the contact with the insert is optimal. The dynamic explicit analysis was first performed on the models containing only the prosthesis components. Since the convergence was reached with those models, the dynamic explicit simulations were then performed on the total models.

6.4.1 Choice of the mass scaling

The mass scaling is used to scale the mass of the entire model at the beginning of each step. When the mass scaling factor is applied, the masses of the elements with a time increment inferior to the user-supplied time increment are scaled so that the time increment of those elements becomes equal to the user-supplied time increment.

Simulations were carried out on one model, the normal mobile bearing cruciate retaining knee, in the full-extension configuration with mass scaling values ranging from 10^{-4} to 10^{-6} to determine

the optimal value to apply to the different models in all the studied configurations. The different mass scaling values that were tested are gathered in the Table 6.1.

Table 6.1: Mass scaling values

Mass scaling					
A	B	C	D	E	F
5×10^{-4}	10^{-4}	5×10^{-5}	10^{-5}	5×10^{-6}	10^{-6}

The parameters that were considered are the average of the output:

- the medial and lateral average contact areas between the femoral component and the tibial insert;
- the medial and lateral average von Mises stresses taken by the tibial insert;
- the medial and lateral average von Mises stresses taken by the tibial cortical bone in the proximal zone;
- the medial and lateral average von Mises stresses taken by both cortical and cancellous tibial bone in the proximal zone;
- the medial and lateral average von Mises stresses taken by the tibial cortical bone in the distal zone;
- and the medial and lateral average von Mises stresses taken by both cortical and cancellous tibial bone in the distal zone;

as well as the simulation time. As it can be seen in Figure 6.7, the computational time increases with the reduction of the mass scaling value. The goal is to find a mass scaling value for which convergence is reached with an acceptable simulation time. The mass scaling value chosen was of 10^{-5}.

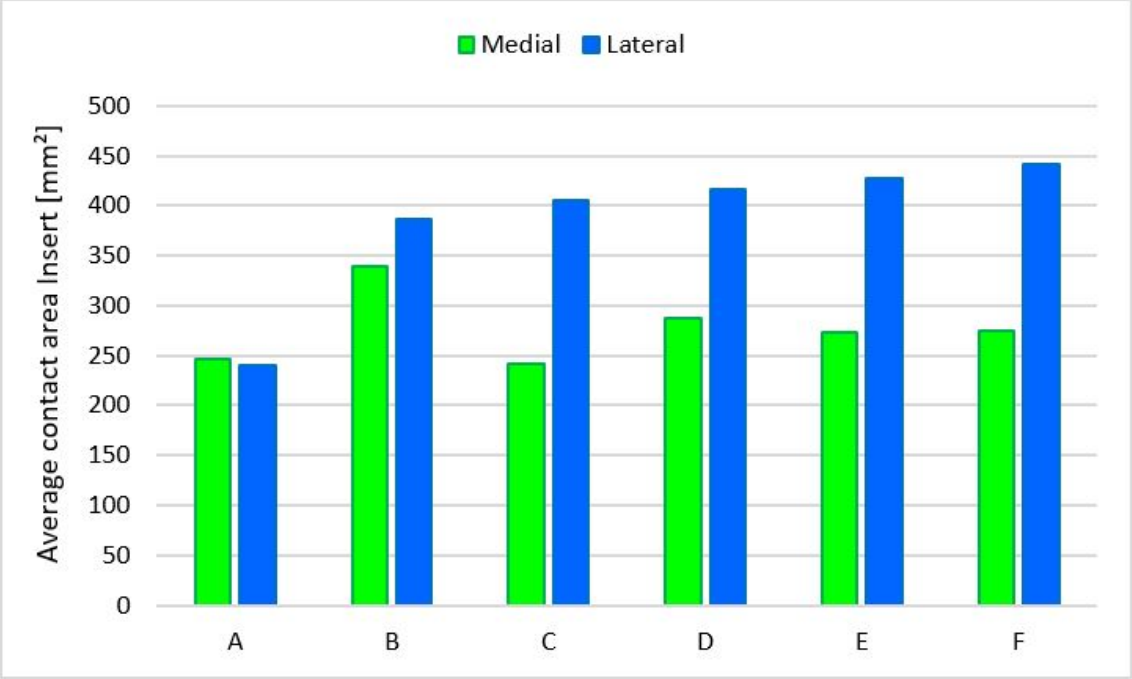

Figure 6.1: Medial and lateral average contact area on the insert for the normal mobile bearing model in the full-extension configuration with A, B, C, D, E, F corresponding to the mass scaling defined in Table 6.1.

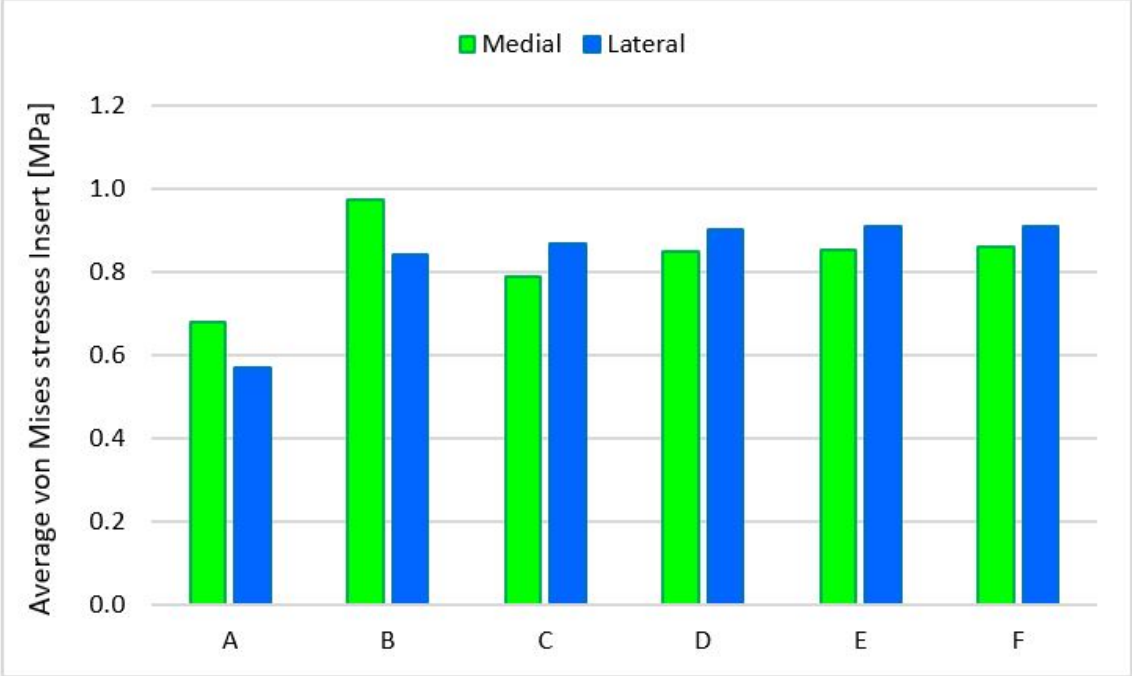

Figure 6.2: Medial and lateral average von Mises stresses of the insert for the normal mobile bearing model in the full-extension configuration with A, B, C, D, E, F corresponding to the mass scaling defined in Table 6.1.

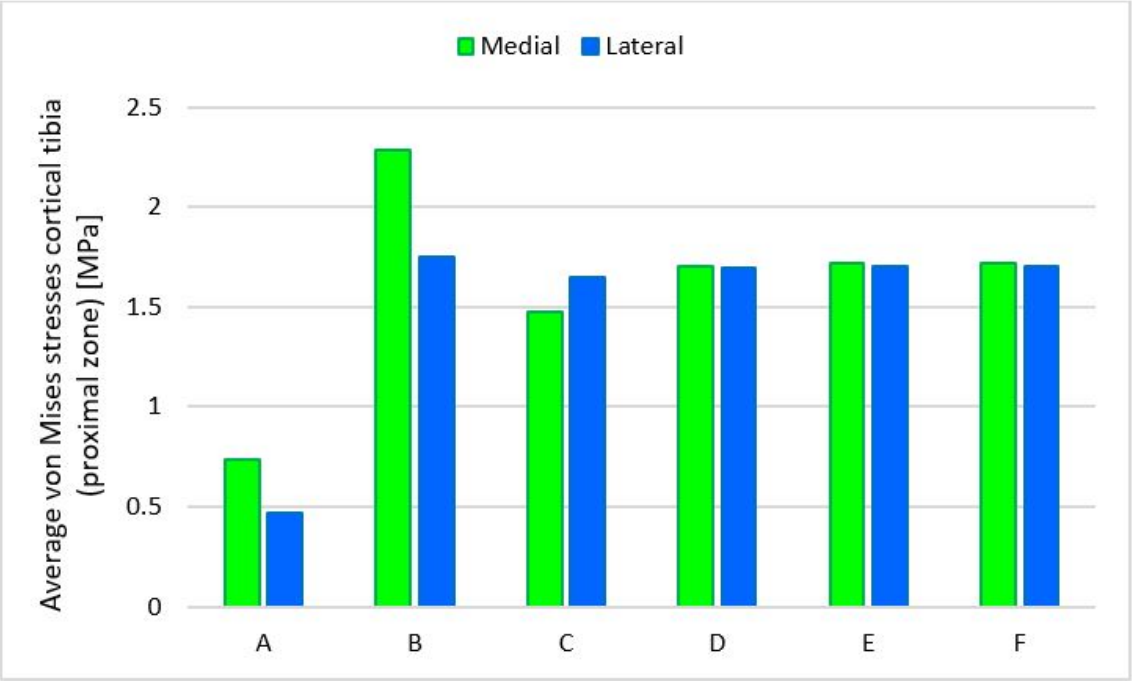

Figure 6.3: Medial and lateral average von Mises stresses of the cortical tibia in the proximal region for the normal mobile bearing model in the full-extension configuration with A, B, C, D, E, F corresponding to the mass scaling defined in Table 6.1.

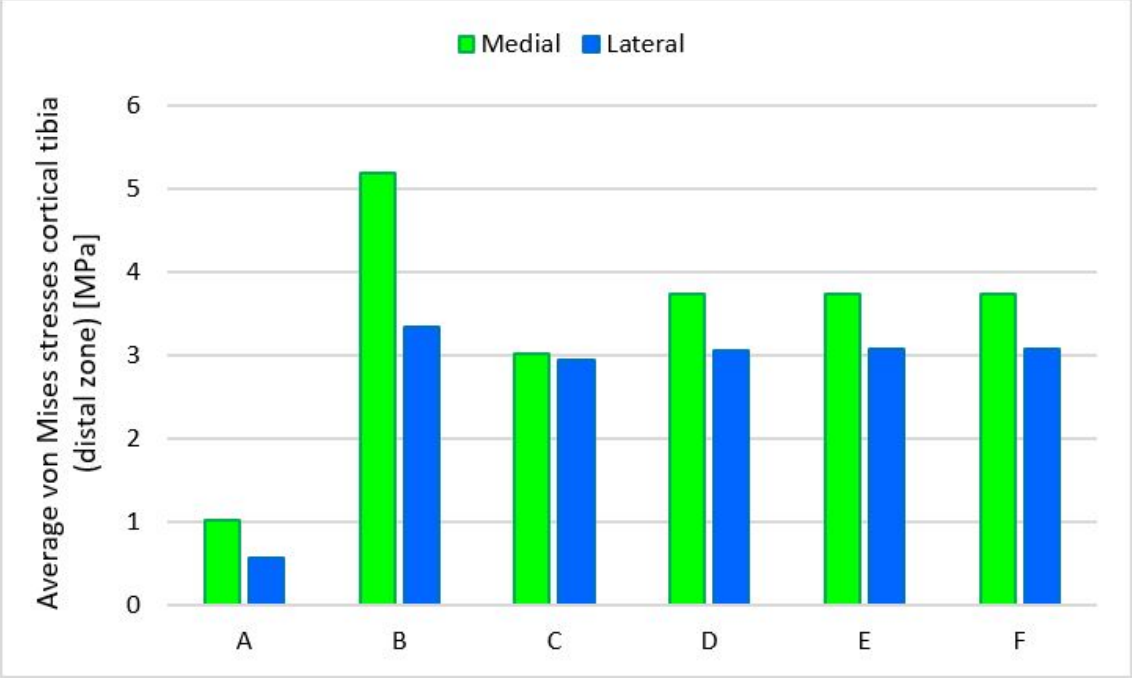

Figure 6.4: Medial and lateral average von Mises stresses of the cortical tibia in the distal region for the normal mobile bearing model in the full-extension configuration with A, B, C, D, E, F corresponding to the mass scaling defined in Table 6.1.

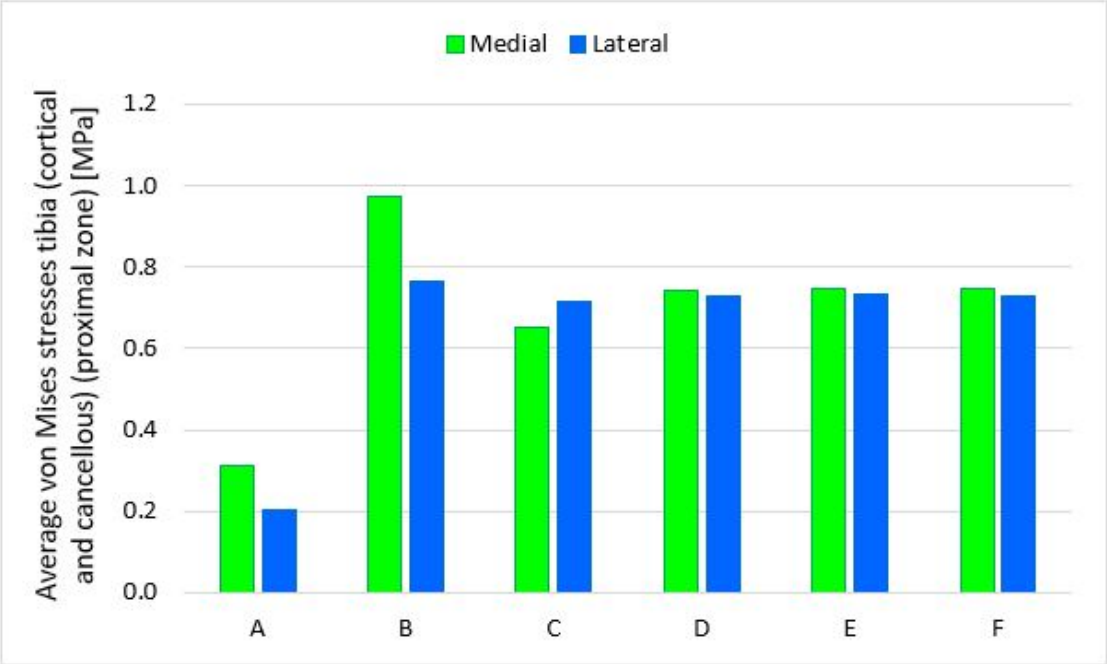

Figure 6.5: Medial and lateral average von Mises stresses of the tibial bone (cortical and cancellous) in the proximal region for the normal mobile bearing model in the full-extension configuration with A, B, C, D, E, F corresponding to the mass scaling defined in Table 6.1.

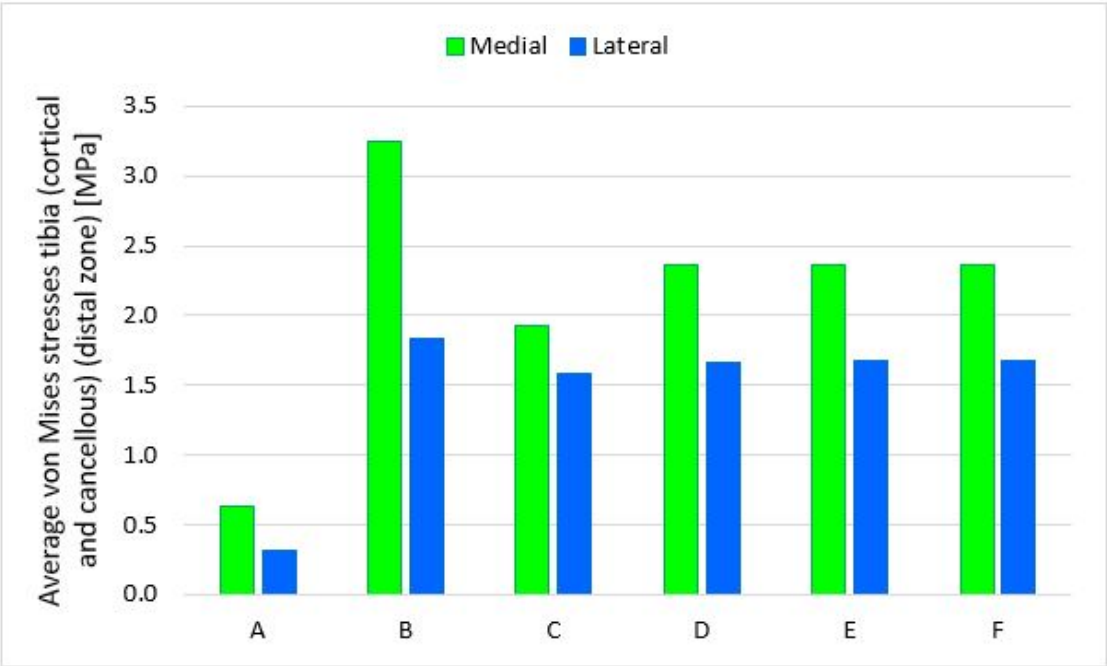

Figure 6.6: Medial and lateral average von Mises stresses of the tibial bone (cortical and cancellous) in the distal region for the normal mobile bearing model in the full-extension configuration with A, B, C, D, E, F corresponding to the mass scaling defined in Table 6.1.

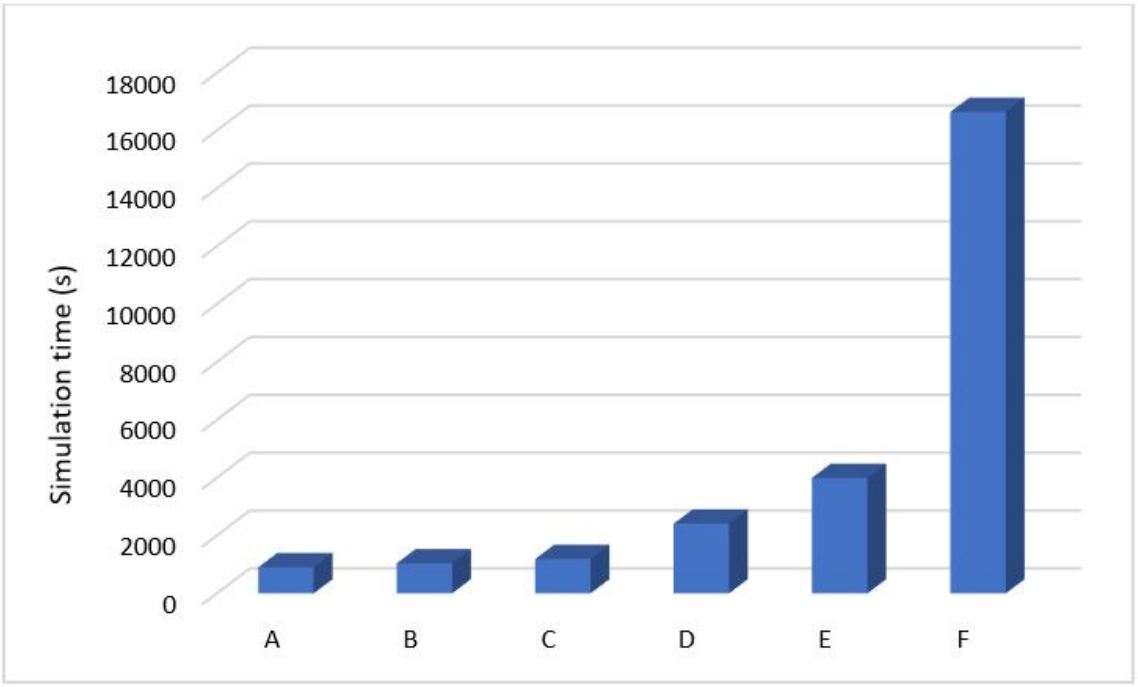

Figure 6.7: Simulation time for the normal mobile bearing model in the full-extension configuration with A, B, C, D, E, F corresponding to the mass scaling defined in Table 6.1.

Chapter 7

Results and discussion

7.1 Quantitative results

7.1.1 Average contact area on the insert

Figure 7.1 reports a graphical overview of the average medial and lateral contact area on the insert for all the considered models in the studied configurations. In all the configurations, the greatest medial and lateral contact areas are found for the mobile bearing ultracongruent insert. Indeed, the surface of the ultracongruent insert is designed to have a maximal contact between the femoral component and the insert.

For all the models in the full-extension configuration, the medial average contact area is lower than the lateral average contact area. In opposition to the previous configuration, the gait one exhibits equivalent medial and lateral contact areas. Regarding the chair-rise configuration, the medial average contact area is slighty greater than the lateral average contact area for the mobile bearing models whereas the medial and lateral average contact areas are similar for the fixed bearing models.

In every configuration, there is a general tendency showing very high contact areas for the ultracongruent mobile bearing model, high contact areas for the normal mobile bearing model and small ones for both fixed bearing models. In the full-extension configuration, the contact areas of the ultracongruent mobile bearing model are twice as high as the values of the normal bearing model which in turn are twice as high as the values of the fixed bearing models. In the gait and chair-rise configuration, the difference between both mobile bearing models is not as important as in the first configuration. Nevertheless, the values of the normal bearing model remain more than twice as high as the values of the fixed bearing models.

For all the models, the gait configuration presents the highest contact areas whereas the chair-rise configuration presents the lowest contact areas.

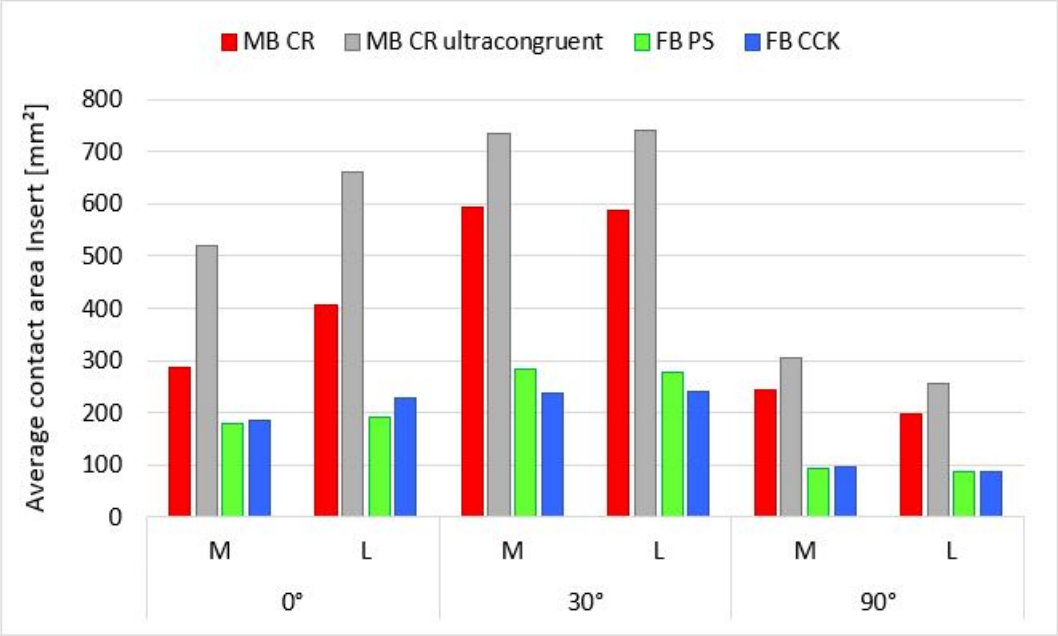

Figure 7.1: Medial (M) and lateral (L) average contact area on the insert for the models - A: MB CR model; B: MB CR ultracongruent model; C: FB PS model; D: FB CCK model in the 0°, 30° and 90° of flexion configuration.

7.1.2 von Mises stresses taken by the insert

7.1.2.1 Average von Mises stresses taken by the insert

Figure 7.2 reports a graphical overview of the average medial and lateral von Mises stresses taken by the insert for all the considered models in the studied configurations. The highest medial and lateral von Mises stresses are observed for the FB CCK model in the gait configuration.

The chair-rise configuration shows the lowest von Mises stresses for all the models with the stress values in this configuration being half of the stress values in the two other ones. In the full-extension configuration, the average medial and lateral von Mises stresses taken by the inserts stay in the same range of values for all the models except for the FB PS insert which shows a higher medial value. The medial and lateral stress values are very close for the gait configuration except for the FB CCK insert which present higher medial and lateral stresses. In the chair-rise configuration, similar values are observed for all the models except for the FB PS which presents higher values. In each studied configuration, there is no significant difference between the models.

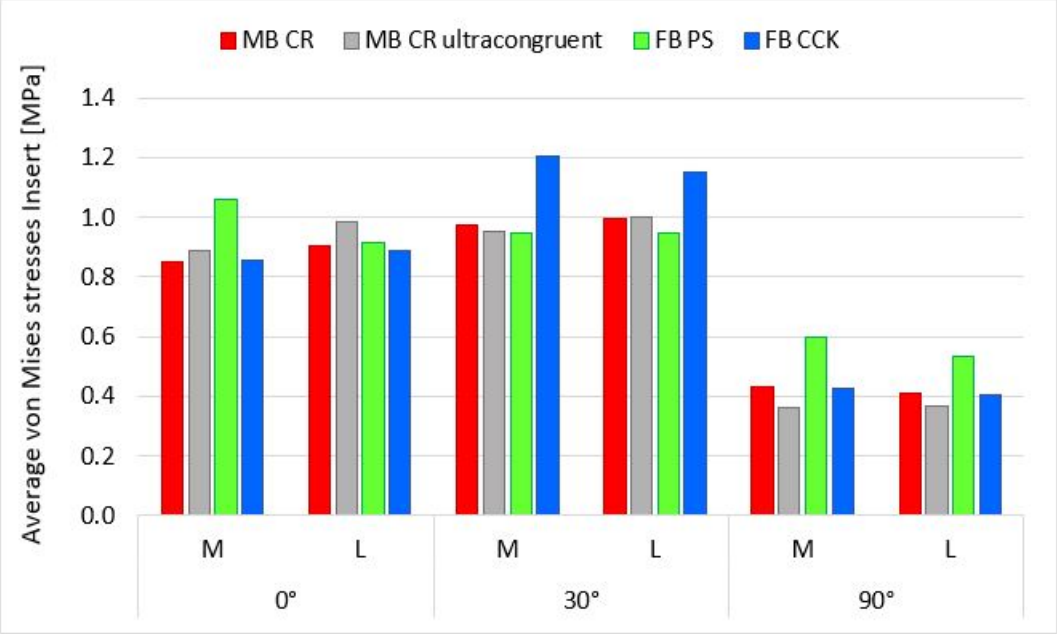

Figure 7.2: Medial (M) and lateral (L) average VM stresses taken by the insert - A: MB CR model; B: MB CR ultracongruent model; C: FB PS model; D: FB CCK model in the 0°, 30° and 90° of flexion configuration.

7.1.2.2 Maximal von Mises stresses taken by the insert

Figure 7.2 reports a graphical overview of the maximal medial and lateral von Mises stresses taken by the insert for all the considered models in the studied configurations.

In the full-extension configuration, the insert undergoing the maximal medial and lateral stresses is the one of the FB PS model with the maximal values being twice as high as the ones of the other models. In the gait configuration, the CCK insert shows the highest maximal medial and lateral stresses. However, the maximal stresses taken by the CCK insert remain close to the ones taken by the other inserts. In the chair-rise configuration, the fixed bearing inserts are subjected to the maximal stresses.

For each configuration, the medial maximal stresses for each model are equivalent to the lateral ones.

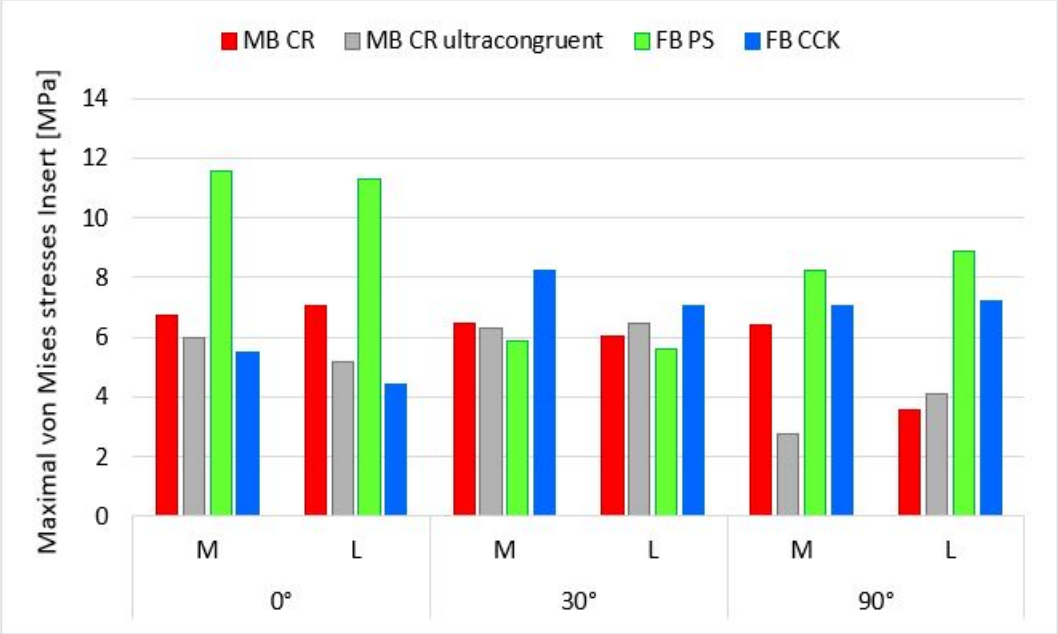

Figure 7.3: Medial (M) and lateral (L) maximal VM stresses taken by the insert - A: MB CR model; B: MB CR ultracongruent model; C: FB PS model; D: FB CCK model in the 0°, 30° and 90° of flexion configuration.

7.1.3 von Mises stresses taken by the cortical tibia in the proximal zone

Figure 7.4 reports a graphical overview of the average medial and lateral von Mises stresses taken by the cortical tibia in the proximal zone for all the considered models in the studied configurations. The lowest average medial and lateral von Mises stresses for all the models are reported for the chair-rise configuration whereas the highest average von Mises stresses are found in the gait configuration. The highest average von Mises stress value is observed for the FB CCK model in the medial proximal tibia in the gait configuration. The second highest average von Mises stress value is reported in the medial proximal tibia for the mobile bearing ultracongruent model in the full-extension configuration.

For all the configurations, there is a general trend showing that the medial average von Mises stresses for all the models are higher than the lateral average von Mises stresses. The difference between the medial and lateral values is more marked for the fixed bearing models in the full-extension and gait configurations. In the chair-rise configuration, the difference between the medial and lateral von Mises average values for those two models becomes negligible.

For all the configurations, the stresses are slightly higher for the mobile bearing model with the ultracongruent insert compared to the normal mobile bearing model. The stresses of the fixed bearing are almost the same in all configurations except for the gait one in which the stress values are slighltly higher for the FB CCK model. Moreover, the cortical distal tibial stresses are slighltly higher for the mobile bearing models compared to the fixed bearing models in the first two configurations and then become equivalent in the chair-rise configuration.

The impact of the different models of prosthesis on the tibia is more marked on the proximal zone compared to the distal one. Indeed, the difference in the average von Mises stresses between the models for the same configuration and for the same model in the different configurations is more noticeable in the proximal zone.

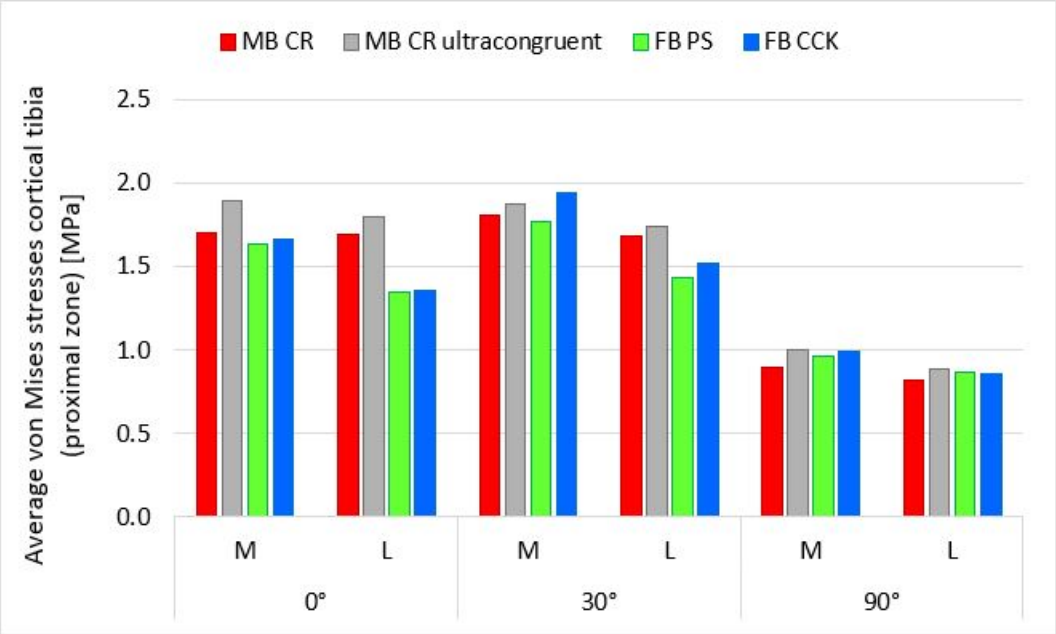

Figure 7.4: Medial (M) and lateral (L) average VM stresses taken by the cortical tibia in the proximal zone for - A: MB CR model; B: MB CR ultracongruent model; C: FB PS model; D: FB CCK model in the 0°, 30 and 90° of flexion configuration.

7.1.4 von Mises stresses taken by the cortical tibia in the distal zone

Figure 7.5 reports a graphical overview of the average medial and lateral von Mises stresses taken by the cortical tibia in the distal zone for all the considered models in the studied configurations. The highest average von Mises stresses for all models values are reported for the full-extension configuration whereas the lowest average von Mises stresses for all models values are found in the chair-rise configuration. For all the models in the different configurations, the medial stresses are higher than the lateral ones. The two mobile bearing models present equivalent values in each configuration.

The different models have similar medial values and similar lateral values in the full-extension configuration. In the gait configuration, the medial and lateral values of the mobile bearing models are slightly higher than the ones of the FB CCK which are in turn slightly higher than the ones of the FB PS model. In the chair-rise configuration, the values of the fixed bearing model are slightly higher to the ones of both mobile bearing models, and this difference is more noticeable in the lateral values.

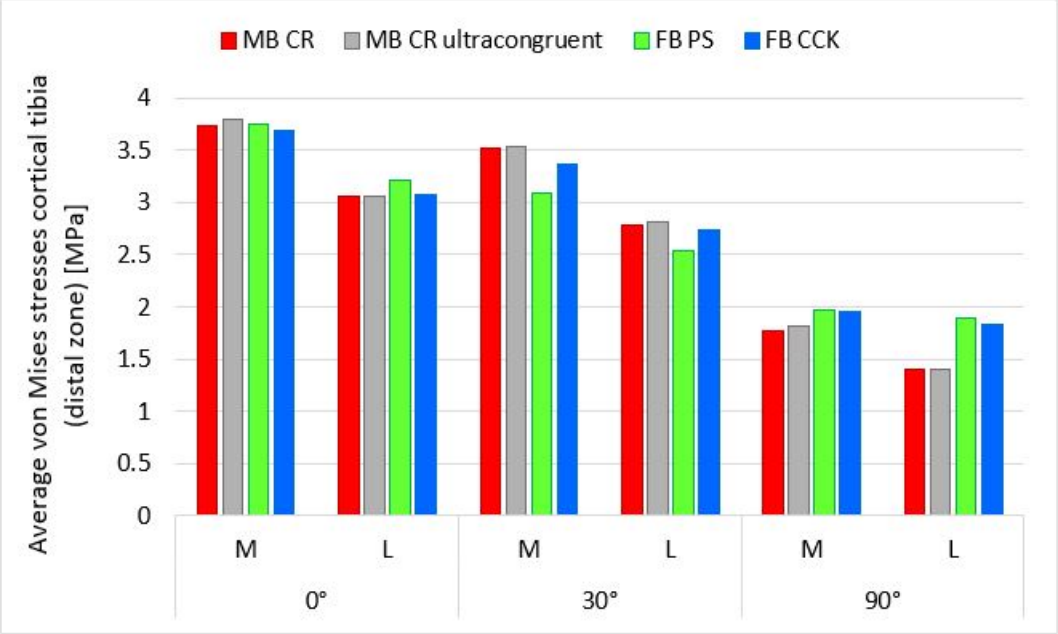

Figure 7.5: Medial (M) and lateral (L) average VM stresses taken by the cortical tibia in the distal zone for - A: MB CR model; B: MB CR ultracongruent model; C: FB PS model; D: FB CCK model in the 0°, 30° and 90° of flexion configuration.

For all the models in the different configurations, the average medial and lateral von Mises stress values are higher in the distal zone than in the proximal zone. In the distal zone, for each configuration, the stresses are more similar between the models as opposed to the proximal zone where the difference is more important in the average values between the models.

7.1.5 von Mises stresses taken by the tibial bone (cortical and cancellous) in the proximal zone

Figure 7.6 reports a graphical overview of the average medial and lateral von Mises stresses taken by the tibial bone in the proximal zone for all the considered models in the studied configurations. For all the models in the different configurations, the average stress values are lower for the tibial bone compared to the cortical tibia in the proximal zone. This difference comes from the fact that the average of the von Mises stresses is realized on a region containing both cortical and cancellous bone with the cancellous bone region being larger than the cortical one with lower von Mises stress values.

The highest average von Mises stresses for all models values are reported for the full-extension configuration (whose values for all models are very similar to the gait configuration) whereas the lowest average von Mises stresses for all models values are found in the chair-rise configuration.

In the full-extension configuration, the medial and lateral values are similar for all models. This trend is also observed in the chair-rise configuration. The gait configuration exhibits greater medial values compared to the lateral ones.

Regardless of the configuration, the mobile bearing model with the ultracongruent insert presents slightly higher values compared to the normal bearing model. For all the configurations excepting the gait one, the fixed bearing models show almost identical values. Indeed, the gait configuration show slightly higher stresses for the FB CCK model compared to the FB PS model. Furthermore, in each configuration, the difference in the stress values between the mobile bearing and fixed bearing models is barely noticeable.

In opposition to the proximal cortical tibial region, for all the models in the different configurations, the difference between the medial and lateral values is negligible. As opposed to the proximal cortical tibial region which present a slight difference in the average values between the models, the proximal tibial region shows more similar values between the models for each configuration.

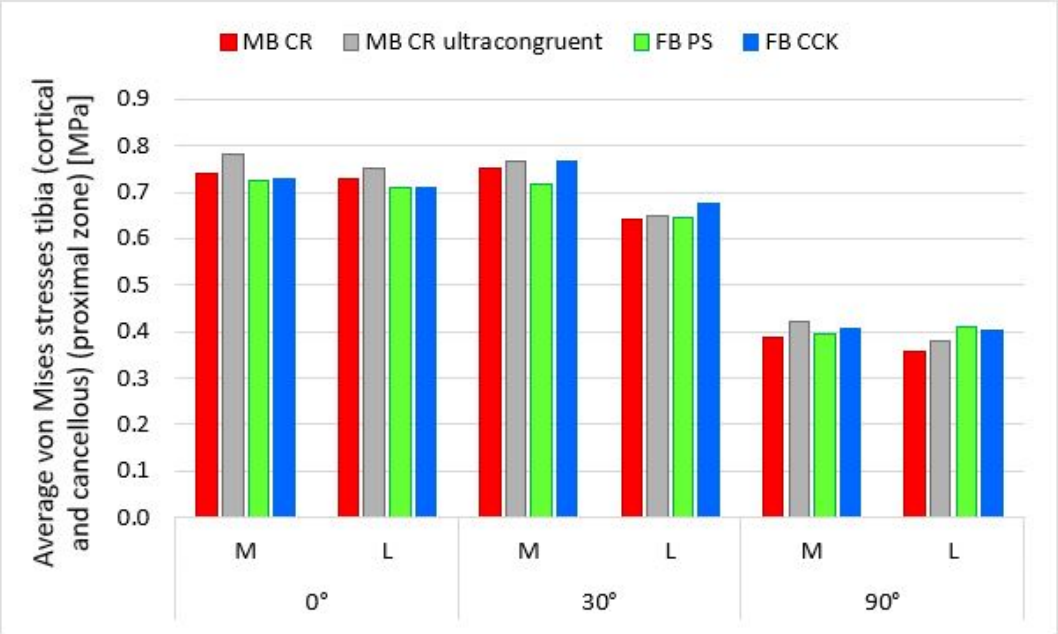

Figure 7.6: Medial (M) and lateral (L) average VM stresses taken by the tibial bone (cortical and cancellous) in the proximal zone for - A: MB CR model; B: MB CR ultracongruent model; C: FB PS model; D: FB CCK model in the 0°, 30° and 90° of flexion configuration.

7.1.6 von Mises stresses taken by the the tibial bone (cortical and cancellous) in the distal zone

Figure 7.7 reports a graphical overview of the average medial and lateral von Mises stresses taken by the tibial bone in the distal zone for all the considered models in the studied configurations. The highest average von Mises stresses for all models values are reported for the full-extension configuration whereas the lowest average von Mises stresses for all models values are found in the chair-rise configuration.

The medial values for all models are greater than the lateral ones in all the configurations. The difference in the values between the mobile bearing models is negligible in every configuration. The mobile bearing models show higher medial values than the fixed bearing models regardless of the studied configuration. This difference is more important in the full-extension and gait configuration and becomes negligible in the chair-rise configuration. The lateral values are slightly higher for the mobile bearing models in the two first configurations but in the third one, this tendency is reversed. The first two configurations show similar medial values and similar lateral values for each model.

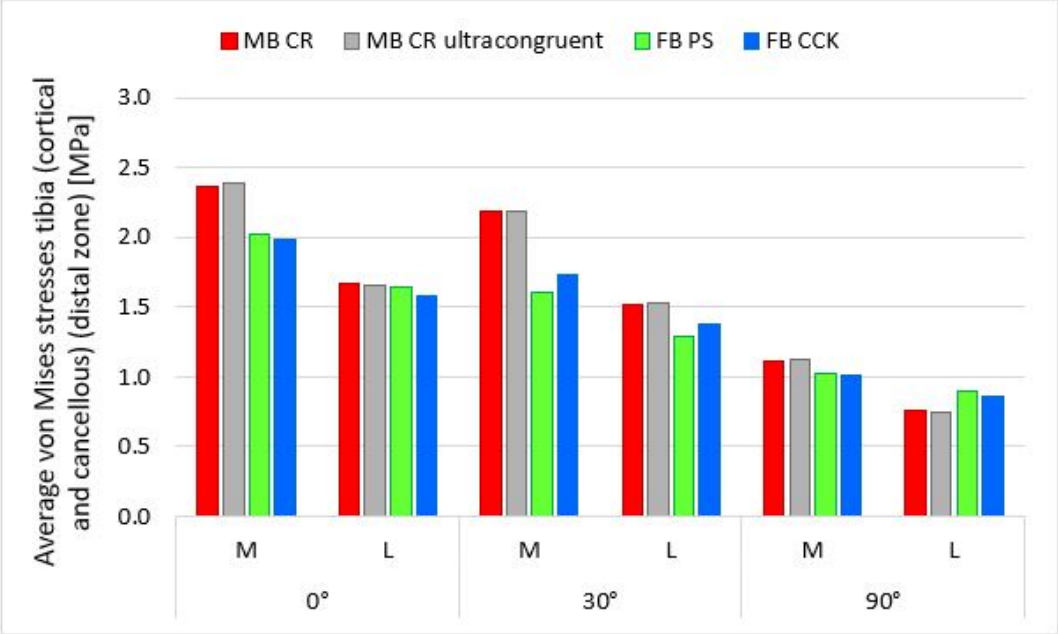

Figure 7.7: Medial (M) and lateral (L) average VM stresses taken by the tibial bone (cortical and cancellous) in the distal zone for - A: MB CR model; B: MB CR ultracongruent model; C: FB PS model; D: FB CCK model in the 0°, 30° and 90° of flexion configuration.

Compared to the proximal tibial region, the distal tibial region presents higher average von Mises stress values for the same model in the different configurations as well as for the different models in the the same configuration. As opposed to the proximal tibial and distal cortical regions which show very similar values between the fixed and mobile bearing models, in the tibial distal zone, the difference between the fixed and mobile bearing models is more marked, especially in the first two configurations.

7.2 Qualitative results

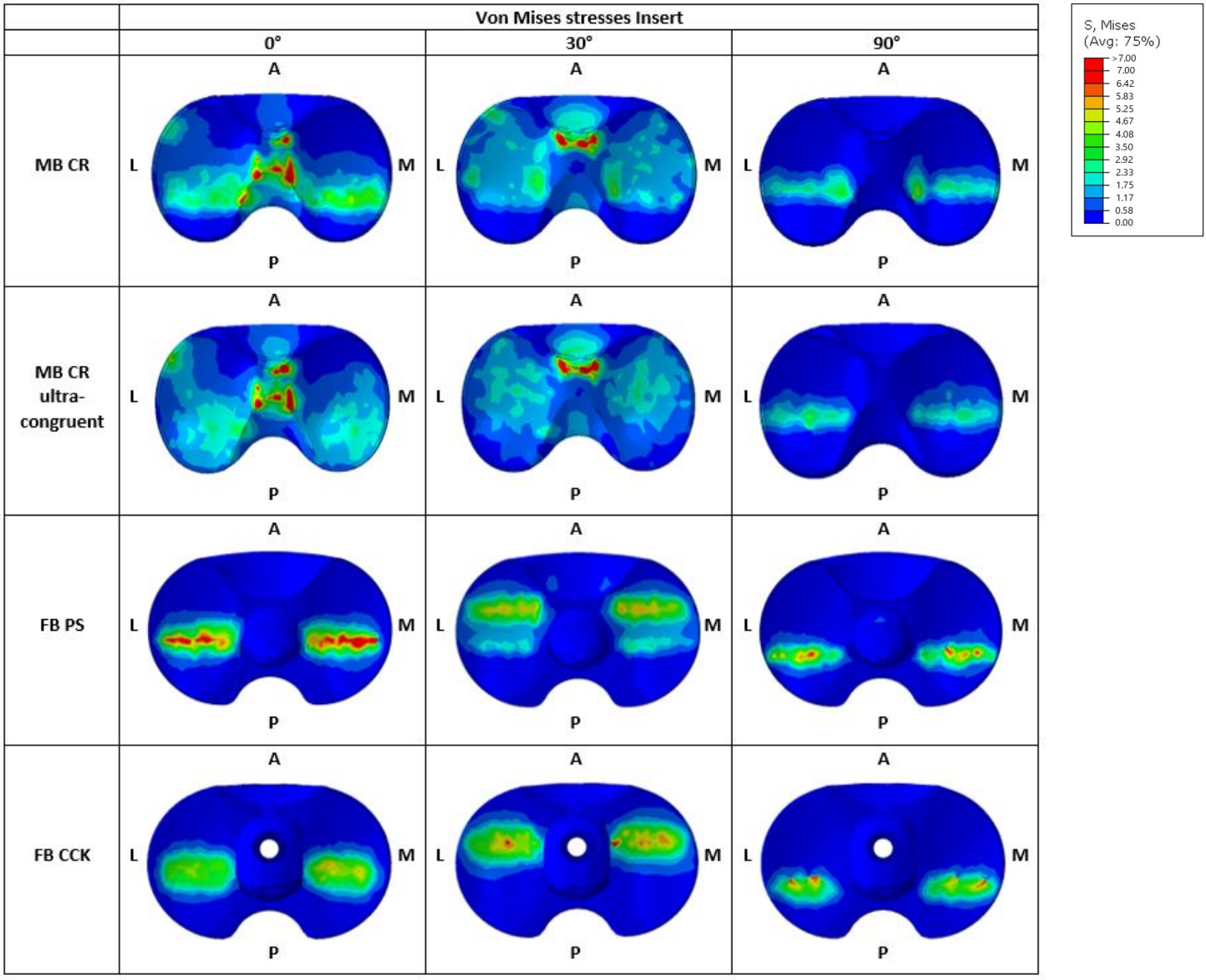

Figure 7.8: Graphical overview of the von Mises stress in the insert for all the considered models in the three different configurations: full-extension (0° of flexion); gait (30° of flexion) and chair-rise (90° of flexion). A=anterior; P=posterior; M=medial; L=lateral.

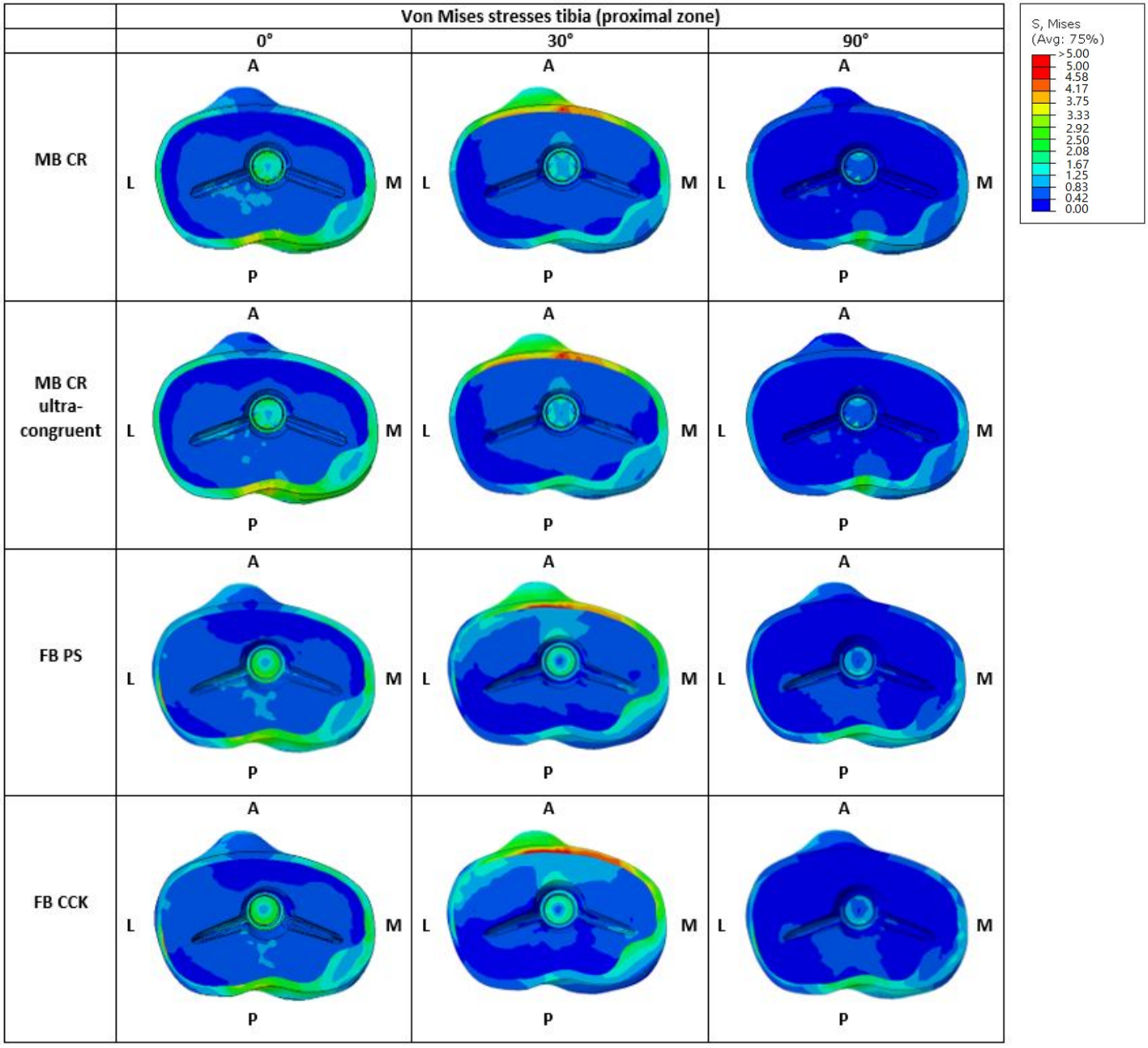

Figure 7.9: Graphical overview of the von Mises stress taken by the tibia in the proximal zone for all the considered models in the three different configurations: full-extension (0° of flexion); gait (30° of flexion) and chair-rise (90° of flexion). A=anterior; P=posterior; M=medial; L=lateral.

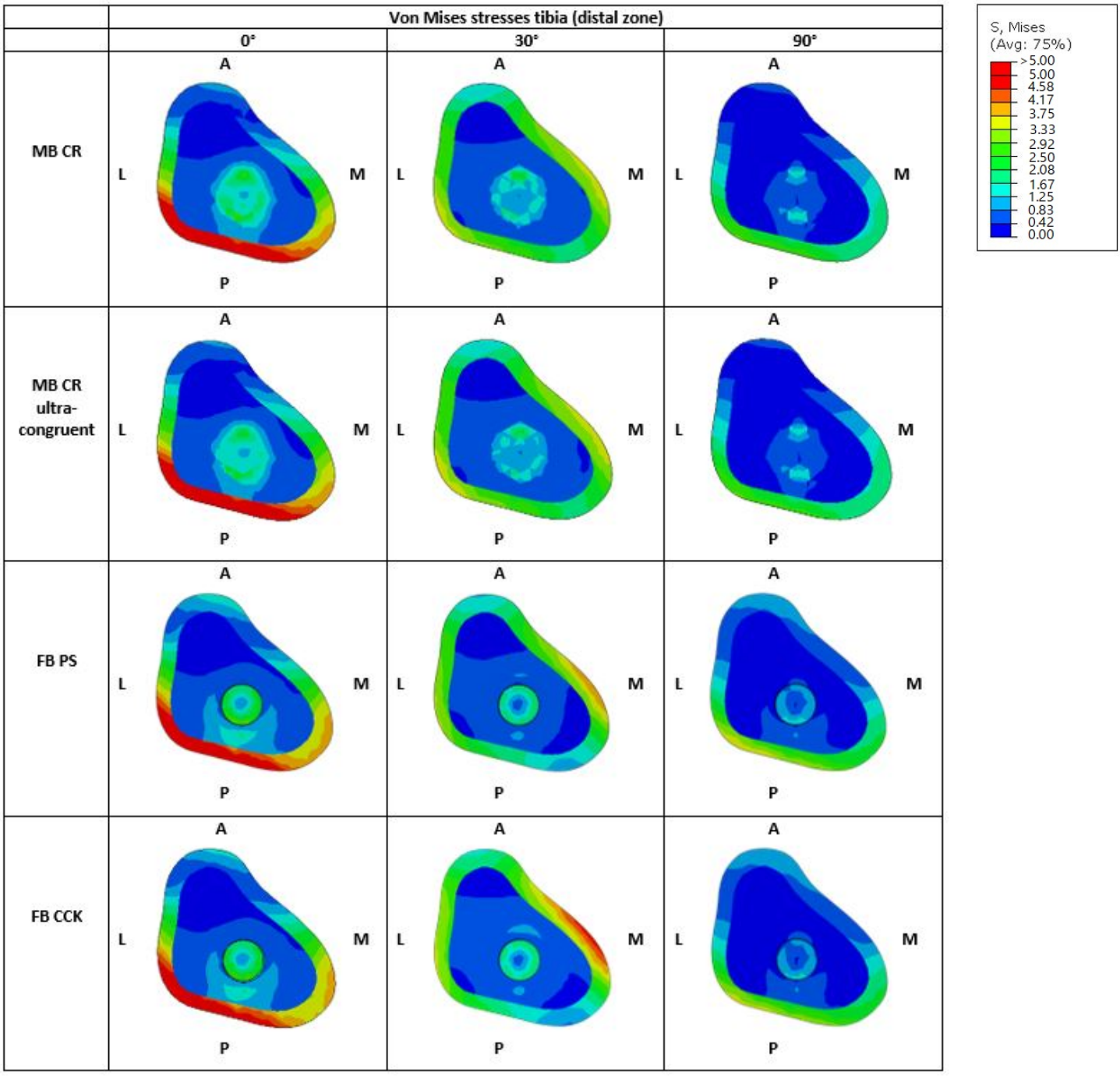

Figure 7.10: Graphical overview of the von Mises stress taken by the tibia in the distal zone for all the considered models in the three different configurations: full-extension (0° of flexion); gait (30° of flexion) and chair-rise (90° of flexion). A=anterior; P=posterior; M=medial; L=lateral.

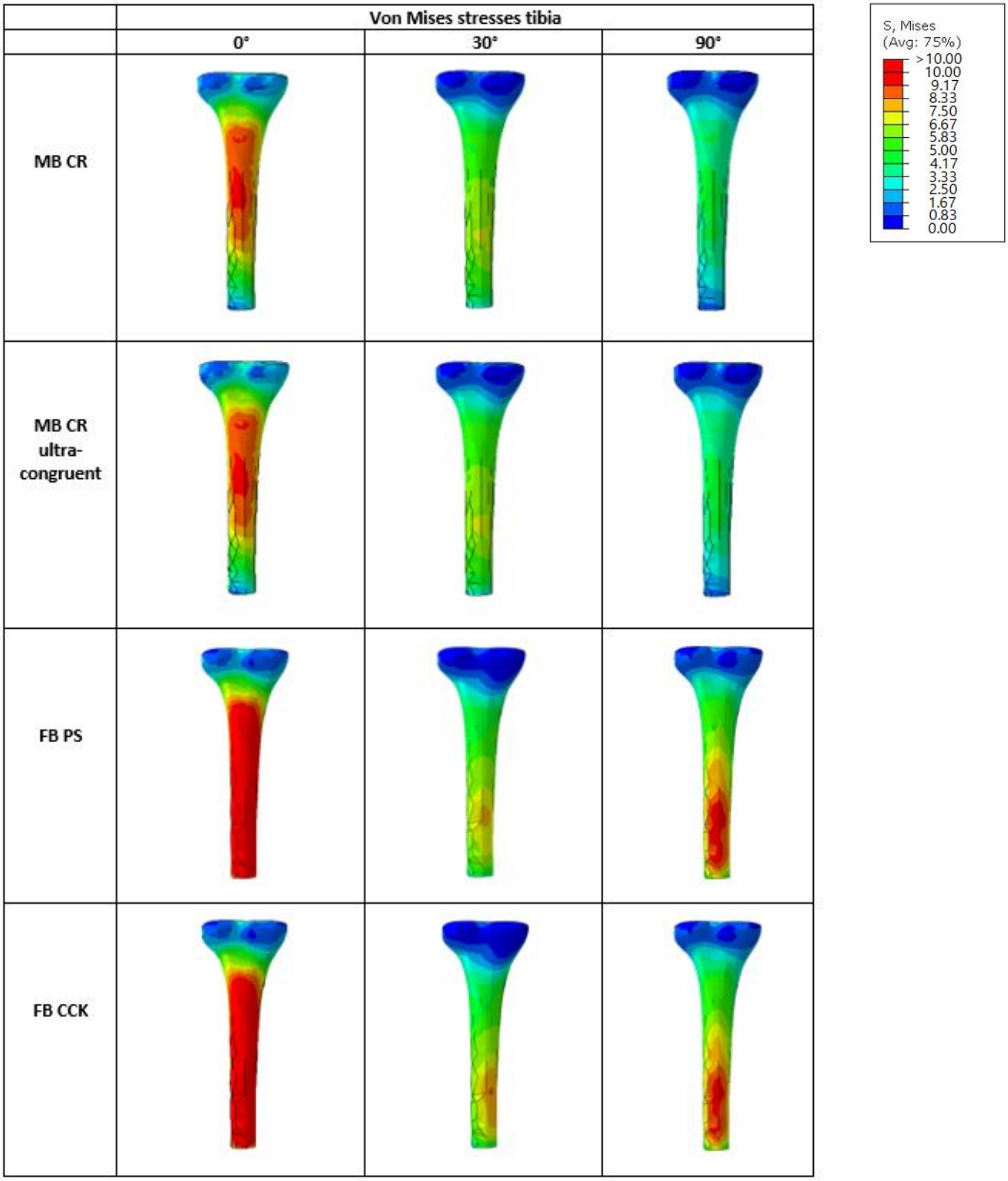

Figure 7.11: Graphical overview of the von Mises stress along the tibial bone for all the considered models in the three different configurations: full-extension (0° of flexion); gait (30° of flexion) and chair-rise (90° of flexion). A=anterior; P=posterior; M=medial; L=lateral.

7.2.1 von Mises stresses taken by the insert

As it can be seen in Figure 7.8, the middle regions of both mobile bearing inserts present peak values (up to 40 [MPa]). The majority of the insert is submitted to stress for those models in the full-extension and gait configuration. Regarding the fixed bearing models in the full-extension configuration, the stress is distributed symmetrically on both medial and lateral center part of the insert. The proportion of insert subjected to stress for the fixed bearing models becomes more important in the gait configuration compared to the previous one. In the chair-rise configuration, this one is less important than in the two previous configurations. Furthermore, the stress location changes with the configuration, becoming more anterior in the gait configuration and more posterior in the chair-rise configuration. The chair-rise configuration present the lowest contact areas among the different configurations, with similar contact areas for all the models. For both mobile bearing models, the stress is distributed at the center part of the insert whereas for the fixed bearing models, the stress is located more posteriorly. The highest stress values are found for the fixed bearing PS model in the full-extension configuration.

7.2.2 von Mises stresses taken by the tibia in the proximal zone

As it can be seen in Figure 7.9, for all the models in the full-extension configuration, the stress distribution is similar and mainly located on the cortical bone. In the gait configuration, the stress is also mainly distributed on the cortical bone with the highest values located on the anterior part of the cortical tibia. In the last configuration, the stress is mainly situated on the posterior part of the cortical tibia with the anterior part quite not subjected to stress.

In the proximal part of the tibia, the highest stress values are observed in the gait configuration in the anterior cortical zone. Furthermore, it is the cortical bone that is taking the majority of the stress.

7.2.3 von Mises stresses taken by the tibia in the distal zone

As it can be seen in Figure 7.10, in the full-extension configuration, all the models present a similar distribution of stress, with the highest stress values located in the posterior part of the cortical bone. In the gait configuration, the stress is uniformly distributed in the cortical distal tibia for both mobile bearing models. In this configuration, the stress distribution is also similar for the fixed bearing models with a peak of stress located on the medial cortical part. In the chair-rise configurations, for all the models, it is the posterior part of the cortical tibia that is taking the most of the stress.

7.2.4 von Mises stresses taken along the tibia

As it can be seen in Figure 7.11, in each configuration, both mobile bearing models exhibit a very similar stress distribution along the tibial bone. This tendency is also observed for the fixed bearing models. Both mobile bearing models in the full-extension configuration present the same stress distribution, with the stress being very low in the proximal zone and progressively increasing to become high in the distal zone and then decreasing to become very low at the end of the tibial bone. For the fixed bearing models in the full-extension configuration, the stress distribution varies along the tibia, being very low in the proximal zone, slightly higher in the distal zone and very high from the end of the distal zone to the end of the tibia. The stress distribution is practically the same for both mobile bearing models in the gait and chair-rise configuration, with a very low stress concentration the proximal zone and the stress being uniformely distributed along the rest of the tibial bone. A similar same stress distribution is observed in the case of the fixed bearing models in the gait configuration but with a concentration of stress slightly higher at the end of the tibial bone. For the fixed bearing models in the chair-rise configuration, the stress is very low in the proximal zone and slightly higher in the distal zone, then progressively increasing from the end of the distal zone to the end of the tibia to become very high at end of the tibial bone. When Increasing the level of constraint: going from the mobile bearing models (less constrained) to the fixed bearing models (more constrained), higher stress values are observed along the tibial bone.

Chapter 8

Validation, limitations and comparison with previous studies

8.1 Limitations

The soft-tissues such as the muscles were not implemented in the different models but were considered when applying the loading conditions.
The ligaments were modeled as beams which is a common approach in the literature and in previously validated ligaments models [68]. All the material models (bony structures as well as the soft tissues) were assumed to be linear elastic and homogeneous even though the cortical and cancellous bone present spatial inhomogeneity in their properties [78]. Another simplification of the study was to consider the behavior of the polyethylene as linear elastic without taking into account the plastic region. The local value of stress could be overestimated under plasticization [75].

The material properties considered for both cortical and cancellous bones correspond to those of an healthy bone and the alteration due to osteoporosis was not taken into account. Moreover, the bone models didn't take in consideration any variation of the bone anatomy and bone deformity that could alter the final TKA outcome [79], [80]. However, this approach is commonly used when modeling clinical situations in the biomechanical field [67], [75], [81], [82].

In this study, the positioning and the alignement of the prosthetic components were assumed to be ideal during the simulations, ignoring the possible post-operative misalignments occurring during TKA surgeries [83]. The tibio-femoral position should also be taken into account in the output as it greatly influences the kinematics of the prosthetic knee and modify the obtained results.

Nevertheless, the main aim of this study was to compare the different levels of constraint in the various loading conditions fixing all the parameters and using the same approach. Consequently, those limitations should not be considered as an issue.

8.2 Validation and comparison with previous studies

This study is difficult to compare with the literature. Indeed, similar stress distributions can be highlighted, but one must be careful when comparing the values due to the possible difference in the materials models, considered material properties, loading and boundary conditions, studied configurations and prosthetic implant which may present a different topology due to the company's specific design features.

The von Mises stresses taken by the cortical tibia in the proximal and distal zone for the MB CR knee stay in the same range of values as those obtained in a previous study [67]. The stress distribution observed on the proximal region of the tibia for the FB PS in the full-extension configuration is compatible with the one obtained in another literature study [63], with the majority of the stress taken by the cortical tibia. In another paper [70], similar contact areas are found for the MB CR ultracongruent knee and the FB PS knee. This one exhibits the same tendency with very high average contact areas for the MB CR ultraconguent model and lower ones for the FB PS knee. In a previous litterature study [75], different stress distributions are found in the proximal region of the tibia and on the insert in the case of a MB CR knee in the full-extension configuration. In opposition to the results obtained in this work, the stress is not distributed symmetrically on the medial and lateral part of the insert, being more anterior in the medial part and presenting higher values. Additionally, the stress distribution on the proximal region of the tibia is not symmetrical, covering a larger medial region and being more important on the cancellous bone compared to the cortical tibial bone.

Chapter 9

Conclusions

The purpose of this study was to compare the biomechanical behaviour of four total knee prostheses with different levels of constraints in a patient-specific TKA using finite element analysis and validate/invalidate the choice of implant made by the surgeon *Gianluca Castellarin* for this patient. The knee joint of the patient was modeled with the four different types of prostheses in three configurations (full-extension, gait and chair-rise) and finite element simulations were carried on those models. The output extracted and the results analyzed from those simulations include the contacts areas on the insert, the von Mises stresses taken by the insert and by the tibia (in different regions).

The conclusions that can be deduced of the results are the followings.
Of all the models in the different configurations, the mobile bearing models present the best constraints regarding all the studied parameters with respect to the other models. In addition, the difference in the average stress values between both mobile bearing models, or between both fixed bearing models is insignificant. The first relevant difference is observed between the mobile and fixed bearing models. The position of the contact points and the contact areas are significantly different between the mobile and fixed models in the different loading conditions but remain acceptable. Moreover, the different models exhibit a symmetrical medial and lateral distribution of the contact areas, which is not always the case. In each configuration, the distribution of the stress on the different zones of the tibia (proximal, distal, cortical, total) is relatively homogeneous between the models. Changing the prosthetic implant would therefore not induce a big variation of the stress distribution in the different regions of the tibial bone. However, it would significantly change the distribution of stress at the interface between the prosthetic components (tibial insert and femoral component).

Based on the von Mises stresses taken by the prostheses's components and the tibia, the mobile bearing cruciate retaining knee is the best implant option which corresponds to the prosthesis implanted on the patient by the surgeon *Gianluca Castellarin*. The result of the study confirms that the choice made by the surgeon to preserve the PCL and rely on it to ensure the stability of the knee was the best one.

Chapter 10

Annex

10.1 Mobile bearing cruciate retaining knee (normal and ultracongruent)

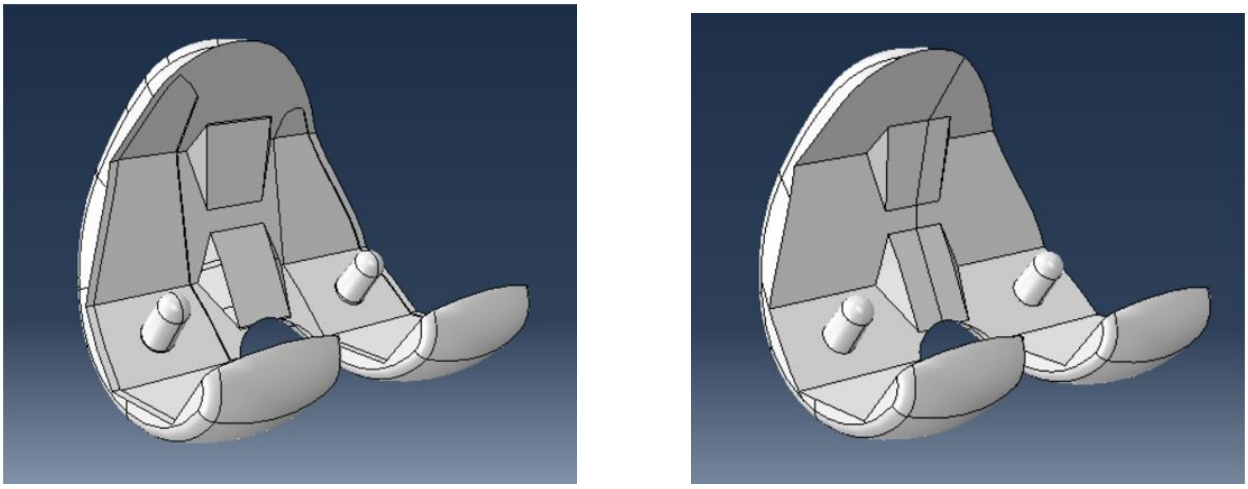

(a) (b)

Figure 10.1: Mobile bearing cruciate retaining knee - femoral component: a) before - b) after the refinement of the geometry

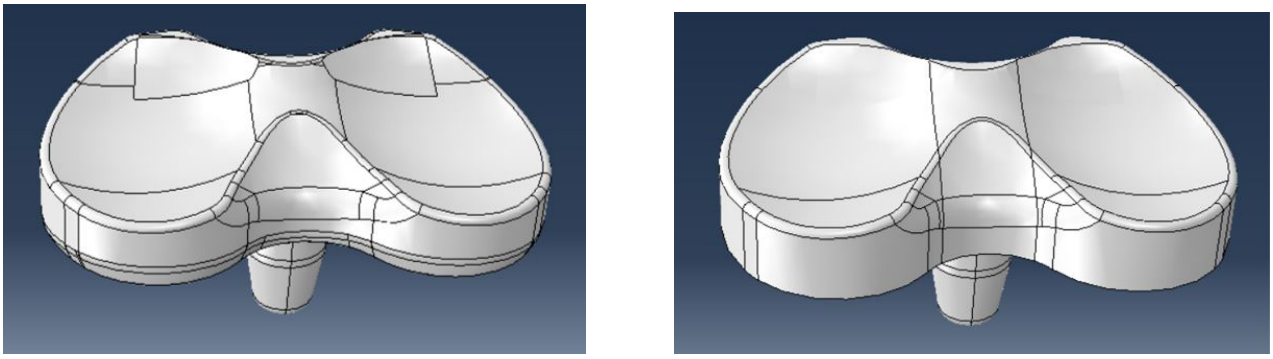

(a) (b)

Figure 10.2: Mobile bearing cruciate retaining knee - insert: a) before - b) after the refinement of the geometry

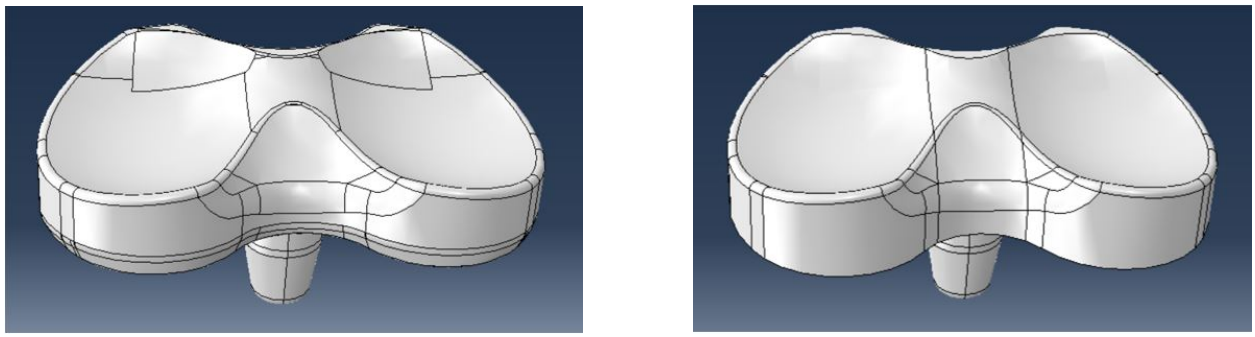

(a) (b)

Figure 10.3: Mobile bearing cruciate retaining ultracongruent knee - insert: a) before - b) after the refinement of the geometry

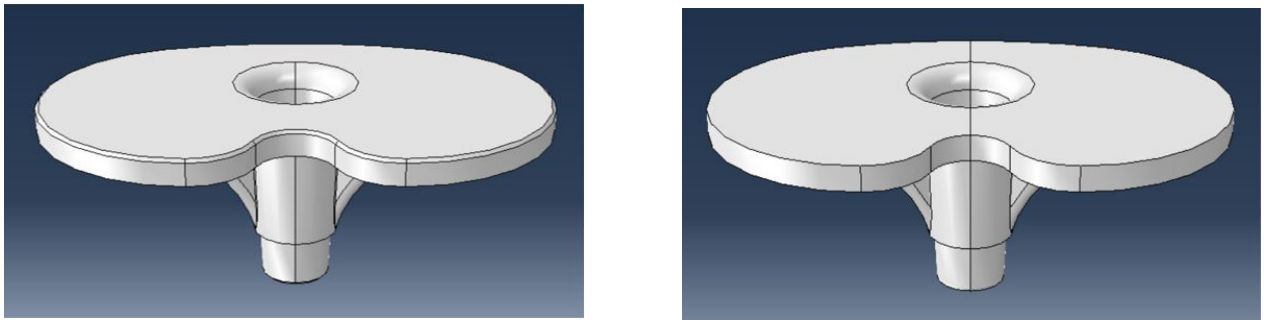

(a) (b)

Figure 10.4: Mobile bearing cruciate retaining knee - tibial tray: a) before - b) after the refinement of the geometry

10.2 Fixed bearing posterior stabilized knee

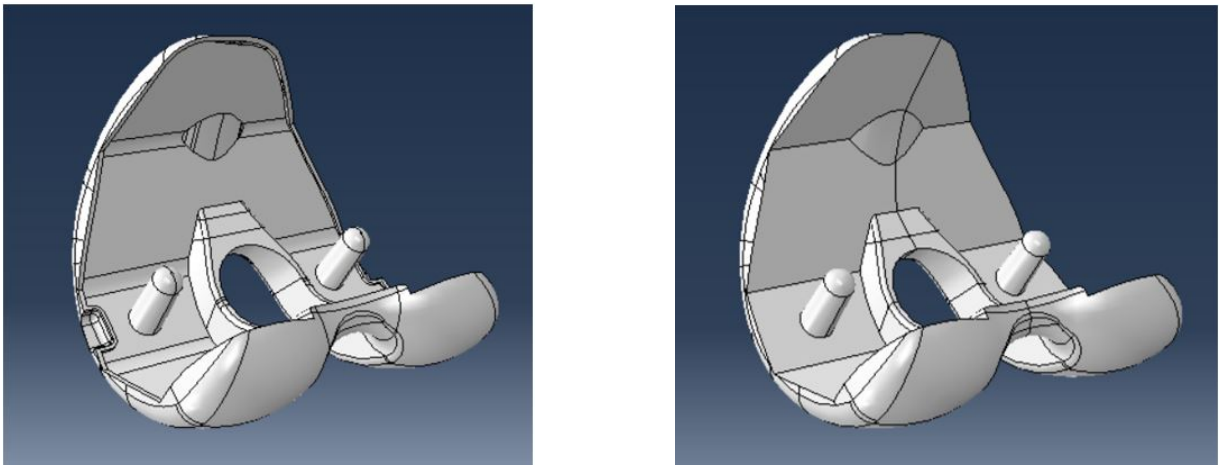

(a) (b)

Figure 10.5: Fixed bearing posterior stabilized knee - femoral component: a) before - b) after the refinement of the geometry

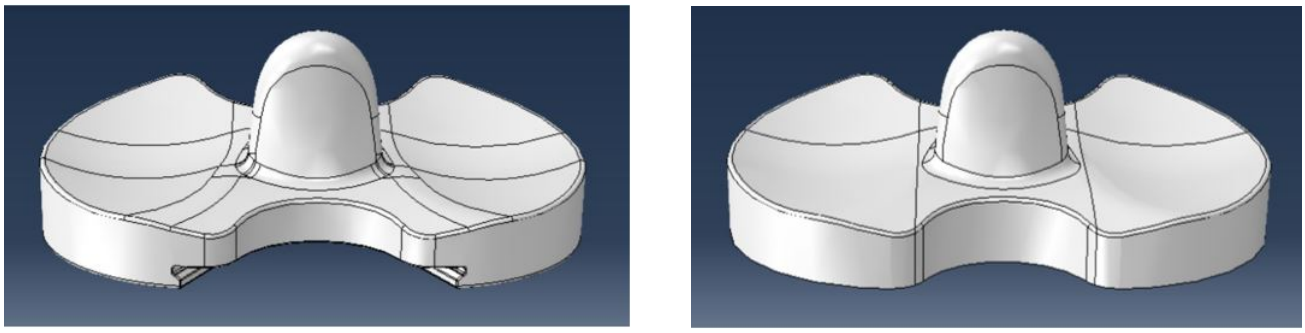

(a) (b)

Figure 10.6: Fixed bearing posterior stabilized knee - insert: a) before - b) after the refinement of the geometry

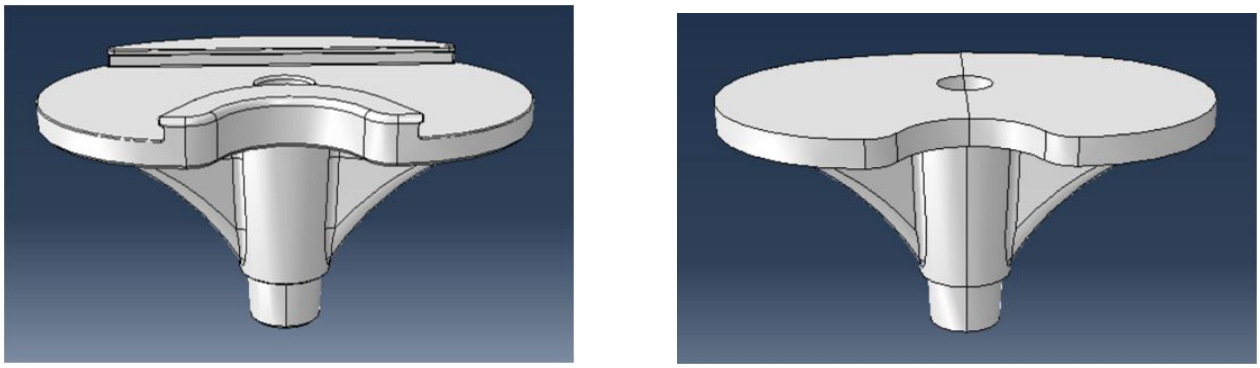

(a) (b)

Figure 10.7: Fixed bearing posterior stabilized knee - tibial tray: a) before - b) after the refinement of the geometry

10.3 Fixed bearing constrained condylar knee

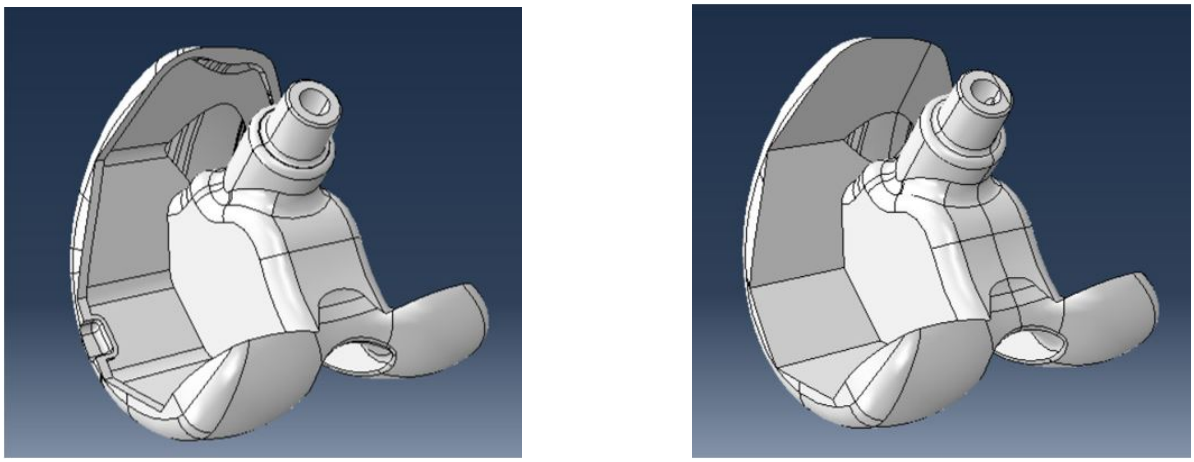

(a) (b)

Figure 10.8: Fixed bearing constrained condylar knee - femoral component: a) before - b) after the refinement of the geometry

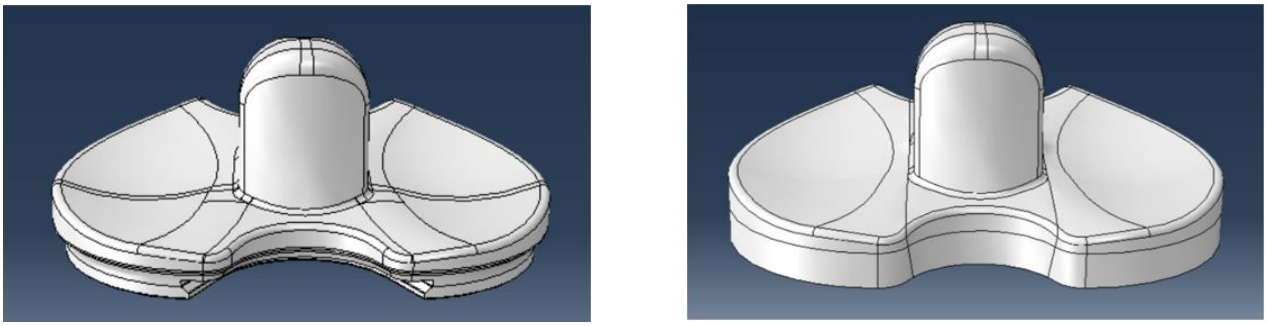

(a) (b)

Figure 10.9: Fixed bearing constrained condylar knee - insert: a) before - b) after the refinement of the geometry

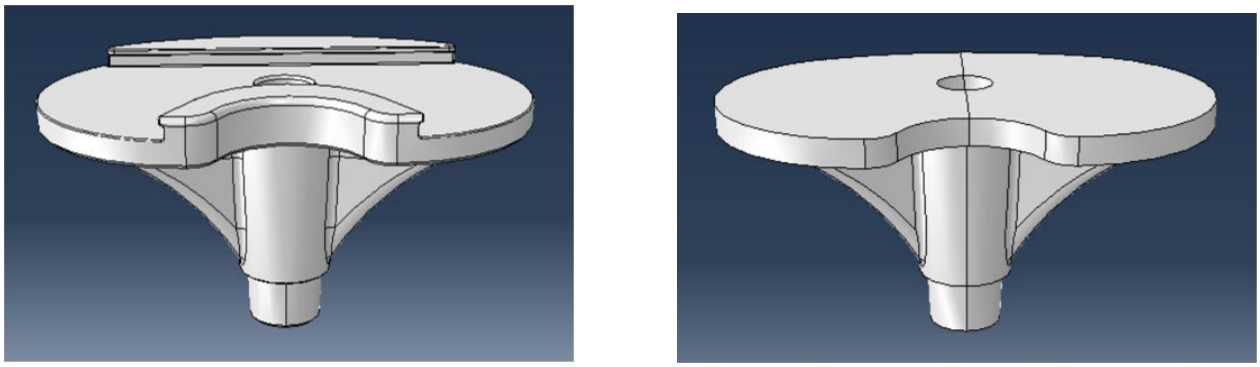

(a) (b)

Figure 10.10: Fixed bearing constrained condylar knee - tibial tray: a) before - b) after the refinement of the geometry

10.4 Model of the femur

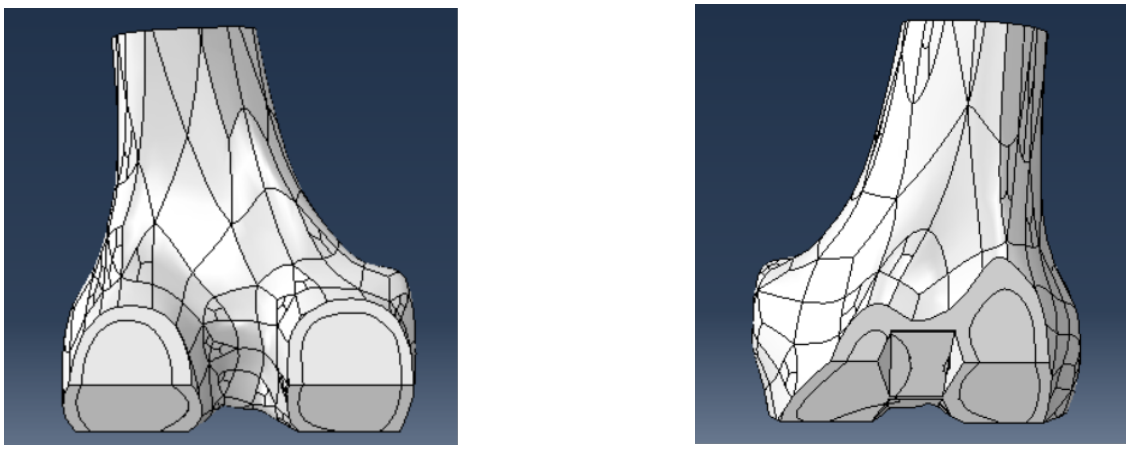

(a) Posterior view of the femur (b) Anterior view of the femur

Figure 10.11: Femur model

10.5 Model of the tibia

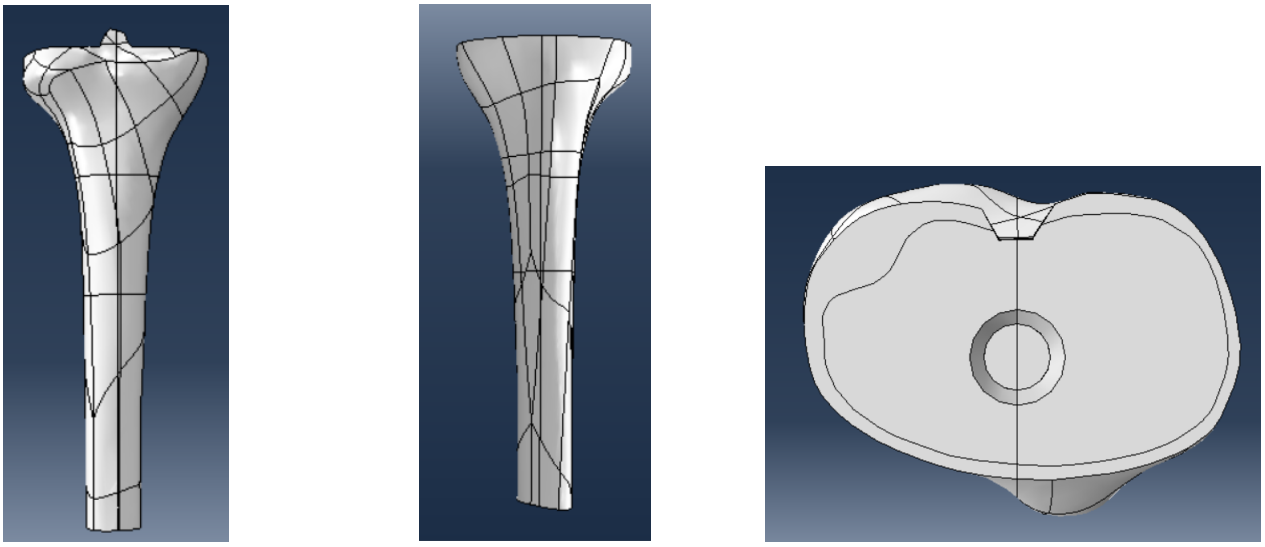

(a) Posterior view of the tibial model

(b) Anterior view of the tibial model

(c) Superior view of the tibial model

Figure 10.12: Tibia model

Bibliography

[1] Chloe Wilson. *Knee Joint Anatomy Motion - Knee Pain Explained*. 2020. URL: https://www.knee-pain-explained.com/knee-joint-anatomy.html.

[2] : Lorenzo Crumbie. *Femur*. 2021. URL: https://www.kenhub.com/en/library/anatomy/femur.

[3] *epicondyle definition anatomy*. 2019. URL: https://gentleforindustrial.blogspot.com/2019/02/epicondyle-definition-anatomy.html.

[4] Bernardo Innocenti. *Orthopaedic Biomechanics: Knee Biomechanics*. 2020.

[5] Uldis Zariņš. *Tibia*. 2021. URL: https://anatomy.net/tibia.

[6] *Atlas of anatomy 25 knee leg*. 2015. URL: https://doctorlib.info/medical/anatomy/27.html.

[7] Colleens Travers. *The Anatomy of the Patella*. 2020. URL: https://www.verywellhealth.com/patella-anatomy-function-and-treatment-4768658#:~:text=%20The%20Anatomy%20of%20the%20Patella%20%201,particularly%20in%20those%20who%20are%20extremely...%20More%20.

[8] Aaron Cassidy. *The Pantella*. 2020. URL: https://teachmeanatomy.info/lower-limb/bones/patella/.

[9] *Patella anatomy*. 2021. URL: https://www.registerednursern.com/patella-anatomy/.

[10] Karola Messner and Jizong Gao. "The menisci of the knee joint. Anatomical and functional characteristics, and a rationale for clinical treatment". In: *Journal of anatomy* 193.2 (1998), pp. 161–178.

[11] Eleftherios A Makris, Pasha Hadidi, and Kyriacos A Athanasiou. "The knee meniscus: structure–function, pathophysiology, current repair techniques, and prospects for regeneration". In: *Biomaterials* 32.30 (2011), pp. 7411–7431.

[12] Arun Pal Singh. *Knee Anatomy and Significance — Bone and Spine*. 2021. URL: https://boneandspine.com/knee-anatomy/.

[13] Chloe Wilson. *Knee Ligaments : Anatomy, Function Injuries - Knee Pain Explained*. 2021. URL: https://www.knee-pain-explained.com/knee-ligaments.html.

[14] Savio LY Woo et al. "Biomechanics of knee ligaments". In: *The American journal of sports medicine* 27.4 (1999), pp. 533–543.

[15] Ritvik Verma. *What is Lateral Collateral Ligament (LCL)? Where is the LCL located?* 2021. URL: https://physio-study.com/lateral-collateral-ligament-anatomy-and-biomechanics/.

[16] Ritvik Verma. *What is the Medial Collateral Ligament (MCL)?* 2021. URL: https://physio-study.com/medial-collateral-ligament-anatomy-and-biomechanics/.

[17] *Anterior cruciate ligament (acl)*. 2021. URL: https://www.physio-pedia.com/Anterior_Cruciate_Ligament_(ACL).

[18] *The Anatomy and Biomechanics of The Posterior Cruciate Ligament*. 2021. URL: https://physio-study.com/posterior-cruciate-ligament-anatomy-and-biomechanics/.

[19] AAOS. *Combined Knee Ligament Injuries - OrthoInfo - AAOS*. 2014. URL: https://orthoinfo.aaos.org/en/diseases--conditions/combined-knee-ligament-injuries.

[20] Jonathan Cluett. *A Patellar Tendon Tear Can Sideline an Athlete for a Long Time*. 2020. URL: https://www.verywellhealth.com/treatment-of-a-patellar-tendon-tear-2549591#:~:text=The%20patellar%20tendon%20is%20the%20structure%20that%20connects,people%20refer%20to%20this%20as%20the%20patellar%20ligament.

[21] Jana Vasković. *Quadriceps femoris muscle*. 2021. URL: https://www.kenhub.com/en/library/anatomy/the-quadriceps-femoris-muscle.

[22] Paul Roger. *How to Stretch and Strengthen Your Hamstrings*. 2021. URL: https://www.verywellfit.com/hamstring-muscle-anatomy-and-stretches-3498372.

[23] David Keil. *Suffering from a hamstring injury?* 2014. URL: https://www.yoganatomy.com/hamstrings-group-muscles-yoga-anatomy/.

[24] Jason Ray Brown and Lynda Sing. *Muscle Anatomy for Yoga: The Quadriceps*. 2016. URL: http://www.asfyt.com/blog/muscle-anatomy-the-quadriceps.

[25] Jenni Tarma. *Upper Hamstring Tendinopathy Treatment - Yoga Medicine*. 2018. URL: https://yogamedicine.com/upper-hamstring-tendinopathy/.

[26] SD Masouros, AMJ Bull, and AA Amis. "(i) Biomechanics of the knee joint". In: *Orthopaedics and Trauma* 24.2 (2010), pp. 84–91.

[27] *Screw home mechanism of the knee joint*. 2021. URL: https://www.physio-pedia.com/Screw_Home_Mechanism_of_The_Knee_Joint.

[28] MUSCULOSKELETAL MEDICINE. *Kinematics of the Natural and Replaced Knee*. 2016. URL: https://musculoskeletalkey.com/kinematics-of-the-natural-and-replaced-knee/.

[29] Prashant Komdeur, Fabian E Pollo, and Robert W Jackson. "Dynamic knee motion in anterior cruciate impairment: a report and case study". In: *Baylor University Medical Center Proceedings*. Vol. 15. 3. Taylor & Francis. 2002, pp. 257–259.

[30] *Lower Limb Alignment*. 2020. URL: https://radiologykey.com/lower-limb-alignment/.

[31] Hamidreza Yazdi et al. "Anatomical axes of the proximal and distal halves of the femur in a normally aligned healthy population: implications for surgery". In: *Journal of orthopaedic surgery and research* 13.1 (2018), pp. 1–8.

[32] UFO Themes. *1 Physiological axes of the lower limb*. URL: https://musculoskeletalkey.com/1-physiological-axes-of-the-lower-limb/.

[33] F Gottschalk, S Kourosh, and M Stills. *Mechanical and anatomic axes of nor — OP Digital Resource Library*. 1989. URL: http://www.oandplibrary.org/popup.asp?frmItemId=92F15493-6EC6-4D13-8197-025F35E3B4A0&frmType=image&frmId=1.

[34] C Daw. *What Is the Difference between Valgus and Varus Deformity?* 2021. URL: https://www.infobloom.com/what-is-the-difference-between-valgus-and-varus-deformity.htm.

[35] Gerard A Engh. "The difficult knee: severe varus and valgus." In: *Clinical Orthopaedics and Related Research (1976-2007)* 416 (2003), pp. 58–63.

[36] *Valgus vs varus knee alignment*. 2021. URL: https://www.allhealthpost.com/valgus-vs-varus/.

[37] Ballis R Neyret P Lustig S Gaillard R Shabani B. "Anatomy, Physiology, and Biomechanics of the Native Knee". In: *Total Knee Arthroplasty* (2015), pp. 1–25.

[38] Karthik Kumar. *What Is Total Knee Arthroplasty (TKA)?* 2020. URL: https://www.medicinenet.com/what_is_total_knee_arthroplasty_tka/article.htm.

[39] *Knee Replacement Surgery Procedure*. 2021. URL: https://www.hopkinsmedicine.org/health/treatment-tests-and-therapies/knee-replacement-surgery-procedure.

[40] CB Physiotherapy. *What is Total Knee Replacement(TKR)? Symptoms, Causes, Diagnosis Physiotherapy Treatment of Total Knee Replacement(TKR)*. 2021. URL: https://cbphysiotherapy.in/condition/total-knee-replacementtkr.

[41] Carol Eustice. *How to Cope With the Symptoms of Degenerative Arthritis*. 2021. URL: https://www.verywellhealth.com/what-is-degenerative-arthritis-189342#:~:text=%20An%20Overview%20of%20Degenerative%20Arthritis%20%201,certainty%20based%20on%20a%20review%20of...%20More%20.

[42] *rheumatoid arthritis - symptoms and causes*. 2021. URL: https://www.mayoclinic.org/diseases-conditions/rheumatoid-arthritis/symptoms-causes/syc-20353648.

[43] Seth S Leopold. "Minimally invasive total knee arthroplasty for osteoarthritis". In: *New England Journal of Medicine* 360.17 (2009), pp. 1749–1758.

[44] Jared Foran. *Arthritis of the Knee - OrthoInfo - AAOS*. 2021. URL: https://orthoinfo.aaos.org/en/diseases--conditions/arthritis-of-the-knee/.

[45] Brian Hatten. *The Knee Prosthesis: The different types*. 2016. URL: https://www.mykneeguide.com/the-knee/the-knee-prosthesis.

[46] Paul Mammer. *Knee Replacement Implants - OrthoInfo - AAOS*. 2016. URL: https://orthoinfo.aaos.org/en/treatment/knee-replacement-implants/.

[47] Bernardo Innocenti. *Medical Devices Total: Knee Arthroplasty*. 2020.

[48] Jeffrey J. Cherian Bhaveen H. Kapadia et al. "Mechanical, anatomical, and kinematic axis in TKA: concepts and practical applications." In: *Current reviews in musculoskeletal medicine* 7.2 (2014), pp. 89–95.

[49] Bert Parcells. *TKA - PRIMARY DESIGN — Hip Knee Book*. 2016. URL: https://hipandkneebook.com/tka-implants/2017/3/15/tka-primary-design.

[50] Vittorio Calvisi et al. "Cruciate-Retaining Total Knee Arthroplasty". In: *Primary Total Knee Arthroplasty* (2018), p. 23.

[51] Morey Vivek Machhindra et al. “Functional outcomes of a new mobile-bearing ultra-congruent TKA system: comparison with the posterior stabilized system”. In: *The Journal of arthroplasty* 30.12 (2015), pp. 2137–2142.

[52] Frank R Kolisek et al. “Posterior-stabilized versus posterior cruciate ligament-retaining total knee arthroplasty”. In: *The Iowa orthopaedic journal* 29 (2009), p. 23.

[53] Takatomo Mine et al. “Kinematic analysis of posterior-stabilized total knee arthroplasty during standing up from and sitting down on a chair”. In: *Journal of orthopaedic surgery and research* 11.1 (2016), pp. 1–6.

[54] Fabio Orozco and Alvin Ong. “Posterior stabilized total knee arthroplasty”. In: *Recent advances in hip and knee arthroplasty* (2012).

[55] P Cholewinski et al. “Long-term outcomes of primary constrained condylar knee arthroplasty”. In: *Orthopaedics & Traumatology: Surgery & Research* 101.4 (2015), pp. 449–454.

[56] Luigi Sabatini et al. “Condylar constrained system in primary total knee replacement: our experience and literature review”. In: *Annals of translational medicine* 5.6 (2017).

[57] *Klinikum solingen: gelenkersatz knie - endoprothetikzentrum — klinikum solingen*. 2021. URL: https://www.klinikumsolingen.de/medizin/zentren/endoprothetikzentrum/gelenkersatz-knie/.

[58] MVZ Gelenk-Klinik and Ostermeier Partner Ärzte-Partnerschaft MVZ Gelenk-Klinik Dres Schneider. *Fixed vs Mobile Bearing Prosthesis — Joint-surgeon.com*. 2012. URL: https://www.joint-surgeon.com/orthopedic-services/knee/total-replacement-knee-types-of-procedures.

[59] PJC Heesterbeek et al. “Superior long-term survival for fixed bearing compared with mobile bearing in ligament-balanced total knee arthroplasty”. In: *Knee Surgery, Sports Traumatology, Arthroscopy* 26.5 (2018), pp. 1524–1531.

[60] Dr. Khokhar. *Cemented and Cementless Knee Replacement*. URL: https://www.cortho.org/knee/cemented-and-cementless-knee-replacement/.

[61] Lützner C. Beyer F. et al. Postler A. “Analysis of Total Knee Arthroplasty revision causes”. In: *BMC Musculoskelet Disord* 19.55 (2018).

[62] AAOS. *Revision Total Knee Replacement - OrthoInfo - AAOS*. URL: https://orthoinfo.aaos.org/en/treatment/revision-total-knee-replacement.

[63] Bernardo Innocenti, Gusztáv Fekete, and Silvia Pianigiani. “Biomechanical analysis of augments in revision total knee arthroplasty”. In: *Journal of biomechanical engineering* 140.11 (2018).

[64] James A.Rand MD. “MODULAR AUGMENTS IN REVISION TOTAL KNEE ARTHROPLASTY”. In: *Orthopedic Clinics of North America* 29.2 (2005), pp. 347–353.

[65] D.Leonett D.Tigani S.Comitini. “Revision total knee arthroplasty (TKA)”. In: *Surgical Techniques in Total Knee Arthroplasty and Alternative Procedures* (2015), pp. 229–242.

[66] Giorgio Burastero et al. “Use of porous custom-made cones for meta-diaphyseal bone defects reconstruction in knee revision surgery: a clinical and biomechanical analysis”. In: *Archives of Orthopaedic and Trauma Surgery* 140.12 (2020), pp. 2041–2055.

[67] Gianluca Castellarin, Silvia Pianigiani, and Bernardo Innocenti. "Asymmetric polyethylene inserts promote favorable kinematics and better clinical outcome compared to symmetric inserts in a mobile bearing total knee arthroplasty". In: *Knee Surgery, Sports Traumatology, Arthroscopy* 27.4 (2019), pp. 1096–1105.

[68] Bernardo Innocenti et al. "Load sharing and ligament strains in balanced, overstuffed and understuffed UKA. A validated finite element analysis". In: *The Journal of arthroplasty* 29.7 (2014), pp. 1491–1498.

[69] Bernardo Innocenti et al. "Biomechanical effects of different varus and valgus alignments in medial unicompartmental knee arthroplasty". In: *The Journal of arthroplasty* 31.12 (2016), pp. 2685–2691.

[70] Bernardo Innocenti. "High congruency MB insert design: stabilizing knee joint even with PCL deficiency". In: *Knee Surgery, Sports Traumatology, Arthroscopy* 28.9 (2020), pp. 3040–3047.

[71] Nigrelli V Tumino V Ricotta V Ingrassia T Nalbone L. "Finite element analysis of two total knee prostheses". In: *Interact Des Manuf* 7.2 (2013), pp. 91–101.

[72] Lewis G Sarathi Kopparti P. "Influence of three variables on the stresses in a three-dimensional model of a proximal tibia-total knee implant construct". In: *Biomed Mater Eng* 17.1 (2007), pp. 19–28.

[73] Bernardo Innocenti et al. "Investigation on the effects induced by TKA features on tibio-femoral mechanics part I: femoral component designs". In: *Journal of mechanics in medicine and biology* 15.02 (2015), p. 1540034.

[74] Silvia Pianigiani et al. "Investigation on the effects induced by TKA features on tibio-femoral mechanics part II: tibial insert designs". In: *Journal of Mechanics in Medicine and Biology* 15.02 (2015), p. 1540035.

[75] Bernardo Innocenti, Johan Bellemans, and Fabio Catani. "Deviations from optimal alignment in TKA: is there a biomechanical difference between femoral or tibial component alignment?" In: *The Journal of arthroplasty* 31.1 (2016), pp. 295–301.

[76] Fanciullacci N Labey L Fuchs-Winkelmann S Innocenti B El-Zayat BF Heyse TJ. "Fixation techniques and stem dimensions in hinged total knee arthroplasty: a finite element study". In: *Arch Orthop Trauma Surg* 136.12 (2016), pp. 1741–1752.

[77] *Implants for surgery. Wear of total knee-joint prostheses; Part 1: Loading and displacement parameters for wear-testing machines with load control and corresponding environmental conditions for test.* Standard. Geneva, CH: International Organization for Standardization, Nov. 2009.

[78] Lewis G Sarathi Kopparti P. "Influence of three variables on the stresses in a three-dimensional model of a proximal tibia-total knee implant construct". In: *Biomed Mater Eng* 17.1 (2007), pp. 19–28.

[79] Wilkinson M Barroso-Rosa S Hazratwala K Matthews B. "Total knee arthroplasty in patients with extra-articular deformity". In: *Arthroplast Today* 2.1 (2016), pp. 26–36.

[80] Ferrara MS Chamnongkich S Kinsey T-Mahoney OM Wang H Simpson KJ. "Biomechanical differences exhibited during sit-to-stand between total knee arthroplasty designs of varying radii". In: *J Arthroplast* 21.8 (2006), pp. 1193–1199.

[81] De Corte R Labey L Innocenti B Soenen M Baracchi M. "Stemmed TKA in a femur with a total hip arthroplasty: is there a safe distance between the stem tips?" In: *J Arthroplasty* 28.8 (1996), pp. 1437–1445.

[82] De Corte R Labey L Innocenti B Soenen M Baracchi M. "All-polyethylene tibial components generate higher stress and micromotions than metal-backed tibial components in total knee arthroplasty". In: *Knee Surg Sports Traumatol Arthrosc* 24.8 (2016), pp. 2550–2559.

[83] Meding JB Pierson JL Berend ME Malinzak RA Ritter MA Davis KE. "The effect of alignment and BMI on failure of total knee replacement". In: *J Bone Jt Surg Am* 93.17 (2011), pp. 1588–1596.